A Thesis

on

THE EXPERIMENTAL INVESTIGATION ON MICROPATTERNING OF BLENDED AND RANDOM COPOLYMER THIN FILMS

Submitted in the partial fulfilment of the requirement

for

Doctor of Philosophy

by

Ankur Pandey

(Roll no. 156107005)

Under the supervision of

Dr. Partho Sarathi Gooh Pattader

DEPARTMENT OF CHEMICAL ENGINEERING

INDIAN INSTITUTE OF TECHNOLOGY

GUWAHATI-781039

JANUARY-2O22

D E C L A R A T I O N

I, *Ankur Pandey*, wholeheartedly declare that the subject matter embedded in this thesis is the outcome of the experiments and analysis carried out by me at the Department of Chemical Engineering and Center for Nanotechnology, Indian Institute of Technology Guwahati, Assam, India, under the supervision of *Dr. Partho Sarathi Gooh Pattader*, Associate Professor, Department of Chemical Engineering, Indian Institute of Technology Guwahati India. In keeping with the general practice of reporting scientific observations, due acknowledgment has been made where the work described is a contribution of another investigator.

Date:

Place: Guwahati

Ankur Pandey
Department of Chemical Engineering
Indian Institute of Technology,
Guwahati, Assam, INDIA 781039

C E R T I F I C A T E

This is to certify that the work contained in this thesis entitled "THE EXPERIMENTAL INVESTIGATION ON MICROPATTERNING OF BLENDED AND RANDOM COPOLYMER THIN FILMS." by Mr. *Ankur Pandey*, has been carried out under my supervision and has not been submitted elsewhere for a degree.

Thesis Supervisor

Date:

Dr. Partho S. G. Pattader

Place: Guwahati

Department of Chemical Engineering

Indian Institute of Technology,

Guwahati, Assam, INDIA 781039

आ नो भद्राः क्रतवो यन्तु विश्वतः ।

Let noble thoughts come to us from every side.

Rig Veda

A C K N O W L E D G E M E N T S

The quest for knowledge and intense desire to contribute to the scientific world and to the nation had filled me up with an intense zeal to pursue Ph.D. It has been a long yet wonderful learning experience for me. Until I joined IIT Guwahati, I have never encountered such a highly motivated and ingenious synod of ignited minds at one place. The kind of research exposure I received from the institution is extraordinary.

At first, with the utmost reverence and deepest gratitude, I would like to acknowledge **Dr. Partho Sarathi Gooh Pattader**, Associate Professor, Department of Chemical Engineering, for his contribution not only in supervising the research work but also modifying my overall thought process of meticulously planning and executing the experiments, and analyzing and summarizing the results obtained. Most importantly, presenting the findings in such a manner that the person at the other end grasps the minutest and intricate details of the experiments. Moreover, under his superintendence, I have got exposed to setting up a highly equipped research laboratory right from scratch.

Next, I would like to acknowledge **Prof Dipankar Bandyopadhyay,** Professor, Department of Chemical Engineering, who, from his very busy schedule, was very kind to spare some time and supervise me whenever I got stuck on some issue. Moreover, during the initial days of my Ph.D., he has been kind to provide us with research facilities in his laboratory until we have got our own fully functional laboratory. Prof. Bandyopadhyay is not only my doctoral committee chairman but more like an elderly head of our small family at IIT Guwahati. Through him, it was such an enriching experience to meet super talented and extraordinary researchers working with him.

I express my deepest gratitude towards doctoral committee members **Prof Amaresh Dalal, Prof. Tapas K Mandal, Prof. Nageshwar Rao Peela** and **Prof. Dipankar N. Basu**. who were very kind in suggesting me improvements in the research work.

I extend my reverence and gratitude towards **Prof. Rabibrata Mukherjee,** Department of Chemical Engineering, IIT Kharagpur, who is my virtual *Guru* and inspiration throughout my course. The research work published under his supervision had laid the foundation for most of my experiments.

Also, I would like to extend my sincere gratidute towards the examiners **Prof. Chiara Neto**, Univeristy of Sydney and **Prof. Saptarshi Majumdar**, IIT Hyderabad for their valuable inputs in the thesis.

I fell short of words to express my thankfulness towards my lab mates. I thank each and every one of them from the bottom of my heart. Moreover, working with enthusiastic and supportive colleagues like **Pritam Da and family, Sunil, Kaniska and family, Prerona** and **Aniruddha** is a blessing in disguise.

I would also like to thank **Dr. Ravi, Dr. Nayan, Dr. Amit, Dr. Saptak, Dr. Mitradip, Dr. Seim, Dr. Tamanna, Dr. Sunny, Dr. Siddharth, Dr. Joydip, Dr. Debadrita, Sagnik, Nayan, Rupam, Nirmal, Vinod, Jiwajyoti,** and **Tanusree,** for their exemplary assistance throughout the course of my research work.

Also, I would like to thank **Mrs. Namrata N. Rynjah**, Student counsellor for her constant support during my stay at IIT Guwahati.

Also, I thank my friends **Miss. Deepmala Singh, Dr**. **Debashri & family, Dr. Soumendu**, **Anupama & family, Dr. Himali & family, Jayakrishnan U, Dr. Arnab, Dr. Saswati & family, Dr. Dharmalingam K & family** and **Kishor** for their suggestions and discussions not restricted to just research work.

I feel myself blessed to have been worked with **Prof. (Retd.) S. Sivashankaran**, MIT Manipal and **Dr. R. Manivannan**, NIT Raipur during my undergraduate and postgraduate research work.

I am grateful to the staff members at the **Department of Chemical Engineering and Centre for Nanotechnology.** Also, a special thank you to my special companion **Atomic Force Microscopy (Bruker, Innova series)**. It was this instrument that enabled me to explore the vast territory of exquisite pattern fabrication.

Lastly, I dedicate this research work to my family members: **Master Jashn Pathak, Master Ved Tiwari, Master Aahan Pandey, Mrs. Jyoti Pandey & Mr. Aseem Kumar Pandey, Mrs. Anubha & Mr. Jeet Pathak, Mrs. Anju Tiwari & Mr. Vinod Tiwari, Mrs. Manorama Tiwari & late Pt. Ambika Prasad Tiwari, late Mrs. Krishna Pandey & Mr. Ramakant Pandey, Col.(Retd.) S.G. Sharma, elders, cousins and almighty.** It was their constant support that empowered me throughout the long journey called Ph.D.

Jai Hind!

Ankur Pandey

Synopsis

Nature is enriched with a variety of highly engineered intricate patterns with multiple functionalities.[1–3] These naturally occurring patterns are formed by the self-assembly of macromolecules like proteins and carbohydrates. To one's amazement, an excellent hierarchy is efficiently maintained for transferring properties from the sub-micron level to the higher level. The highly efficient naturally occurring structures kindle the cogitation of the scientific world, and there is an urge to mimic these structures using synthetic materials, like polymers.[4–7] These patterns attract a broad spectrum of multidisciplinary applications such as fabrications of anti-reflection coatings,[4,5] robust membrane materials,[6–10] highly ordered magnetic bit pattern media,[11,12] bio-inspired super-hydrophobic and self-cleaning surfaces,[2,13–17] solar cells,[18] and many others.

Munch et al. reported ice-template technology to form tougher microstructures using polymer composite of PMMA and aluminum oxide.[19] Muehlberger et al. successfully fabricated multilevel and intricate patterns in *Morpho* butterfly structures using simple techniques like nanoimprint lithography (NIL).[20] Moreover, taking inspiration from the *Stenocara* beetle, Neto and co-worker successfully utilized alternate arrangements of hydrophilic (poly 4-vinyl pyridine, P4VP) and hydrophobic polymers (polystyrene, PS) dew harvesting.[21] The reports related to polymer pattern generation are multitudinous. Hence based on the patterning methodology, these studies are divided into *Top-down* and *Bottom-up* approaches.[22] Moreover, in the presented work, the synergies of both the approaches and present state-of-the-art methods for the complex pattern generation using homopolymer blends and random copolymer.

OUTLINE OF THE THESIS

Based on the understanding of various methods available in the reported works of literature, the methods presented here are facile, low-cost, and innovative to fabricate complex patterns. The present work is divided into five chapters. **Chapter 1** is the introduction of the thesis. It gives a brief account of the works of literature available for polymer pattern generation. The chapter summarizes the *Top-down* and *Bottom-up* techniques. Some theoretical concepts related to dewetting of thin polymer films and phase separation in blend films are also included in the account. Moreover, existing research works available for the fabrication of polymer patterns are also discussed.

Chapter 2 is an experimental study that explains how phase separation occurs in the polymer bilayer system. The upper layer is a blend of polystyrene (PS) and polymethyl methacrylate (PMMA) in toluene. The under layer consists of PS, PMMA, blend PS-PMMA, or random copolymer of PS and PMMA (PS-r-PMMA). The complete experimental process is schematically represented in Figure 1. The polymer chains were not tethered and thus labile over the silicon wafer (substrate). Strong evidence was obtained that showed the underlayer strongly affects the phase separation in the blend upper layer. For example, a lower surface energy PS underlayer assisted in phase separation during spin coating, unlike higher surface energy underlayers like PMMA, blend PS/PMMA, or PS-r-PMMA. The study also shows that the short-duration rapid thermal annealing (RTA) at a high temperature of 300ºC enhances the rate of phase separation in a bilayer system. The final equilibrium morphology in the bilayer system was achieved much faster than conventional solvent vapor annealing or thermal annealing at lower temperatures. The thermal stability of polymers at higher temperatures was also checked using Raman spectroscopy, thermogravimetry analysis (TGA), and differential Scanning Calorimetry (DSC). It was found that the polymers were stable at high temperatures for shorter durations. The study also deals with the fabrication of multiple-length scale

structures. When a bilayer of blend/RCP was thermally annealed using RTA, phase separation occurs in both blend upper layer and RCP under layer. The upper blend layer phase separates and forms a larger PS droplet-like structure in the PMMA matrix. However, in the underlayer, the RCP domains also self-assemble to form isolated PS droplet structures within the PMMA matrix but, owing to the covalent bonds present, cannot self-assemble to an extent to form larger domains. This concept was further utilized to generate complex hierarchical patterns. The patterning of the RCP underlayer was done using capillary force lithography (CFL). Like the previous case, phase separation occurs when the system was subjected to RTA. Later by using the solvents for etching out one polymer component, keeping others intact selectively, can fabricate complementary patterns.

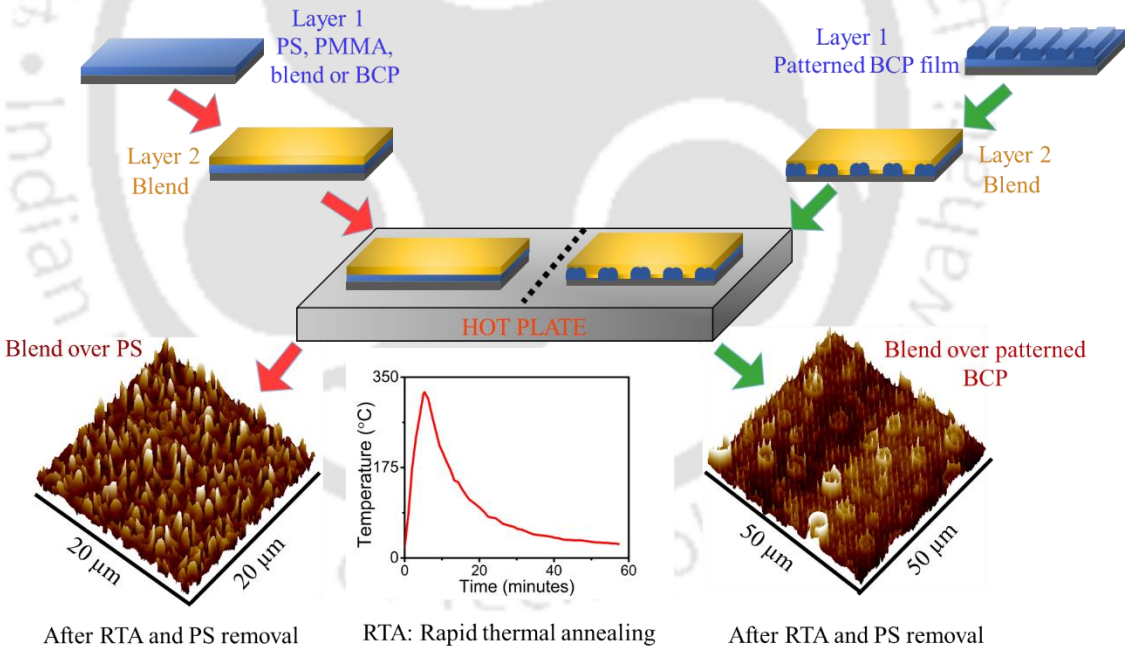

Figure 1. The schematic depicts the protocol adopted to study phase separation over different types of the polymer layer.

Chapter 3 primarily focuses on blend PS/PMMA coated PS underlayer. The thickness of the PS underlayer was kept constant, and the ratio of the individual polymer was varied. It was found that during spin coating, blend upper layer tend to phase separate due to rapid evaporation of solvent and presence of marginally low surface energy PS underlayer. By

altering the ratio PS: PMMA, various patterns can be obtained. Later, the PS underlayer was patterned using CFL and thus used to generate orderly arrangements of the phase-separated domains.

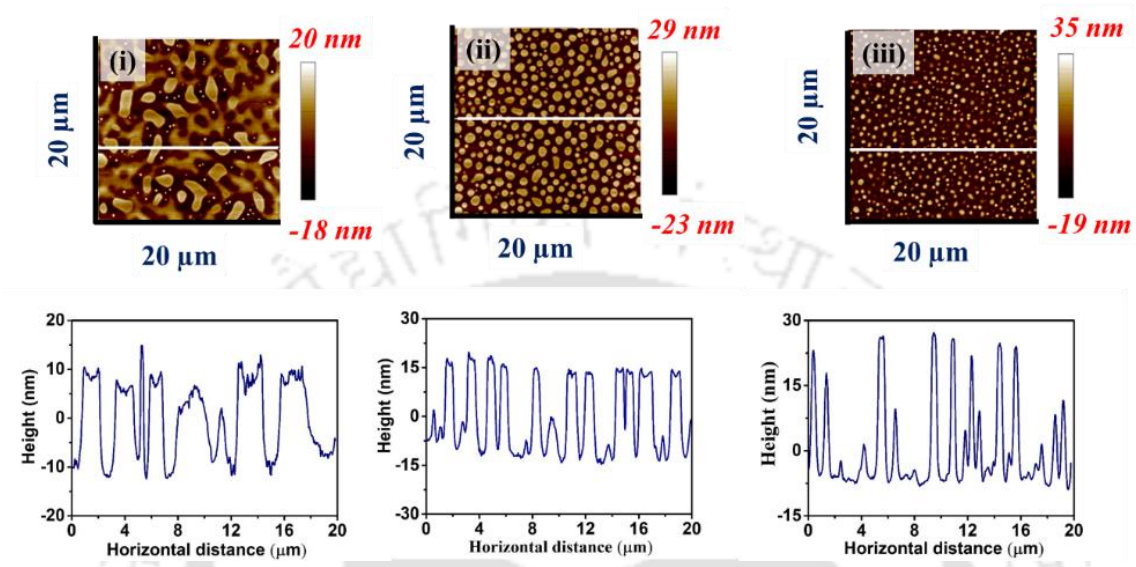

Figure 2. The AFM images were obtained after spin coating of Blend PS/PMMA over PS underlayer by varying the PS: PMMA ratio. The PS:PMMA ratio was varied from (i) 20:80, (ii) 50:50 and (iii) 80:20.

In Chapter 2, it was shown that a bilayer of blend and RCP could be utilized to generate multi-length scale structures. **Chapter 4** is a detailed study of blend PS/PMMA over RCP underlayer. Here, the underlayer RCP was patterned using CFL. The top layer of blend PS/PMMA was then spin-coated over the patterned RCP layer. A parametric study was presented in which the concentration of blend PS/PMMA was varied by diluting it in toluene. When the system was annealed using RTA, phase separation resulted in multi-length scale structures discussed in Chapter 2. However, due to the change in the polymer concentration in the blend upper layer, a variety of patterns can be generated. With a decrease in the concentration of blend in the upper layer, there was a decrease in the droplet diameter and wavelength. Also, a comparative study was done by coating the blend upper layer over silicon wafers.

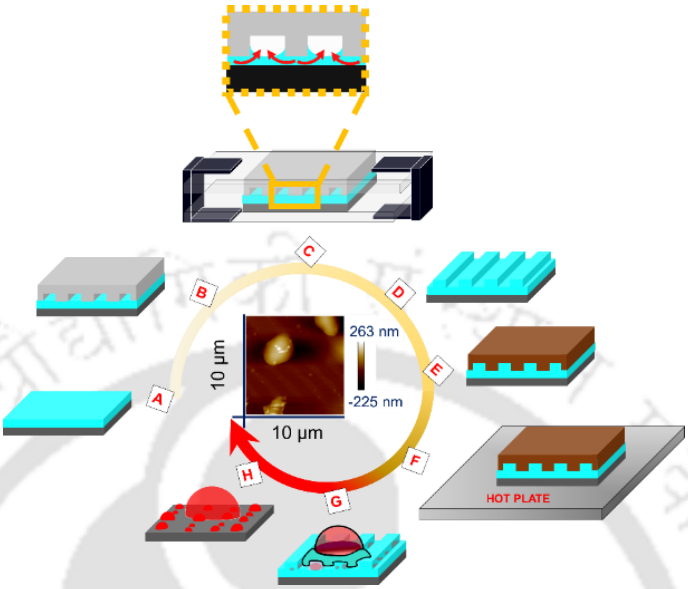

Figure 3. The figure is showing the steps followed during the experiment. The sequence of steps are as follows (A) spin coating of RCP film at 2500 rpm for 120 s (B) placement of aluminium foil mould over the RCP film (C) the film with flexible mould over it firmly sandwiched between two glass slides and heated over 120℃ for 12 h (D) pattern transfer from mould to RCP films (E) a second coat of blend over pre-patterned RCP layer (F) rapid thermal annealing (RTA) of bilayer films (G) patterns obtained after RTA and (H) selective solvent etching after immersion in acetic acid to remove PMMA (for the simplicity selective solvent etching for PS removal using cyclohexane is not shown here).

A study presented in **Chapter 5** describes the evolution of morphology in random copolymer when exposed to the highly focussed electron beam. The process is schematically shown in Figure 4. The copolymer used here contained blocks of PS and PMMA. The e-beam dose was varied from 180 µC/cm^2-10,000 µC/cm^2. At low e-beam dose, the bond scission occurs in the PMMA segments while PS blocks are crosslinked and form trenches in the exposed zone. The solvent-induced dewetting was observed in the exposed PMMA blocks to form nanopatterns at room temperature. During this process, the unexposed region is intact. The key highlight of the present work is the tone reversal of the PMMA block. At a higher dose of the electron beam, the PMMA block present gets crosslinked in the area of exposure. In the vicinity of the zone of exposure, weak interaction of the polymer with scattered electrons

causes scission PMMA chains. The broken PMMA chains undergo solvent-induced dewetting to develop large-area nanopatterns. Also, the study reports that a further size reduction of features by ~50% by the selective removal of a particular polymer from the RCP using suitable solvents. The study presented opens up a gateway to generate complex and intricate multi-length scale structures merely by the variations in film thickness, e-beam dosage, pattern, or composition/MW of RCP.

Lastly, **Chapter 6** gives a detailed conclusion of the thesis; the scope, future, and further applications of the complex patterns are also mentioned.

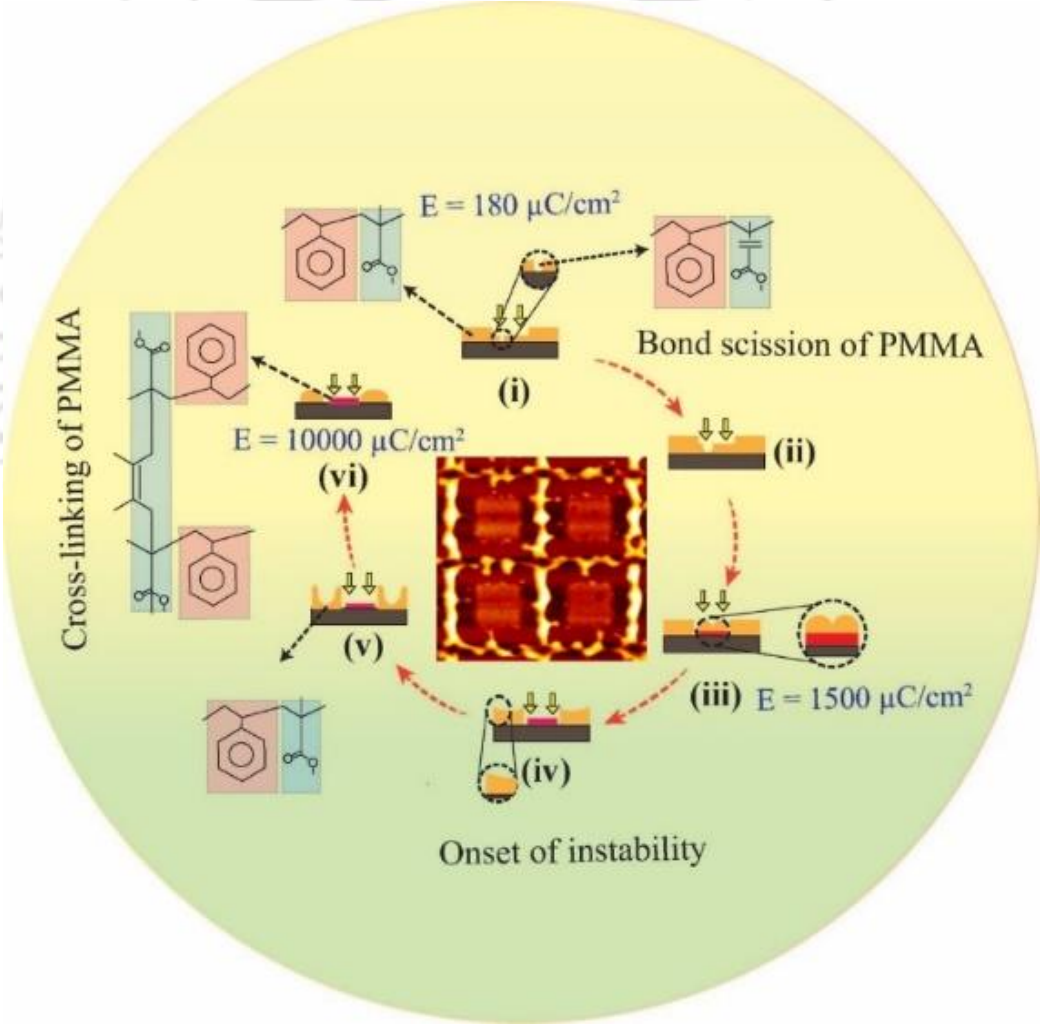

Figure 4. The schematic representation showing the mechanism for morphological changes occurring at varying dose of e-beam viz. (i) 180 μC/cm² (ii) 300-700 μC/cm² (iii) 1500 μC/cm² (iv) 2000 μC/cm² (v) 3000 μC/cm² and (vi) 6000-10000 μC/cm².

LIST OF RESEARCH OUTPUT

Research articles

1. **A. Pandey**, K. Murmu, P.S. Gooh Pattader, Non-equilibrium thermal annealing of a polymer blend in bilayer settings for complex micro/nano-patterning, RSC Adv. 11 (2021) 10183–10193. https://doi.org/10.1039/d1ra00017a.

2. **A. Pandey**, S. Maity, K. Murmu, S. Middya, D. Bandyopadhyay, P.S. Gooh Pattader, Self-organization of random copolymers to nanopatterns by localized e-beam dosing, Nanotechnology. 32 (2021) 285302. https://doi.org/10.1088/1361-6528/abf197.

3. P. Gogoi, S. K. Singh, **A. Pandey**, A. Chattopadhyay; P. S. Gooh Pattader, Nanometer Thick Superhydrophobic Coating Renders Cloth Mask Potentially Effective Against Aerosol-driven Infections, (2021) Advanced Bio Materials (Submitted).

** Two manuscript are at drafting stage.

Poster presentations

1. **Ankur Pandey**, Himanshu Raturi and Partho Sarathi Gooh Pattader, Multistage Patterning of Composite Polymeric Thin Film, International Conference on Functional Nanomaterials, IIT BHU, 2019.
2. **Ankur Pandey**, Surjendu Maity, Partho Sarathi Gooh Pattader and Dipankar Bandhyopadhyay, Biomimicking: Fabrication of insect eye type polymer structures using spin dewetting, Research Conclave, IITG, 2019. (2^{nd} rank for poster presentation).
3. **Ankur Pandey** and Partho Sarathi Gooh Pattader, An experimental investigation of phase separation in polymer-polymer bilayer system, International Conference on Functional Materials-2020, IIT Kharagpur.
4. **Ankur Pandey**, Aniruddha Deb and Partho Sarathi Gooh Pattader, Phase separation in polymer-polymer bilayer systems, International Conference Advances in Chemical Engineering-2020, UPES, Dehradun.
5. **Ankur Pandey** and Partho Sarathi Gooh Pattader, A study on phase separation in polymer-polymer bilayer thin film, EMRS spring meeting 2020, Strasbourg-France. (Accepted for poster presentation).

Oral presentations

1. **Ankur Pandey**, Dipankar Bandhyopadhyay and Partho Sarathi Gooh Pattader, Investigation of blend and block copolymer self-assembly on thin polymer interlayer, REFLUX IIT G, 2018.
2. **Ankur Pandey**, Aniruddha Deb and Partho S G Pattader, Effect of a labile under layer on phase separation of PS-PMMA blend, ACS Spring 2021, 2021.
3. Aniruddha Deb, **Ankur Pandey** and Partho S G Pattader, Effect of vibration on spontaneous dewetting morphology, kinetics and self-assembly of thin films, ACS Spring 2021, 2021.

REFERENCES

[1] M. Ghasemlou, F. Daver, E.P. Ivanova, B. Adhikari, Bio-inspired sustainable and durable super-hydrophobic materials: from nature to market, J. Mater. Chem. A. 7 (2019) 16643–16670. https://doi.org/10.1039/c9ta05185f.

[2] K. Liu, L. Jiang, Bio-inspired design of multiscale structures for function integration, Nano Today. 6 (2011) 155–175. https://doi.org/10.1016/j.nantod.2011.02.002.

[3] N. Desert, T.N. Desert, Water capture by a desert beetle, Nature. 414 (2001) 33–34.

[4] S. Walheim, E. Schäffer, J. Mlynek, U. Steiner, Nanophase-separated polymer films as high-performance antireflection coatings, Science. 283 (1999) 520–522. https://doi.org/10.1126/science.283.5401.520.

[5] W. Joo, M.S. Park, J.K. Kim, Block copolymer film with sponge-like nanoporous strucutre for anti-reflection coating, Langmuir. 22 (2006) 7960–7963. https://doi.org/10.1021/la061441k.

[6] L. Chen, W.A. Phillip, E.L. Cussler, M.A. Hillmyer, Robust nanoporous membranes templated by a doubly reactive block copolymer, J. Am. Chem. Soc. 129 (2007) 13786–13787. https://doi.org/10.1021/ja0753041.

[7] S.Y. Yang, I. Ryu, H.Y. Kim, J.K. Kim, S.K. Jang, T.P. Russell, Nanoporous membranes with ultrahigh selectivity and flux for the filtration of viruses, Adv. Mater. 18 (2006) 709–712. https://doi.org/10.1002/adma.200501500.

[8] W.A. Phillip, J. Rzayev, M.A. Hillmyer, E.L. Cussler, Gas and water liquid transport through nanoporous block copolymer membranes, J. Memb. Sci. 286 (2006) 144–152. https://doi.org/10.1016/j.memsci.2006.09.028.

[9] G. Liu, J. Ding, A. Guo, M. Herfort, D. Bazett-Jones, Potential skin layers for

membranes with tunable nanochannels, Macromolecules. 30 (1997) 1851–1853. https://doi.org/10.1021/ma961530b.

[10] R.M. Dorin, W.A. Phillip, H. Sai, J. Werner, M. Elimelech, U. Wiesner, Designing block copolymer architectures for targeted membrane performance, Polymer (Guildf). 55 (2014) 347–353. https://doi.org/10.1016/j.polymer.2013.09.038.

[11] O. Hellwig, J.K. Bosworth, E. Dobisz, D. Kercher, T. Hauet, G. Zeltzer, J.D. Risner-Jamtgaard, D. Yaney, R. Ruiz, Bit patterned media based on block copolymer directed assembly with narrow magnetic switching field distribution, Appl. Phys. Lett. 96 (2010) 052511–052513. https://doi.org/10.1063/1.3293301.

[12] S. Xiao, X. Yang, E.W. Edwards, Y.H. La, P.F. Nealey, Graphoepitaxy of cylinder-forming block copolymers for use as templates to pattern magnetic metal dot arrays, Nanotechnology. 16 (2005) S324–S329. https://doi.org/10.1088/0957-4484/16/7/003.

[13] M. Ma, R.M. Hill, J.L. Lowery, S. V. Fridrikh, G.C. Rutledge, Electrospun poly(styrene-block-dimethylsiloxane) block copolymer fibers exhibiting superhydrophobicity, Langmuir. 21 (2005) 5549–5554. https://doi.org/10.1021/la047064y.

[14] J.T. Han, X. Xu, K. Cho, Diverse access to artificial super-hydrophobic surfaces using block copolymers, Langmuir. 21 (2005) 6662–6665. https://doi.org/10.1021/la051042+.

[15] P. Pareo, G.L. De Gregorio, M. Manca, M.S. Pianesi, L. De Marco, F. Cavallaro, M. Mari, S. Pappadà, G. Ciccarella, G. Gigli, Ultra lightweight PMMA-based composite plates with robust super-hydrophobic surfaces, J. Colloid Interface Sci. 363 (2011) 668–675. https://doi.org/10.1016/j.jcis.2011.07.075.

[16] D. Adak, S. Ghosh, P. Chakraborty, K.M.K. Srivatsa, A. Mondal, H. Saha, R. Mukherjee, R. Bhattacharyya, Non lithographic block copolymer directed self-

assembled and plasma treated self-cleaning transparent coating for photovoltaic modules and other solar energy devices, Sol. Energy Mater. Sol. Cells. 188 (2018) 127–139. https://doi.org/10.1016/j.solmat.2018.08.011.

[17] N.A. Gengec, U. Cengiz, H.Y. Erbil, Superhydrophobic perfluoropolymer/polystyrene blend films induced by nonsolvent, Appl. Surf. Sci. 383 (2016) 33–41. https://doi.org/10.1016/j.apsusc.2016.04.160.

[18] S.I. Na, S.S. Kim, J. Jo, S.H. Oh, J. Kim, D.Y. Kim, Efficient polymer solar cells with surface relief gratings fabricated by simple soft lithography, Adv. Funct. Mater. 18 (2008) 3956–3963. https://doi.org/10.1002/adfm.200800683.

[19] E. Munch, M.E. Launey, D.H. Alsem, E. Saiz, A.P. Tomsia, R.O. Ritchie, Tough, Bio-Inspired Hybrid Materials, Science. 322 (2008) 1516–1520.

[20] M. Muehlberger, S. Ruttloff, D. Nees, A. Moharana, M.R. Belegratis, P. Taus, S. Kopp, H.D. Wanzenboeck, A. Prinz, D. Fechtig, Nanoimprint replication of biomimetic, multilevel undercut nanostructures, Nanomaterials. 11 (2021) 1–10. https://doi.org/10.3390/nano11041051.

[21] S.C. Thickett, C. Neto, A.T. Harris, Biomimetic surface coatings for atmospheric water capture prepared by dewetting of polymer films, Adv. Mater. 23 (2011) 3718–3722. https://doi.org/10.1002/adma.201100290.

[22] A. Perl, D.N. Reinhoudt, J. Huskens, Microcontact printing: Limitations and achievements, Adv. Mater. 21 (2009) 2257–2268. https://doi.org/10.1002/adma.200801864.

TABLE OF CONTENTS

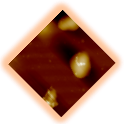

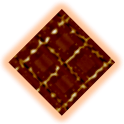

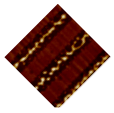

LIST OF FIGURES

LIST OF TABLES

ABBREVIATIONS

1	**PS**	Polystyrene
2	**PMMA**	Polymethyl methacrylate
3	**PVP**	Poly(2-vinylpyridine)
4	**PVME**	Poly (vinyl methyl ether)
5	**P4VP**	Poly(4-vinylpyridine)
6	**BCP**	Block copolymer
7	**RCP**	Random copolymer
8	**SD**	Spinodal decomposition
9	**NG**	Nucleation and growth
10	**EBL**	Electron Beam Lithography
11	**Mw**	Molecular weight
12	**AFM**	Atomic Force Microscopy
13	**XPS**	X-Ray Photoelectron Spectroscopy
14	**FE-SEM**	Field Emission Scanning Electron Microscope.
15	**TGA**	Thermogravimetric Analysis
16	**DSC**	Differential Scanning Calorimetry

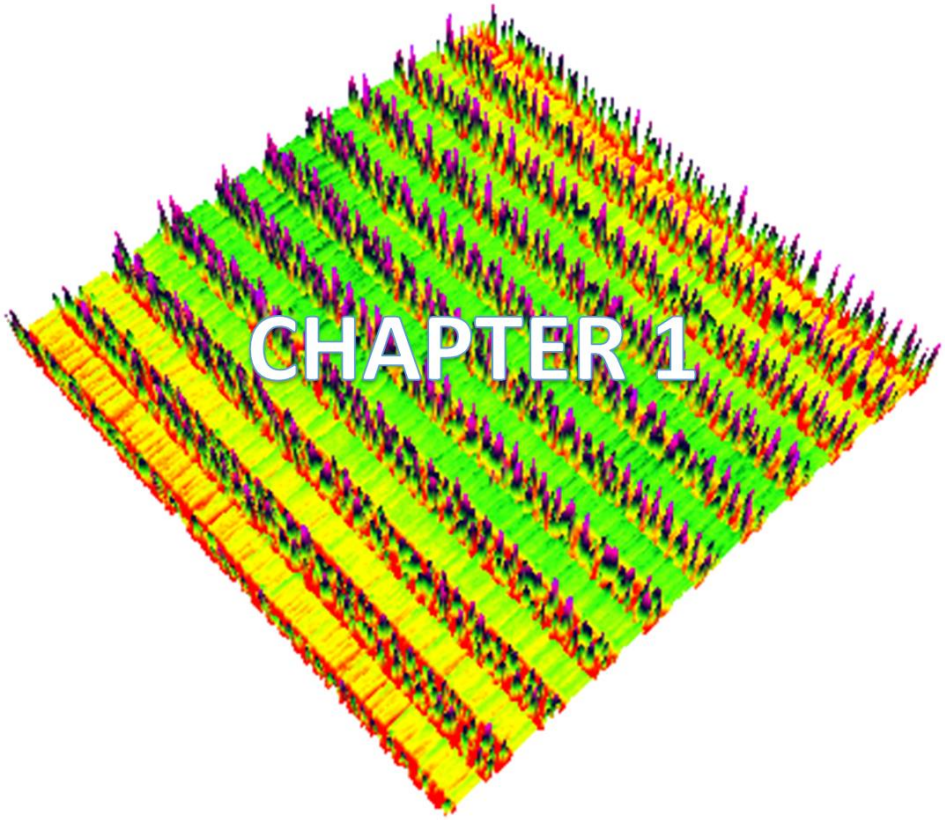

CHAPTER 1

Chapter 1

Introduction

The polymer films can be prepared using a variety of techniques like spin-coating, dip-coating, or drop casting. By using suitable patterning techniques or methods, these films can be transformed to generate polymeric micro/nano patterns over the substrate. Herein, a brief literature survey of the techniques/methods used for pattern generation is presented. These techniques are broadly classified into two broader sections viz. top-down and bottom-up approaches.

1. TOP-DOWN APPROACHES FOR PATTERNING

The top-down methods are the size reduction processes that involves breaking down a larger dimension structure into a smaller one. One such technique that involves UV lasers is photolithography.[1] The typical features obtained using this technique are of the order of few microns. However, with the use of electron beam lithography, feature sizes are further reduced to the nanometer scale. The polymer on which direct writing is done is broadly classified into positive resists (for example, polymethyl methacrylate) and negative resists (for example, polystyrene).[2,3] The former type resist is exposed with a focussed beam the bonds between the polymer units break down in the exposed area. These broken chains are removed using a suitable solvent. This process is known as development. On the contrary to this, in the negative

type resist, the crosslinking of the polymer occurs in the exposed area. Subsequently, the unexposed polymer is removed in the development process.[1] Direct writing using e-beam assisted dewetting is successfully demonstrated by Verma and Sharma. The process involved exposing the polystyrene (PS) or polymethyl meth acrylate (PMMA) films with electron beam and development using solvent mixture containing water, butanone and acetone. Here, PS is negative resist (chain entanglement upon interaction with e beam) and PMMA is positive resist (chain scission upon interaction with e beam). The solvent diffuses into the polymer making chains mobile thereby assisting dewetting.[4–8]

2. BOTTOM-UP FOR PATTERNING

On the contrary to the top-down methods, the bottom-up approach involves molecule by molecule or atom by atom building of larger length scale structures. This phenomenon is also known as self-assembly.[9,10] The commonly used methods for fabrication utilizing a bottom-up approach are dewetting of polymer films and phase separation of blend/block copolymers.

2.1 Dewetting of polymer thin films

In the bulk polymer system, the polymer chains adopt a *random coil model,* and thus along the chain backbone, the physical orientation of each repeating unit is essentially not correlated with the orientation of another unit. However, unlike the bulk polymer system, the properties of a thin film supported on a rigid substrate deviate substantially from the random coil model.[11–14] The film supported on a rigid substrate is confined between two interfaces 1) substrate-polymer interfaces 2) air polymer interfaces. This confinement reduces the degree of freedom, and polymer thin film adopts a modified random coil model due to the influences from air-polymer and polymer substrate.[15] These influences give rise to instabilities in the film in the form of capillary waves. Under certain conditions, these capillary waves are

amplified and subsequently rupture, marking the onset of what is popularly known as *dewetting*. The phenomenon of dewetting is the opposite of wetting, where a film coated over a non-wettable substrate disintegrates into polymer droplets. The based on the interface potential (ϕ) versus film thickness h curve the films can be stable, metastable and unstable.[16] The ultra-thin films (thickness around 10 nm) dewet spontaneously and is engendered by van der Waals interaction between air-liquid and liquid-solid interface. This phenomenon is popularly known as spinodal dewetting.[17–19] The initial film contains nanoscopic undulations for the thicker films with thickness in the range of 10-100 nm. When this film is perturbed externally (heating over a temperature higher than the glass transition temperature of polymer or at room temperature, infusion of solvent vapour to reduce the viscosity of polymeric thin-film or by using electric or magnetic field), the nanoscopic undulations grows. When the air-liquid interface merges with the liquid-solid interface, the holes are generated. This marks the onset of the dewetting process. Also, in a separate case, where the heterogeneities present over the substrate lead to the formation of holes.[16] The holes merge and form interconnected cellular ribbons or rims. Finally, the rims disintegrate into smaller droplets due to Rayleigh instability.[20,21] The droplets' wavelength, number density, and size depend upon the initial thickness of the polymer films.[16,22] In some cases, synergies of spinodal and nucleated dewetting are also observed.[23] Also dewetting is observed in a large spectrum of polymers like PS,[19,22,24–28] PMMA,[29] P4VP,[30] PDMS,[31] liquid crystals[32,33] etc. The factors affecting dewetting process are discussed as follows:

2.1.1 Effect of annealing

2.1.1.1 Thermal annealing

Initially prepared films using techniques like spin coating are smooth and stable at a temperature lower than glass transition temperature (T_G). This is because most of the polymers

have their glass transition temperature > 100°C. However, annealing the films to a temperature higher than glass transition temperature (T_G) leads to the amplification of capillary waves and eventually hits the solid substrate, leading to the formation of holes, which subsequently merge to form rims. In the late stage, the rims break up due to Rayleigh instability to form polymer droplets.[28,34,35]

2.1.1.2 Solvent vapour annealing

The solvent vapour assisted dewetting involves the prepared film being placed inside a chamber saturated with good solvent vapours. At the interface, osmosis leads to swelling of the polymer chains, thereby reducing the glass transition temperature (T_G) below room temperature. The chain mobility increases, engendering hole formation, hole coalescing, and rim formation. In the final stages, the rims break to form polymer droplets.[36–38] The difference between thermal dewetting and solvent vapour dewetting is that the former is caused by instability in long-range van der Waals forces. On the contrary, later is engendered by short-range polar interactions.[39]

2.1.2 Highly ordered patterned generation using dewetting

Irrespective of the dewetting mechanism, the polymeric micro/nano droplets formed by dewetting are randomly oriented. The orderly arrangement of the dewetted structures can be achieved either by using a pre-patterned substrate. These pre-patterned substrates either have topographical protrusions [40,41] or have alternating chemically wetting and non-wetting patches.[42–44]

The early report of generating a pre-patterned substrate with topographical protrusions utilizes simple techniques like the unidirectional rubbing of the substrates like glass with emery paper.[45] Later, when the polymer solution is dispensed over the substrate, the scratches

guided the polymer solution to flow along the direction of the scratches.[46] The topographically pre-patterned substrates can also be prepared using soft lithography [36,47,48] or other lithographic techniques like optical lithography.[49,50]

The dewetting over topographically patterned substrates can be achieved by directly spin coating the polymer solution over the patterned substrates[48] or by transferring the film with uniform thickness over the pre-patterned substrate by floating.[36,51] When directly dispensing the polymer solution over the patterned substrate, the film formed over the patterns contains the undulations as the portion of liquid fills inside the gaps between protrusions. Thus, the film has nonuniform thickness throughout.[48,52] When the films were annealed, the rupture of the film first occurred at the places where the film thickness is thinnest.[53] However, the polymer concentration is sufficiently low and/or spin coating is performed at high spin speed. The film ruptures during spin coating. This phenomenon is known as *spin dewetting*.[53,54] In another innovative approach, the spin coated film was first detached from the substrate by floating it in water. Subsequently, the film was lifted on the topographically pre-patterned substrate. The nature of binding of the film with the topographically pre-patterned substrate determines the final morphology of the structures. There are two types of contact of films-protrusion contacts reported: focal and conformal. Upon dewetting, the dewetted polymer droplet encapsulates the protrusions in case of focal adhesion. Whereas, when the film adheres conformally, the final dewetted droplets occupy interstitial sites between the protrusions.[36,51]

Ordering of the dewetted structures can also be done using a substrate with alternating wettable and non-wettable patches.[43,44,52,55,56] The primary aim of this approach is to induce chemical heterogeneity in the substrate. This can be done in a variety of ways like micro-contact printing of non-wettable self-assembled monolayers (SAMs) over the

substrate[57,58] or by using a mask (such as TEM grid) over the substrate (PDMS). When substrate and the mask are exposed to UV-Ozone, the interaction at the exposed region creates periodic chemical heterogeneities.[59] When a thin film is coated over a chemically pre-patterned substrate, mass transfer of polymer occurs from non-wettable (or partially wettable) to more wettable regions of the substrate.[52,56,60–62] The film ruptures at less wettable patches revealing the underlying non-wettable region of the substrate. The film becomes undulated with a thickness on the less wettable region than thicker film on the more wettable region. As the dewetting progresses, the polymer accumulated inside the more wettable stripe ruptures due to Rayleigh instability, forming the droplets.[57,58]

The techniques discussed above use pre-patterned substrate; however, direct-write techniques can also create nanoscopic, highly ordered dewetted droplets. A highly focused low dose e-beam shined over PS and PMMA films. Later, after e-beam exposure, the prepared films were immersed in a solvent mixture of water, acetone, and butanone in the ratio of 15:3:7. Arguably, PS and PMMA behave differently upon interaction with e-beam. The bond scission occurs in the case of PMMA (positive tone resist) whereas cross-linking takes place in the case of PS (negative tone resist).[2,63] The solvent mixture percolated inside the polymer films and makes them mobile, thereby reducing the glass transition temperature T_G of the films leading to film rupture. For positive tone polymer film, rupture occurs in the shined part of the films, whereas for negative tone polymer films, the rupture occurs in the region where the e-beam is not shined.[7,64–66]

2.2 Polymer blends and phase separation in thin films

2.2.1 Phase separation in polymer blends: bulk

A few sets of polymers are mutually immiscible due to the long-chain and low energy of mixing. The blending of polymers is done when it is desirable to have some properties of each

component or completely different characteristics.[67] This is done by mixing the polymers in a common solvent (for example, PS and PMMA in chloroform or toluene). However, under appropriate conditions, phase separation in blend occurs. This leads to a variety of morphologies like bicontinuous or sea-island type.[68]

2.2.1.1 Flory Huggins Theory

The free energy of mixing determines the miscibility of two polymers. It is the difference in the free energy of the mixture and the total free energy of the individual polymers. Flory and Huggins independently put forward an expression for the free energy of mixing of polymers, which later came to be known as Flory-Huggins Theory.[69,70] The complete derivation of the theory has been provided in Appendix 1. According to the theory, free energy change of mixing per unit lattice is:

$$\frac{\Delta G_m}{RT} = \mathrm{n}_2 \ln(\phi_2) + \mathrm{n}_1 \ln(\phi_1) + \mathrm{n}_1 \phi_2 \chi$$

The first two terms on the right-hand side account for the combinatorial entropy of mixing, ΔS_m. During mixing, the randomness of the system increases hence, $\Delta S_m > 0$, thereby decreasing the free energy of the system. The last term in the right-hand side represents enthalpy of mixing, ΔH_m. The value of enthalpy depends upon the Flory-Huggins interaction parameter, χ. The Flory-Huggins interaction parameter, χ can be approximately predicted by following expression:

$$\chi = \frac{1}{\kappa_B T}[\varepsilon_{AB} - 0.5(\varepsilon_{AA} - \varepsilon_{BB})]$$

Where, $\kappa_B$is Boltzmann constant, $\varepsilon_{ij}$is the contact energy between i and j and T is temperature.

2.2.1.2 Phase diagram

The phase behaviour in polymer blends, i.e., whether a system will exhibit phase separation or complete/partial miscibility, can be qualitatively predicted using a phase diagram. For miscibility, the free energy of mixing should be less than zero, $\Delta G_m < 0$. However, this is insufficient to precisely determine the phase behavior of the system, and criteria for equilibrium and stability should be established. For a symmetric system at constant pressure and temperature, i.e., an equal degree of polymerization, the following equations of equilibrium and stability should be satisfied:

1. Equilibrium

$$\frac{\partial \Delta G_m(\varphi_A')}{\partial \varphi_A} = \frac{\partial \Delta G_m(\varphi_A'')}{\partial \varphi_A}$$

2. Stability

$$\frac{\partial^2 \Delta G_m}{\partial {\varphi_A}^2} = 0$$

The locus of the two equations is shown in the form of the phase diagram (**Figure 1.1**). It is a qualitative plot between the temperature and composition. The equilibrium line forms the boundary between one phase and two-phase region. The two-phase region is further divided into metastable and stable regions. Phase separation in polymer blends occurs when a system changes temperature or composition. Broadly two types of mechanisms have been observed 1) spinodal decomposition (SD) and 2) nucleation and growth (NG). The SD type phase separation occurs due to concentration fluctuations. The phase diagram can be visualized by crossing through the critical point into the unstable region without crossing the metastable region. However, in another case, when NG type phase separation occurs, the system enters

into the metastable region. The phase separation occurs in two stages, i.e., slow nucleation followed by growth of phase-separated domains.[71,72]

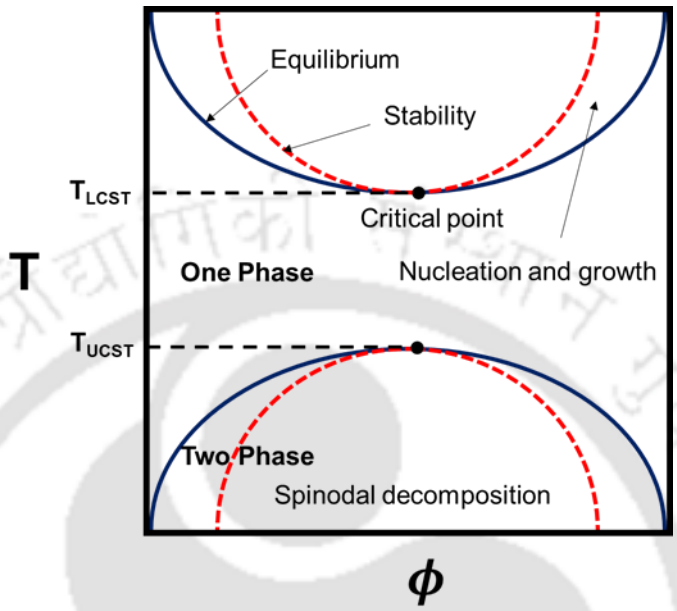

Figure 1.1. *The figure showing schematic phase separation for symmetric system ($N_A = N_B$) binary mixture of linear homopolymer blends.*

2.2.2 Phase separation in polymer blends: films

So far, we have discussed the phase separation of polymer blends in bulk. The scenario changes for thin polymer films as the synergistic effect of various parameters give rise to many phase-separated structures in blend thin films.[68] The various parameters that affect the demixing and subsequent pattern generation in blend films are thickness, polymer-substrate interaction, surface energy χ Flory-Huggins parameter, the molecular weight of the polymers, compositions, polymer solubility, evaporation speed in blend or presence of additives. One by one, these parameters are discussed here:

2.2.2.1 Evaporation rate of solvent and roughness of the films.

During the spin coating process, the evaporation rate of the solvent directly impacts the roughness of the film. As the spin coating progresses, the excess solution is thrown out at the system due to centrifugal force forming a layer over the substrate. Also, there is solvent loss due to evaporation at air-film interfaces. If the evaporation rate is high owing to the high vapor pressure of the solvent, the solvent is quickly depleted. Thus, a concentration gradient is generated between near-surface (solvent lean) and near substrate (polymer-rich) region. Thereby assisting in Marangoni instability and formation of large cellular structures and rougher films.[73,74]

2.2.2.2 Thickness of films

The polymer-polymer phase separation is strongly affected by the thickness of the film. Ogawa et al. studied the demixing mechanism for polystyrene (PS): poly(vinyl methyl ether) (PVME) blend for a wide range of thickness ranging from 65 μm to 42 nm using optical microscopy, atomic force microscopy, and small-angle light scattering.[75] The solution in toluene was spun cast to prepare films of various thicknesses over a glass substrate. Later the films were soft baked at 60ºC for 24 h followed by annealing the films at 115ºC for different time intervals. For the thicker films ($t > 15$ μm), the phase separation mechanism was found to exhibit spinodal decomposition as in the case of bulk. In films with a thickness range (15 μm $< t < 1$ μm), the dewetting is induced by spinodal decomposition. Irregularities in the morphology were reported for the films with thickness in the range of 1 μm $> t > 200$ nm indicating the simultaneous occurrence of spinodal decomposition and dewetting. Finally, for the films with thickness $t < 200$ nm, the phase separation was found to be governed by the affinity of one component with the substrate (here PVME) of the blend.

In another study based on the phase separation of PS/PMMA/Toluene on the Au substrate, for the thickness in the range of 140 nm-80 nm, the final morphologies in each case

exhibited a similar type of vertical phase separation. However, the films with higher film thickness had coarser domains as compared to that thinner films.[76]

2.2.2.3 Solvent dependence of the phase-separated structures

Walheim et al. presented a comprehensive study showing the respective solubility of polymers present in the blend determines the final phase-separated structures after film formation. They used model polymer blends of PS/PMMA in toluene, tetrahydrofuran (THF), and methyl ethyl ketone (MEK). The local evaporation rate of the solvent played a crucial role in the formation of the final structures of the polymers. Like in the case of PS/PMMA/toluene or PS/PMMA/THF system, these solvents were common solvents for both of these polymers. However, PS showed more affinity towards toluene and THF than PMMA. As the evaporation of the solvent took place, PMMA rich phase was quickly deprived of the solvent and was solidified faster than PS. The final morphology was obtained when the PS-rich domains get deprived of the solvent resulting in vertical phase-separated structures with protruding, sharp-edged PMMA domains surrounded by the PS-rich phase. The case was reversed when the solvent used was MEK, which had more affinity towards PMMA. In this case, PS-rich domains were protruded vertically and were surrounded by PMMA domains. Interestingly, the domains did not exhibit sharp edges. As a rule of thumb suggested in the study, the structures formed when lower surface energy polymer (PS) had an affinity towards common solvents (toluene or THF), the polymer with a lower solubility in the solvent protruded vertically with a sharp edge and were surrounded by lower surface energy polymer. However, the case was reversed when the higher surface energy (PMMA) had an affinity towards the common solvent (MEK). The final structures obtained did not had sharp edges and the polymer with least affinity was vertically phase-separated surrounded by polymer with higher affinity towards the common solvent.[76]

2.2.2.4 Substrate dependence

The type of substrate used to support strongly influence the final morphology in polymer blend phase separation.[77] It was shown by Walheim et al. that phase separation is affected by the type of substrate used.[76]

2.2.2.5 Molecular weight

Tanaka et al. reported that for a blend of high Mw PS and low Mw PMMA in toluene, surface segregation of PMMA rich domains was observed albeit $\gamma_{PMMA} > \gamma_{PS}$. It had been argued that surface energy of chain-end groups (γ_e) was less than the main chain, which further reduces with the reduction of Mw. Therefore, the chain end effect dominates the segregation of low Mw PMMA at the air-polymer interface. Also, a polymer adopts random coil conformation in a bulk system, and conformational entropy increases with the increase in Mw. However, polymers at the surface of the film were compressed perpendicular to the film surface. Thus, the polymer present at the surface of the air-polymer interface has lower conformational entropy than at the bulk. The difference between conformational entropy at bulk and at the surface decreases with the decrease in Mw, which allows lower Mw PMMA to be enriched at the surface as compared to high Mw PS.[78]

Apropos to the Mw dependence of preferential surface segregation of one of the polymer blend components, Li et al. reported the morphological changes that occurred when the molecular weight of PS was varied in PS/PMMA blend in toluene. The molecular weight of PMMA was fixed at 10.6 k, while the PS molecular weight was varied from 2.9 k to 129 k. To prepare blend films, the individual polymers were dissolved in toluene and mixed in equal volume. Thereafter, the solution was spun coated over the cleaned silicon wafers. Later the films (thickness ~ 70-90 nm) were dried under vacuum at 50ºC for 10 h. Later the films were

annealed at 156ºC for various times. The characterization was done using AFM and XPS techniques. For the blend consisting of PS component in the Mw range < 4 k the nano-phase separation occurred with PS, with no clear distinction between respective PS and PMMA rich domains. Next, for the blend with Mw of PS in the range of 5.6-31.6 k, after the spin coating, the PMMA chains were first to get depleted, thereby forming solidified interconnected matrix. However, at this stage, PS chains were still swelled by toluene and get dispersed over previously solidified PMMA matrix such that PS islands were formed inside the matrix of PMMA. Lastly, all PS was deprived of toluene, giving rise to sea-island morphology. A similar argument was proposed when blend contained high molecular-weight PS (> 35 k), PMMA chains depleted of toluene faster than PS, thereby getting solidified as a stratified layer over the substrate. Later after the evaporation of solvents from PS chains, PS-rich domains were formed and were embedded inside the PMMA rich domains.[79]

2.2.2.6 Effect of annealing on the morphologies

2.2.2.6.1 Thermal annealing

Ton-That et al. studied the PS/PMMA blend in chloroform film spun coated over Mica substrate. After the spin coating, demixing occurs after spin coating of the polymer blend solution. The maximum solvent is evaporated during the spin coating due to faster evaporation rates, and the polymer gets deprived of most of the chloroform. However, chloroform has more affinity towards PMMA than PS; PMMA domains enrich the air-polymer interface over the stratified PS layer during polymer demixing. The morphology presented after the spin coating is far from equilibrium. The holes were present in the morphology due to high surface energy PMMA over the PS stratified layer. Later, upon annealing over-temperature 142ºC, which is higher than glass transition temperature, the top PMMA layer starts dewetting over the PS layer. In the late stages, PMMA domains form a stable layer over the substrate, and the air-

polymer interface was found to be enriched by PS domains. Thus annealing the blend above glass transition temperature drastically modifies the morphologies.[80]

Li et al. presented a study for PS/PMMA/toluene system spun coated over silicon wafer having thickness 67.1, 27.2, and 16.3 nm. All the films were annealed at 156ºC for various time intervals ranging up to 1088 h. For the film having a thickness of 67.1 nm, the as-cast film showed sea-islands type morphology with high surface energy elevated PMMA mounds were surrounded by PS rich phase. However, the morphology was far from equilibrium due to the rapid evaporation of solvent from the bulk of the casted film. During the solvent evaporation process, PMMA was deprived of solvent faster than PS due to the lower solubility of PMMA in toluene as compared to PS. Hence, PMMA gets solidified faster than PS, forming raised PMMA rich domains surrounded by PS-rich domains, as argued by Walheim et al.[76] The PMMA mounds gradually migrate towards the substrate upon prolonged annealing, replacing PS that migrates towards the air-polymer interface. Finally, the PS-rich phase was layer-stacked over PMMA, indicating complete reversal PMMA rich phase at the air-polymer interface before annealing to PS-rich phase in the air-polymer interface after annealing giving rise to foam like morphology. The same phenomenon was observed for 27.2 nm film, with a reduced vertical height of the features and bicontinuous morphology after prolonged annealing. For the thinnest film, 16.3 nm, along with the migration of the PS-rich phase from the substrate to the air-polymer interface at secondary phase separation, was also observed after prolonged annealing.[81]

Rui et al. discussed the three stages of morphological evolution for phase separation when a 50 nm PS/PMMA blend film was spun coated over a silicon wafer. The common solvent used here was 160ºC. The optical monographs were recorded at different time intervals. In the initial stage, the air-polymer interface was enriched by PMMA. In the intermediate stage

phase separation was evident with coarsening of PS-rich domains at the air-polymer interface. In the late stage isolated droplets were formed. These droplets were randomly distributed with PS-rich mounds were surrounded by PMMA rims. Interestingly when PS domains were selectively removed by carbon tetrachloride, the trenches were observed inside and outside of the remaining PMMA rims. This indicated that PS domains extended considerably inside the PMMA domains.[82]

2.2.2.6.2 Solvent vapour annealing

Self-organization based on thermal annealing of blend films is a slower process. A faster process that achieves self-organization in the blend films is solvent vapour annealing. The prepared blend films were confined inside a chamber saturated with vapours of the solvent. As the vapour interacts with the polymers, present the final morphology is determined by the factors like composition, film thickness, and relative interaction between polymers-solvent.[83,84] Roy and Sharma presented a study for PS and PMMA blend in toluene spun casted films exposed to thermal annealing, toluene vapour, and chloroform.[85] Significant differences were observed in the final morphology owing to the relative mobility of the polymers. The process involved the preparation of a thin polymer blend film containing PS and PMMA dissolved in toluene. After spun coating to remove residual toluene, the films were allowed to dry under vacuum ($T< T_G$). These prepared films, as discussed above, were far from equilibrium and at this stage, the morphology obtained had phase separated PS, and PMMA rich domains with PMMA columns protruded outwards and are surrounded by the PS matrix. The high M_w polymers displayed low mobility thus slower kinetics when subjected to thermal annealing at 160ºC for 70 h. However, when as cast films were placed inside a chamber of toluene and chloroform vapour separately, the relative solubility of polymers in these solvents significantly affects the final morphology. Albeit both toluene and chloroform are common

solvent for PS and PMMA, toluene exhibits more affinity towards PS than PMMA. Likewise, PMMA has more affinity towards chloroform than to PS ($\chi_{PS-T} = 0.3469$ $\chi_{PMMA-T} = 0.3829$ $\chi_{PS-C} = 0.3452$ $\chi_{PMMA-C} = 0.3413$, where, T and C represents toluene and chloroform, respectively). The solvent vapours penetrate inside the polymers, reduces the T_G and enhances the chain mobility. After 3 h of solvent vapour exposure, the authors showed that holes begin to emerge in PS rich domains while there was a reduction in the height of PMMA columns, later forming bicontinuous morphology with PMMA rich phase being uneven containing domains and columns. After 9 h of solvent vapour exposure, the PS micro droplets get entrapped inside the PMMA rich phase. Interestingly the PS micro droplets still contained slender PMMA columns embedded inside the PS droplets. In the later stages of prolonged solvent vapour exposure of 48 h, the embedded PMMA columns subsided, and PS micro droplets surrounded the PMMA matrix. Likewise, the as-cast blend films were exposed to chloroform vapours. However, the kinetic was found to be very fast, with an immediate reduction in the heights of PMMA columns and PS domains forming with holes forming Swiss cheese-like morphology on top PMMA rich domains. The PMMA migrates towards the substrate due to high affinity towards SiO_2 layer. Over this stratified PMMA layer, PS domains get dewetted. The final equilibrium morphology was attained in just 60 h of exposure, with PS droplets were embedded inside the PMMA rich matrix. Thus, the study indicates the selective affinity of one polymer towards solvent vapour and M_w plays a crucial role in relative mobility, thereby determining the phase separation kinetics when blend films are subjected to solvent vapour.

2.2.2.7 Concentration of polymer

Polymer-Polymer demixing and subsequent pattern formations are significantly affected by overall polymer concentration and individual polymer volume fraction. A study by Ton-That

et al. showed for a blend PS-PMMA in chloroform coated over cleaned mica, the structures formed when 0.2% polymer was significantly smaller than that of 1%. Moreover, the individual volume fractions of PS: PMMA in the blend resulted in either pitted, sea-island type, or labyrinth type morphology.[86] The same group demonstrated that the overall polymer concentration and individual polymer ratio significantly affect the final morphologies. It was shown for PS-PMMA blend in chloroform spin-cast over Mica substrate. When PS/PMMA ratio was greater than equal to 50:50, the morphology showed the formation of the pits. This was because after solvent rapidly evaporated from the films during spin coating, surface segregation of the PMMA occurs on top of the PS under-layer.[87] However, owing to the negative spreading coefficient, PMMA over the PS layer is unstable, and thus, pits were formed. The square root diameter with respect to film thickness was found to exhibit linear variation. On the contrary, granular domains were formed when the PMMA concentration was higher in the blend than PS. The size of the granules was found to increase with the increase in the PMMA concentration in the blend.[88]

2.2.2.8 Mechanism of morphology formation during spin coating

Heriot and Jones used time-resolved small-angle light scattering during spin coating to propose the mechanism of vertical phase separation in thin polymer blend films. The polymers used were PS, and PMMA dissolved in toluene spun coated over a silicon wafer. A drop of solution was dispensed over the wafer and was spun coated at 1500 rpm for 20 s. Simultaneously, a laser (633 nm) was focussed over the system at an angle of 40º. As the spun coating progresses, the thickness of the dispensed liquid decreases, and at a certain critical thickness, the polymer domains phase separate and layer stack parallel to the substrate, with one polymer-forming an unstable stratified layer over another. A further decrease in the thickness makes the polymer-polymer interface unstable and marks the manifestation of the capillary waves. These capillary

waves are further amplified, and in the later stages, when the polymer-polymer interface meets the air-polymer interface the stratified layer breaks and give rise to phase separated structures vertically.[89]

2.2.2.9 Ordering of phase-separated structures

Like in the case of dewetting, phase-separated domains are randomly oriented over the sample. To overcome this difficulty, a synergistic approach is often utilized such that phase separated domains are aligned by using conventional lithographic processes. Some of the earlier reported techniques are discussed as follows:

In nano imprint lithography (NIL), a pre-patterned mould is placed over the polymeric film, and pattern transfer occurs when the system is annealed at an elevated temperature. In some variation, UV-assisted-NIL has also been reported.[90,91] Wang et al. demonstrated that highly ordered domains could be generated by the application of NIL and phase separation in PS/PMMA blend films.[92] Capillary force lithography (CFL) is a variant of conventional NIL. Unlike in NIL, patterning using CFL requires low pressure.[93] Liu et al. proposed a method in which capillary force lithography was used to create orderly arrangements of phase separation domains.[94] Dip pen lithography can also be used to generate highly ordered phase separated structures.[95] The orderly arrangement of phase separated domains can also be created using a pre-patterned substrate. Chen et al. used topographically patterned silicon wafers to create highly ordered patterns when the PS and PMMA phases separate over the pre-patterned silicon wafer.[96] Interestingly, orderly arrangements of phase separated domains can also be formed by using pre-pattered PDMS stamps as substrates.[97] Controlled evaporation of solvent and phase separation in blend using a Sphere on flat geometry can also be used to create the hierarchical arrangement of domains over silicon wafer.[98] The above

mentioned techniques and concepts associated with those techniques are used to design the methodologies and experiments in the present thesis.

REFERENCES

[1] A. del Campo, E. Arzt, Fabrication approaches for generating complex micro- and nanopatterns on polymeric surfaces, Chem. Rev. 108 (2008) 911–945. https://doi.org/10.1021/cr050018y.

[2] A.A. Tseng, K. Chen, C.D. Chen, K.J. Ma, Electron beam lithography in nanoscale fabrication: Recent development, IEEE Trans. Electron. Packag. Manuf. 26 (2003) 141–149. https://doi.org/10.1109/TEPM.2003.817714.

[3] S. Ma, C. Con, M. Yavuz, B. Cui, Polystyrene negative resist for high-resolution electron beam lithography, Nanoscale Res. Lett. 6 (2011) 1–6. https://doi.org/10.1186/1556-276X-6-446.

[4] A. Verma, A. Sharma, Self-organized nano-lens arrays by intensified dewetting of electron beam modified polymer thin-films, Soft Matter. 7 (2011) 11119–11124. https://doi.org/10.1039/c1sm06229h.

[5] A. Verma, A. Sharma, Enhanced self-organized dewetting of ultrathin polymer films under water-organic solutions: fabrication of sub-micrometer spherical lens arrays., Adv. Mater. 22 (2010) 5306–5309. https://doi.org/10.1002/adma.201002768.

[6] A. Verma, A. Sharma, G.U. Kulkarni, Ultrafast large-area micropattern generation in nonabsorbing polymer thin films by pulsed laser diffraction, Small. 7 (2011) 758–765. https://doi.org/10.1002/smll.201001939.

[7] A. Verma, A. Sharma, Sub-40 nm polymer dot arrays by self-organized dewetting of

electron beam treated ultrathin polymer films, RSC Adv. 2 (2012) 2247–2249. https://doi.org/10.1039/c2ra00956k.

[8] A. Verma, A. Sharma, Submicrometer pattern fabrication by intensification of instability in ultrathin polymer films under a water-solvent mix, Macromolecules. 44 (2011) 4928–4935. https://doi.org/10.1021/ma200113w.

[9] D. Mijatovic, J.C.T. Eijkel, A. van den Berg, Technologies for nanofluidic systems: top-down vs. bottom-up—a review, Lab Chip. 5 (2005) 492–500. https://doi.org/10.1039/b416951d.

[10] A. Biswas, I.S. Bayer, A.S. Biris, T. Wang, E. Dervishi, F. Faupel, Advances in top-down and bottom-up surface nanofabrication: Techniques, applications & future prospects, Adv. Colloid Interface Sci. 170 (2012) 2–27. https://doi.org/10.1016/j.cis.2011.11.001.

[11] K. Tanaka, A. Taura, S.R. Ge, A. Takahara, T. Kajiyama, Molecular weight dependence of surface dynamic viscoelastic properties for the monodisperse polystyrene film, Macromolecules. 29 (1996) 3040–3042. https://doi.org/10.1021/ma951378y.

[12] K. Tanaka, A. Takahara, T. Kajiyama, Effect of polydispersity on surface molecular motion of polystyrene films, Macromolecules. 30 (1997) 6626–6632. https://doi.org/10.1021/ma970057e.

[13] O.K.C. Tsui, H.F. Zhang, Effects of chain ends and chain entanglement on the glass transition temperature of polymer thin films, Macromolecules. 34 (2001) 9139–9142. https://doi.org/10.1021/ma0102159.

[14] Y. Grohens, L. Hamon, G. Reiter, A. Soldera, Y. Holl, Some relevant parameters affecting the glass transition of supported ultra-thin polymer films, Eur. Phys. J. E. 8

(2002) 217–224. https://doi.org/10.1140/epje/i2001-10088-4.

[15] J. Liu, X. Yu, L. Xue, Y. Han, Polymer Morphology Principles, Characterization and Processing, John Wiley & Sons, Inc., Hoboken, New Jersey, 2016.

[16] R. Seemann, S. Herminghaus, K. Jacobs, Dewetting patterns and molecular forces: A reconciliation, Phys. Rev. Lett. 86 (2001) 5534–5537. https://doi.org/10.1103/PhysRevLett.86.5534.

[17] U. Thiele, M.G. Velarde, K. Neuffer, Dewetting: Film rupture by nucleation in the spinodal regime, Phys. Rev. Lett. 87 (2001) 016104/1-016104/4. https://doi.org/10.1103/physrevlett.87.016104.

[18] R. Verma, A. Sharma, Defect sensitivity in instability and dewetting of thin liquid films: Two regimes of spinodal dewetting, Ind. Eng. Chem. Res. 46 (2007) 3108–3118. https://doi.org/10.1021/ie060615q.

[19] R. Xie, A. Karim, J.F. Douglas, C.C. Han, R.A. Weiss, Spinodal dewetting of thin polymer films, Phys. Rev. Lett. 81 (1998) 1251–1254. https://doi.org/10.1103/PhysRevLett.81.1251.

[20] T.G. Stange, D.F. Evans, W.A. Hendrickson, Nucleation and growth of defects leading to dewetting of thin polymer films, Langmuir. 13 (1997) 4459–4465. https://doi.org/10.1021/la962090k.

[21] G. Reiter, Dewetting of Thin Polymer Films, Phys. Rev. Lett. 68 (1992) 75–80.

[22] A. Sharma, G. Reiter, Instability of thin polymer films on coated substrates: Rupture, dewetting, and drop formation, J. Colloid Interface Sci. 178 (1996) 383–399. https://doi.org/10.1006/jcis.1996.0133.

[23] K.M. Ashley, J.C. Meredith, E. Amis, D. Raghavan, A. Karim, Combinatorial investigation of dewetting: Polystyrene thin films on gradient hydrophilic surfaces, Polymer (Guildf). 44 (2002) 769–772. https://doi.org/10.1016/S0032-3861(02)00779-6.

[24] R.A.L. Jones, The dynamics of thin polymer films, Curr. Opin. Colloid Interface Sci. 4 (1999) 153–158. https://doi.org/10.1016/S1359-0294(99)00025-4.

[25] A. Oron, S.H. Davis, S.G. Bankoff, Long-scale evolution of thin liquid films, Rev. Mod. Phys. 69 (1997) 931–980. https://doi.org/10.1103/revmodphys.69.931.

[26] G. Krausch, Surface induced self assembly in thin polymer films, Mater. Sci. Eng. R. 14 (1995) 5–6. https://doi.org/10.1016/0927-796X(94)00173-1.

[27] K.R. Shull, T.E. Karis, Dewetting Dynamics for Large Equilibrium Contact Angles, (1994) 334–339.

[28] G. Reiter, Dewetting of Thin Polymer Films, Phys. Rev. Lett. 68 (1992) 75–78.

[29] M.D. Morariu, E. Schäffer, U. Steiner, Molecular forces caused by the confinement of thermal noise, Phys. Rev. Lett. 92 (2004) 14–17. https://doi.org/10.1103/PhysRevLett.92.156102.

[30] D. Chen, H. Handa, L. Wan, G. Mao, Surface morphological evolution of ultrathin P4VP films and generation of ordered patterns on graphite, Macromol. Rapid Commun. 28 (2007) 1619–1623. https://doi.org/10.1002/marc.200700342.

[31] C. Redon, F. Brochard-Wyart, F. Rondelez, Dynamics of Dewetting, Phys. Rev. Lett. 66 (1991).

[32] M.W.J. Van Der Wielen, M.A.C. Stuart, G.J. Fleer, Autophobicity and Layering

Behavior of Thin Liquid-Crystalline Polymer Films, 66 (1998) 7065–7071.

[33] B. Ravi, R. Mukherjee, D. Bandyopadhyay, Solvent vapour mediated spontaneous healing of self-organized defects of liquid crystal film, Soft Matter. 11 (2015) 139–146. https://doi.org/10.1039/c4sm02111h.

[34] G. Reiter, Unstable Thin Polymer Films: Rupture and Dewetting Processes, Langmuir. 9 (1993) 1344–1351. https://doi.org/10.1021/la00029a031.

[35] R. Fetzer, M. Rauscher, R. Seemann, K. Jacobs, K. Mecke, Thermal noise influences fluid flow in thin films during spinodal dewetting, Phys. Rev. Lett. 99 (2007) 1–4. https://doi.org/10.1103/PhysRevLett.99.114503.

[36] R. Mukherjee, M. Gonuguntla, A. Sharma, Meso-patterning of thin polymer films by controlled dewetting: From nano-droplet arrays to membranes, J. Nanosci. Nanotechnol. 7 (2007) 2069–2075. https://doi.org/10.1166/jnn.2007.771.

[37] S.H. Lee, P.J. Yoo, S.J. Kwon, H.H. Lee, Solvent-driven dewetting and rim instability, J. Chem. Phys. 121 (2004) 4346–4351. https://doi.org/10.1063/1.1770475.

[38] L. Xue, Y. Han, Autophobic dewetting of a poly(methyl methacrylate) thin film on a silicon wafer treated in good solvent vapor, Langmuir. 25 (2009) 5135–5140. https://doi.org/10.1021/la8041814.

[39] N.H. Frick, H.L. Gerhart, H.E. Gilbert, E.E. Parker, Polymer Coatings, 1969. https://doi.org/10.1021/ie50716a010.

[40] S. Roy, K.J. Ansari, S.S.K. Jampa, P. Vutukuri, R. Mukherjee, Influence of substrate wettability on the morphology of thin polymer films spin-coated on topographically patterned substrates, ACS Appl. Mater. Interfaces. 4 (2012) 1887–1896.

https://doi.org/10.1021/am300201a.

[41] N. Rehse, C. Wang, M. Hund, M. Geoghegan, R. Magerle, G. Krausch, Stability of thin polymer films on a corrugated substrate, Eur. Phys. J. E. 4 (2001) 69–76. https://doi.org/10.1007/s101890170144.

[42] M. Geoghegan, C. Wang, N. Rehse, R. Magerle, G. Krausch, Thin polymer films on chemically patterned, corrugated substrates, J. Phys. Condens. Matter. 17 (2005). https://doi.org/10.1088/0953-8984/17/9/007.

[43] A. Sehgal, D. Bandyopadhyay, K. Kargupta, A. Sharma, A. Karim, From finite-amplitude equilibrium structures to dewetting in thin polymer films on chemically patterned substrates, Soft Matter. 8 (2012) 10394–10402. https://doi.org/10.1039/c2sm26369f.

[44] K. Kargupta, A. Sharma, Creation of ordered patterns by dewetting of thin films on homogeneous and heterogeneous substrates, J. Colloid Interface Sci. 245 (2002) 99–115. https://doi.org/10.1006/jcis.2001.7860.

[45] A.M. Higgins, R.A.L. Jones, Anisotropic spinodal dewetting as a mute to self-assembly of patterned surfaces, Nature. 404 (2000) 476–478. https://doi.org/10.1038/35006597.

[46] X. Zhang, F. Xie, O.K.C. Tsui, Microscopic surface patterning by rubbing induced dewetting, Polymer (Guildf). 46 (2005) 8416–8421. https://doi.org/10.1016/j.polymer.2005.06.066.

[47] R. Mukherjee, A. Sharma, G. Patil, D. Faruqui, P.S.G. Pattader, Soft lithography meets self-organization: Some new developments in meso-patterning, Bull. Mater. Sci. 31 (2008) 249–261. https://doi.org/10.1007/s12034-008-0043-z.

[48] S. Roy, K.J. Ansari, S.S.K. Jampa, P. Vutukuri, R. Mukherjee, Influence of substrate wettability on the morphology of thin polymer films spin-coated on topographically patterned substrates, ACS Appl. Mater. Interfaces. 4 (2012) 1887–1896. https://doi.org/10.1021/am300201a.

[49] B. Yoon, H. Acharya, G. Lee, H.C. Kim, J. Huh, C. Park, Nanopatterning of thin polymer films by controlled dewetting on a topographic pre-pattern, Soft Matter. 4 (2008) 1467–1472. https://doi.org/10.1039/b800121a.

[50] B. Yoon, H. Acharya, G. Lee, H.C. Kim, J. Huh, C. Park, Nanopatterning of thin polymer films by controlled dewetting on a topographic pre-pattern, Soft Matter. 4 (2008) 1467–1472. https://doi.org/10.1039/b800121a.

[51] R. Mukherjee, D. Bandyopadhyay, A. Sharma, Control of morphology in pattern directed dewetting of thin polymer films, Soft Matter. 4 (2008) 2086–2097. https://doi.org/10.1039/b806925e.

[52] K. Kargupta, A. Sharma, Morphological self-organization by dewetting in thin films on chemically patterned substrates, J. Chem. Phys. 116 (2002) 3042–3051. https://doi.org/10.1063/1.1434949.

[53] N. Bhandaru, A. Das, N. Salunke, R. Mukherjee, Ordered alternating binary polymer nanodroplet array by sequential spin dewetting, Nano Lett. 14 (2014) 7009–7016. https://doi.org/10.1021/nl5033205.

[54] Z. Xin, B. Su, J. Wang, X. Zhang, Z. Zhang, M. Deng, Y. Song, L. Jiang, Continuous microwire patterns dominated by controllable rupture of liquid films, Small. 9 (2013) 722–726. https://doi.org/10.1002/smll.201202515.

[55] K. Kargupta, A. Sharma, Dewetting of Thin Films on Periodic Physically and

Chemically Patterned Surfaces, (2002) 1893–1903.

[56] K. Kargupta, A. Sharma, Templating of thin films induced by dewetting on patterned surfaces, Phys. Rev. Lett. 86 (2001) 4536–4539. https://doi.org/10.1103/PhysRevLett.86.4536.

[57] A. Sehgal, V. Ferreiro, J.F. Douglas, E.J. Amis, A. Karim, Pattern-directed dewetting of ultrathin polymer films, Langmuir. 18 (2002) 7041–7048. https://doi.org/10.1021/la020180l.

[58] A. Sehgal, D. Bandyopadhyay, K. Kargupta, A. Sharma, A. Karim, From finite-amplitude equilibrium structures to dewetting in thin polymer films on chemically patterned substrates, Soft Matter. 8 (2012) 10394–10402. https://doi.org/10.1039/c2sm26369f.

[59] B. Ravi, S. Chakraborty, M. Bhattacharjee, S. Mitra, A. Ghosh, P.S.G. Pattader, D. Bandyopadhyay, Pattern Directed Ordering of Spin-dewetted Liquid Crystal Micro or Nanodroplets as Pixelated Light Reflectors and Locomotives Pattern Directed Ordering of Spin-dewetted Liquid Crystal Micro or Nanodroplets as Pixelated Light Reflectors and Locomotives, Appl. Mater. Interfaces. 9 (2017) 1066–1076. https://doi.org/10.1021/acsami.6b12182.

[60] K. Kargupta, A. Sharma, Dewetting of thin films on periodic physically and chemically patterned surfaces, Langmuir. 18 (2002) 1893–1903. https://doi.org/10.1021/la010469n.

[61] K. Kargupta, A. Sharma, Mesopatterning of thin liquid films by templating on chemically patterned complex substrates, Langmuir. 19 (2003) 5153–5163. https://doi.org/10.1021/la026634w.

[62] K. Kargupta, R. Konnur, A. Sharma, Instability and pattern formation in thin liquid films on chemically heterogeneous substrates, Langmuir. 16 (2000) 10243–10253. https://doi.org/10.1021/la000759o.

[63] M. Stepanova, S. Dew, Nanofabrication: Techniques and principles, 2014. https://doi.org/10.1007/978-3-7091-0424-8.

[64] A. Verma, S. Sekhar, P. Sachan, P.D.S. Reddy, A. Sharma, Control of morphologies and length scales in intensified dewetting of electron beam modified polymer thin films under a liquid solvent mixture, Macromolecules. 48 (2015) 3318–3326. https://doi.org/10.1021/acs.macromol.5b00029.

[65] A. Verma, A. Sharma, Self-organized nano-lens arrays by intensified dewetting of electron beam modified polymer thin-films, Soft Matter. 7 (2011) 11119–11124. https://doi.org/10.1039/c1sm06229h.

[66] A. Verma, A. Sharma, Enhanced self-organized dewetting of ultrathin polymer films under water-organic solutions: fabrication of sub-micrometer spherical lens arrays., Adv. Mater. 22 (2010) 5306–5309. https://doi.org/10.1002/adma.201002768.

[67] P. Mokarian-Tabari, Controlling the Morphology of Spin coated Polymer Blend Films, The University of Sheffield, 2009.

[68] L. Xue, J. Zhang, Y. Han, Phase separation induced ordered patterns in thin polymer blend films, Prog. Polym. Sci. 37 (2012) 564–594. https://doi.org/10.1016/j.progpolymsci.2011.09.001.

[69] P.J. Flory, Themodynamics of high polymer solutions, J. Chem. Phys. 10 (1942) 51–61. https://doi.org/10.1063/1.1723621.

[70] L. Huggins, Theory of Solutions of High Polymers, J. Am. Chem. Soc. 417 (1942) 1712–1719.

[71] L. Robeson, Historical perspective of advances in the science and technology of polymer blends, Polymers (Basel). 6 (2014) 1251–1265. https://doi.org/10.3390/polym6051251.

[72] E. Manias, L.A. Utracki, Polymer Blends Handbook, Second, Springer, 2014.

[73] P. Müller-Buschbaum, J.S. Gutmann, M. Wolkenhauer, J. Kraus, M. Stamm, D. Smilgies, W. Petry, Solvent-induced surface morphology of thin polymer films, Macromolecules. 34 (2001) 1369–1375. https://doi.org/10.1021/ma0009193.

[74] P. Mokarian-Tabari, M. Geoghegan, J.R. Howse, S.Y. Heriot, R.L. Thompson, R.A.L. Jones, Quantitative evaluation of evaporation rate during spin-coating of polymer blend films: Control of film structure through defined-atmosphere solvent-casting, Eur. Phys. J. E. 33 (2010) 283–289. https://doi.org/10.1140/epje/i2010-10670-7.

[75] H. Ogawa, T. Kanaya, K. Nishida, G. Matsuba, Phase separation and dewetting in polystyrene/poly(vinyl methyl ether) blend thin films in a wide thickness range, Polymer (Guildf). 49 (2008) 254–262. https://doi.org/10.1016/j.polymer.2007.11.031.

[76] S. Walheim, M. Böltau, J. Mlynek, G. Krausch, U. Steiner, Structure formation via polymer demixing in spin-cast films, Macromolecules. 30 (1997) 4995–5003. https://doi.org/10.1021/ma9619288.

[77] S. Reich, Y. Cohen, Phase Separation of Polymer Blends in Thin Films., J. Polym. Sci. Part A-2, Polym. Phys. 19 (1981) 1255–1267.

[78] K. Tanaka, A. Takahara, T. Kajiyama, Surface molecular aggregation structure and surface molecular motions of high-molecular-weight polystyrene/low-molecular-weight

poly(methyl methacrylate) blend films, Macromolecules. 31 (1998) 863–869. https://doi.org/10.1021/ma9709866.

[79] X. Li, Y. Han, L. An, Surface morphology control of immiscible polymer-blend thin films, Polymer (Guildf). 44 (2003) 8155–8165. https://doi.org/10.1016/j.polymer.2003.10.012.

[80] C. Ton-That, A.G. Shard, R. Daley, R.H. Bradley, Effects of annealing on the surface composition and morphology of PS/PMMA blend, Macromolecules. 33 (2000) 8453–8459. https://doi.org/10.1021/ma000792h.

[81] X. Li, Y. Han, L. An, Annealing effects on the surface morphologies of thin PS/PMMA blend films with different film thickness, Appl. Surf. Sci. 230 (2004) 115–124. https://doi.org/10.1016/j.apsusc.2004.02.046.

[82] X. Rui, Z. Song, S. Jing, T. Decheng, Phase separation and dewetting induced surface pattern in PS/PMMA blend films, Polym. J. 37 (2005) 560–564. https://doi.org/10.1295/polymj.37.560.

[83] S. Zhang, T. Shi, J. You, Y. Li, Solvent annealing induced phase separation and dewetting in PMMA/SAN blend films: Composition dependence, Polym. Chem. 4 (2013) 3943–3948. https://doi.org/10.1039/c3py00290j.

[84] J. You, S. Zhang, G. Huang, T. Shi, Y. Li, Solvent annealing induced phase separation and dewetting in PMMA/SAN blend film: Film thickness and solvent dependence, J. Chem. Phys. 138 (2013) 1–8. https://doi.org/10.1063/1.4811471.

[85] S. Roy, A. Sharma, Self-organized morphological evolution and dewetting in solvent vapor annealing of spin coated polymer blend nanostructures, J. Colloid Interface Sci. 449 (2015) 215–225. https://doi.org/10.1016/j.jcis.2014.12.095.

[86] C. Ton-That, A.G. Shard, D.O.H. Teare, R.H. Bradley, XPS and AFM surface studies of solvent-cast PS/PMMA blends, Polymer (Guildf). 42 (2001) 1121–1129. https://doi.org/10.1016/S0032-3861(00)00448-1.

[87] C. Ton-That, A.G. Shard, R. Daley, R.H. Bradley, Effects of annealing on the surface composition and morphology of PS/PMMA blend, Macromolecules. 33 (2000) 8453–8459. https://doi.org/10.1021/ma000792h.

[88] C. Ton-That, A.G. Shard, R.H. Bradley, Surface feature size of spin cast PS/PMMA blends, Polymer (Guildf). 43 (2002) 4973–4977. https://doi.org/10.1016/S0032-3861(02)00333-6.

[89] S.Y. Heriot, R.A.L. Jones, An interfacial instability in a transient wetting layer leads to lateral phase separation in thin spin-cast polymer-blend films, Nat. Mater. 4 (2005) 782–786. https://doi.org/10.1038/nmat1476.

[90] S. Chou, Nanoimprint lithography, Technol. Rev. 106 (2003) 42. https://doi.org/10.1116/1.588605.

[91] H. Schift, Nanoimprint lithography: An old story in modern times? A review, J. Vac. Sci. Technol. B Microelectron. Nanom. Struct. 26 (2008) 458. https://doi.org/10.1116/1.2890972.

[92] Z. Wang, D.U. Ahn, Y. Ding, Topographically uniform but chemically heterogeneous nanostructures by nanoimprinting demixed polymer blends, Langmuir. 26 (2010) 14909–14914. https://doi.org/10.1021/la102523t.

[93] D. Ho, J. Zou, B. Zdyrko, K.S. Iyer, I. Luzinov, Capillary force lithography: The versatility of this facile approach in developing nanoscale applications, Nanoscale. 7 (2015) 401–414. https://doi.org/10.1039/c4nr03565h.

[94] X. Liu, N. Bhandaru, M. Banik, X. Wang, A.M. Al-Enizi, A. Karim, R. Mukherjee, Capillary Force Lithography Pattern-Directed Self-Assembly (CFL-PDSA) of Phase-Separating Polymer Blend Thin Films, ACS Omega. 3 (2018) 2161–2168. https://doi.org/10.1021/acsomega.7b02078.

[95] D.C. Coffey, D.S. Ginger, Patterning Phase Separation in Polymer Films with Dip-Pen Nanolithography, J. Am. Chem. Soc. 69 (2004) 4564. https://doi.org/10.1063/1.347325.

[96] X.C. Chen, H.M. Li, F. Fang, Y.W. Wu, M. Wang, G. Bin Ma, Y.Q. Ma, D.J. Shu, R.W. Peng, Confinement-induced ordering in dewetting and phase separation of polymer blend films, Adv. Mater. 24 (2012) 2637–2641. https://doi.org/10.1002/adma.201200089.

[97] N. Bhandaru, A. Karim, R. Mukherjee, Directed ordering of phase separated domains and dewetting of thin polymer blend films on a topographically patterned substrate, Soft Matter. 13 (2017) 4709–4719. https://doi.org/10.1039/c7sm00799j.

[98] M. Byun, S.W. Hong, F. Qiu, Q. Zou, Z. Lin, Evaporative organization of hierarchically structured polymer blend rings, Macromolecules. 41 (2008) 9312–9317. https://doi.org/10.1021/ma801864n.

CHAPTER 2

Chapter 2

Effect of Labile Underlayer on the Morphology of Thermally Annealed Polymer Blend

GRAPHICAL ABSTRACT

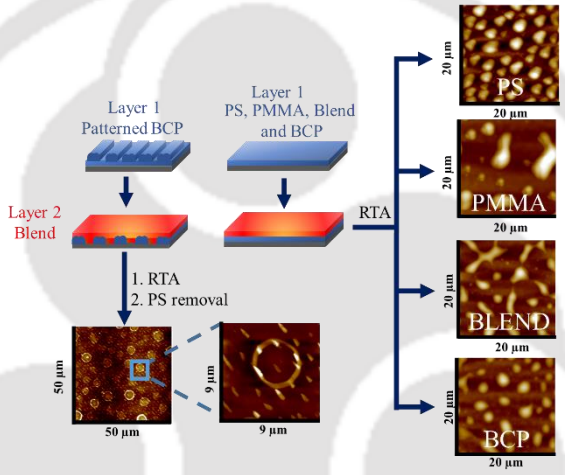

ABSTRACT

Microphase separation in a thin film of a polymer blend leads to interesting patterns on different substrates. The plethora of studies in this field discussed the effect of the surface energy of the underlying tethered polymer brush or substrate on the final morphology of the polymer blend. The conventional process toward the final morphology is relatively slow. Here, aiming the fast lithography, we induce the kinetically driven morphological evolution by rapid thermal annealing (RTA) of the polymer blend of polystyrene (PS) and polymethylmethacrylate (PMMA) in bilayer settings at a very high temperature. The underlying film consists of untethered constituent homopolymers or their blend or random-co-polymer (RCP). Apart from the phase inversion of the blend on PS homopolymer, a rich morphology of the blend on RCP underlayer is uncovered with the systematic investigation of the film using sequential washing with selective solvents. The dissolution characteristics and the thermal stability of the constituent polymers corroborated the observation. Based on the understanding of the morphological evolution, fabrication of a complex shaped micro/nanopattern with multiple length scales is demonstrated using a blend/RCP system. This study shows a novel methodology for easy fabrication of hierarchical small length scale complex structure.

Keywords: *Thin Film Instability, Rapid Thermal Annealing, Polymer Blend, Random-co-polymer, Hierarchical patterns.*

1. INTRODUCTION

On-demand alteration of the surface properties of a given surface using small scale structured polymeric domains finds a broad spectrum of interdisciplinary applications such as fabrications of robust membrane materials,[1–5] highly ordered magnetic bit pattern media,[6,7] bio-inspired super-hydrophobic and self-cleaning surfaces,[8–13] anti-reflection coatings,[14,15] negative refractive index materials[16] etc. Fabrication of micro/nanoscale morphology involves different techniques such as photolithography,[17] e-beam lithography,[18,19] reactive ion etching (RIE),[20] vapour deposition methods,[21] nanoimprint lithography (NIL),[22–24] micro-contact printing (μCP),[25–28] elastic contact lithography (ECL),[29] electric field-induced pattern generation,[30–35] dewetting of polymer films,[36–39] phase separation mediated pattern generation,[40–42] etc.

Self-assembly in polymer blend and block copolymer thin films has gained attraction in the last few decades due to its scientific and technological importance in the fabrication of micro-nano structures. The blend polymer solution contains two or more dissimilar polymers in the form of a physical homogeneous mixture in a common solvent. In random copolymers (RCP), the two or more dissimilar polymers blocks of random chain lengths are chemically bonded to each other. Owing to the differences in their chemical and physical properties, the respective polymers of the blend or RCP blocks tend to form segregation into micro/nano phases.

The thermodynamics of the blend system dictates the phase separation of the polymer blend. Upon altering the conditions like temperature, pressure or compositions, the system can be forced to move from single phase to metastable or to the two phase spinodal regime. Metastable regime involves slow nucleation followed by growth of phase-separated domains. However, in spinodal decomposition, phase separation starts with instantaneous density

fluctuations of segments that progressively increase in amplitude and wavelengths in later stages, resulting in coarser phase-separated domains.[43]

In this respect, the phase separation in microdomains is somewhat restricted in the case of RCP compared to the blend due to the presence of covalent bonds between two different polymer blocks in RCP. Nevertheless, rich morphology, such as a stratified layer, horizontal or vertical cylinders, gyroid[41] etc., can be obtained using blend and block copolymers depending on their mole fraction, solvent /temperature used for annealing[44,45] etc. The phase separation of a polymer blend or RCP within a thin film over a substrate is a complex process and is influenced by various parameters such as solubility, Flory-Huggins parameter, molecular weights, mobility, evaporation of the solvent, which is associated with viscosity and concentration of the components, the thickness of the film[40] etc. The formation of nanoscale structures using blend polymers is thus challenging and provides a controlling handle to tune the morphology. One can obtain diverse morphology by varying the volume fraction as well as the substrate characteristics.[46]

The polymer-polymer phase separation in a thin film is quite different from a bulk phase separation and strongly affected by the film thickness. As the film thickness reduces, the characteristic length scale of spinodal decomposition decreases, and at film thickness less than ~ 200 nm, the film dewets with spinodal length scale.[47] The final morphology obtained is far from thermodynamic equilibrium and is often governed by the kinetics of the process. Demixing of a spin-cast polymer blend can be attributed to different substrate preferences of the component polymers and the different solubility of them in the common solvent.[48,49] Mansky et al. showed that the PS wets over a grafted PS-r-PMMA brush if the fraction of the Styrene is more than ~ 0.7 in the tethered brush.[50] The interfacial energy difference, $\Delta\gamma = \gamma_{PS-brush} - \gamma_{PMMA-brush} \approx 0$ when the fraction of Styrene in the tethered brush is ~ 0.6 that

renders the surface neutral to both PS and PMMA. Here, $\gamma_{PS-brush}$ ($\gamma_{PMMA-brush}$) represent the interfacial energy between PS (PMMA) and the grafted PS-r-PMMA brush.

In view of the above discussion, here in this article, we have investigated the morphological evolution of PS/PMMA blend on an untethered labile polymer (PS, PMMA, PS/PMMA blend, and PS-r-PMMA copolymer) layer of different thicknesses. To achieve the fast patterning of polymer in contrast to the conventional thermal dewetting, the non-equilibrium kinetics of morphological evolution is probed for a relatively short duration (~12-15 min) to attain a high temperature of ~ 300°C called rapid thermal annealing (RTA). The chapter is organized as follows: after the experimental procedure described in the next section, the results and discussion section begins with few characterizations of the process parameters, which are crucial to validate the results. Then the morphological evolutions of as cast and annealed polymer blends over different polymer settings are discussed. Next, based on the findings, the fabrication of complex hierarchical patterns is demonstrated. Lastly, concluding remarks are offered with the future direction of this study.

2. MATERIALS AND METHODS

2.1 Preparation of polymer solutions

A homogeneous 1 % (by wt.) solution of random copolymer PS-r-PMMA (Sigma Aldrich, average Mw 1,00,000-1,50,000, styrene 40 mol %) was prepared by dissolving the polymer in toluene. Likewise, the 1% solutions of PS (Sigma Aldrich, Mw = 1,92,000) and PMMA (Sigma Aldrich, Mw = 1,20,000) were prepared in toluene (Sigma Aldrich). In order to prepare a homogeneous blend of PS-PMMA, separate solutions of PS (1% wt.) and PMMA (1% wt.) in toluene were prepared and mixed thoroughly with PS : PMMA :: 40 : 60 volume ratio.

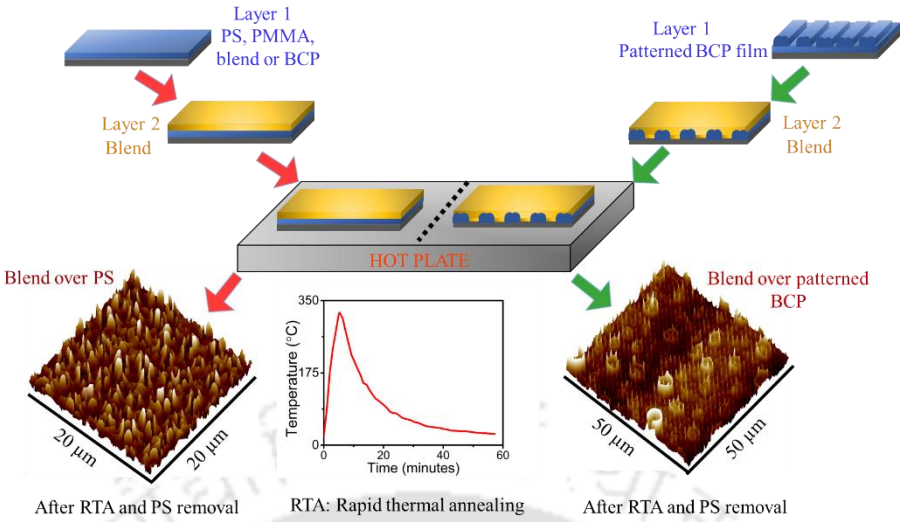

***Figure 2.1**. The schematic depicts the protocol adopted for the study of phase separation over different types of the polymer layer.*

2.2 Preparation of polymer thin film

A polymer solution was spin-coated at 5000 rpm for 2 min over cleaned silicon wafers of 1 cm x 1 cm dimensions. Before spin coating, the silicon wafers (<100>) were cleaned using Piranha solution consisting of H_2SO_4 and H_2O_2 in the volume ratio of 80:20. The prepared films were left at room temperature for 12 h in a vacuum desiccator to remove the excess solvent. This will serve as the underlayer thin film. Subsequently, the second layer of the polymer was spin-coated over the first layer at 2500 rpm for 2 min. **Table 2.1** shows the concentrations of polymer used to prepare the films, and corresponding film thicknesses are reported.

2.3 Rapid Thermal Annealing (RTA)

All the bilayer systems were thermally annealed by raising the temperature rapidly up to 300 °C on a hot plate. When the 300°C is attained, the system was allowed to remain at that temperature for 30 s and thereafter, cooled down by natural convection to room temperature of 23°C.

The temperature profile was monitored using an IR thermometer (Fluke 59 MAX, 650 nm laser). The complete process is shown in **Figure 2.1**. Here one point to note that the during RTA, the polymer films remain above its glass transition temperatures (~ 100°C for PS and ~ 105°C for PMMA) for about ~ 12-15 min. This time frame is not sufficient to achieve the thermodynamic equilibrium state, even though the maximum temperature is much higher than the glass transition temperature of the polymer. This study is aiming given the smaller time window, how the morphological variation took place for different underlayer settings so that it can be implemented as a faster patterning tool. Moreover, there is a possibility of considerable thermal degradation if the temperature is maintained at high temperature for longer duration.

2.4 Preferential dissolution of polymer

The RTA allowed polymer chains to self-organize and PS / PMMA segregate to form microdomains. To get an insight into the self-organization mechanism after RTA, selective solvent etching of the sample was performed. In this process, the polymer thin film of PS/PMMA blend and/or RCP was immersed in a solvent that selectively removes only one of the component polymers present, keeping another polymer structure intact. Here we used acetic acid to wash away PMMA domains and cyclohexane for the removal of the PS regime. The immersion was carried out in 25 ml of appropriate solvent for 5 min without any stirring or sonication. For samples with hierarchical patterns (discussed later), the immersion time was 10 min. After immersion, a slow stream of nitrogen was used to remove residual solvent from the samples. Subsequently, the samples were vacuum dried at 60°C for 6 h.

2.5 Preparation of complex multiscale structures

For the complex pattern, 1% solution of PS-r-PMMA RCP was spun coat (spin speed was maintained at 5000 rpm for 2 min) over a clean Si wafer. The film thickness of 48 nm was confirmed by ellipsometric measurement. A structured aluminium foil was peeled off from a

compact disk (CD) to use it as a flexible stamp with alternate lines of grooves and crests with periodicity, width and height of about 1.6 µm, 800 nm and 120 nm respectively.[51] This flexible CD foil was carefully placed on the thin RCP film prepared and sandwiched between two glass slides with the help of a pair of binder clips to induce uniform pressure. The whole set up then heated over 120°C for 12 h to induce capillary force lithography (CFL). The film then cooled down to room temperature, and the foil was removed carefully. Based on the thickness of the film and the intensity of the applied pressure, different types such as inverted "ω", "u" shaped or complete negative replica of the stamp can be achieved.[52] Over this patterned RCP film, PS-PMMA blend was coated at 2500 rpm for 2 min from 1% toluene solution.

2.6 Characterization

Surface morphology of the samples was analysed using atomic force microscopy (AFM, Bruker, Innova series) using sharp-edged antimony doped silicon tips (TESPA-V2, Bruker) having a resistivity of 0.01-0.025 Ohm-cm, frequency 320 kHz, and force constant 42 N/m. The scan rate was maintained at 0.7-0.8 Hz in tapping mode. Raman spectroscopy was performed using the Laser micro-Raman system (Horiba Scientific, LabRam HR evolution Raman spectrometer) using a 532 nm laser beam. Thermogravimetric (TGA) analysis was performed using TG 209 F1 Libra, Netzsch, Germany, with sample amount of about 10 mg and a heating rate of 10°C/min under nitrogen gas flow (purge: 40 mL/min, protective: 20 mL/min) in an alumina crucible. DSC was performed under nitrogen condition using DSC 3500 Sirius Netzsch, Germany. TGA was also performed in the aerial condition of the experiments and the results are shown in section S1 of the **Appendix 3**. The thickness of the composite bilayer films was measured using ellipsometer (EP3 Nanofilm, Accurion, Germany) with a Cauchy model for fitting the data.

***Table 2.1**: Film thickness obtained from ellipsometer (all the concentrations are in wt. %).*

S. No.	Under layer	Thickness (nm)	Upper layer	Total Thickness (nm) (under layer + upper layer)
1	0.5% PS	17.02 ± 0.28	1 % Blend#	*
2	0.5% PMMA	19.72 ± 0.11	1 % Blend#	96.48 ± 0.22
3	0.5 %Blend#	23.48 ± 0.55	1 % Blend#	95.74 ± 0.21
4	0.5% RCP	22.32 ± 0.13	1 % Blend#	97.89 ±0.16
5	1 % PS	53.6 ± 0.18	1 % Blend#	*
6	1 % PMMA	46.87 ± 0.26	1 % Blend#	120.16 ± 0.04
7	1 % Blend#	52.78 ± 0.47	1 % Blend#	120.25 ± 0.06
8	1 % RCP	48.82 ± 0.56	1 % Blend#	119.53 ± 0.13

*spin dewetted structures, # overall polymer concentration that includes both PS and PMMA.

3. RESULTS AND DISCUSSIONS

Before going on to describe the morphological evolution of the thin film in the bilayer polymer settings and the complex patterning, it is vital to discuss few parameters such as dissolution characteristics of the polymers, extent of degradation of the polymers due to RTA etc. which is relevant to this study and will be corroborated at the appropriate places.

3.1 Dissolution characteristics

A known amount of each polymer (PS, PMMA, and PS-r-PMMA) was taken in a specific amount of toluene, and the weight of the polymer was monitored with time. The solvent was decanted before each weight measurement, and the left-over polymer was dried in a vacuum desiccator. The percentage weight loss per ml of solvent was estimated, and the whole process was performed with and without stirring conditions. The dissolution characteristics (Figure 2.2) reveal that within 2 min the percentage dissolution of polymer is less than 1% per ml of pure toluene even in stirring conditions. This ensures that the dissolution of underlying polymer

thin film during the spin coating of the second layer is almost negligible, given that the polymer solution used during second spin coating is in the order of µl range, loaded with 1% polymer.

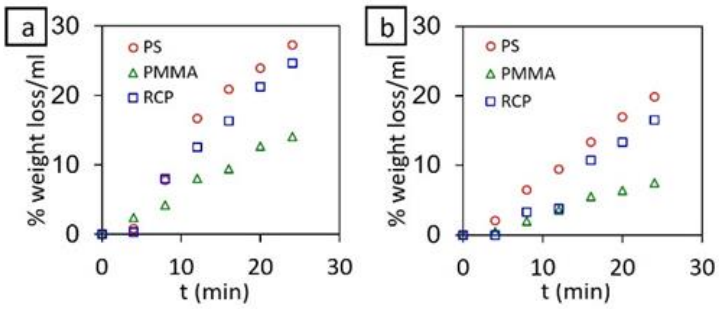

***Figure 2.2**. %weight loss/ml of toluene for PS, PMMA and PS-r-PMMA (RCP) (a) with stirring (b) without stirring. The error is significantly less in the experiment.*

3.2 Chemical stability of polymers

As the fast thermal dewetting process involves very high temperatures, it is essential to characterize the extent of polymer degradation due to RTA. To characterise this, Thermogravimetric analysis (TGA) and Raman spectroscopic study were performed on the polymer sample.

Thermogravimetric Analysis (TGA): Thermal stability of PS, PMMA and RCP was investigated by thermo-gravimetric analysis (TGA). TGA curves of all samples are shown in **Figure 2.3(a-c). Figure 2.3a** shows one-step decomposition for PS with onset temperature of ~ 350°C and end temperature of 430 ºC. In the case of PMMA, two prominent decomposition steps were observed with first mass loss of approx. 40% (from ~250°C to 310°C) and second mass loss of approx. 60% (from 310°C to 430°C). Degradation at ~ 270°C is attributed mainly due to the cleavage of the unsaturated ends primarily resulting from the disproportionate termination.[53,54] Degradation at higher temperatures is due to the random scissions of the main PMMA chain. RCP, On the other hand, showed a single decomposition step starting from 310°C to 410°C. Even though RCP possesses PS and PMMA components, a single

decomposition temperature of RCP is due to the strong covalent bond present between PS and PMMA domains. The TGA at the experimental condition also shows that the polymers are stable till 300 °C (see **Appendix 3**). DSC results are shown in **Figure 3.3(a-c)** also supports this observation.

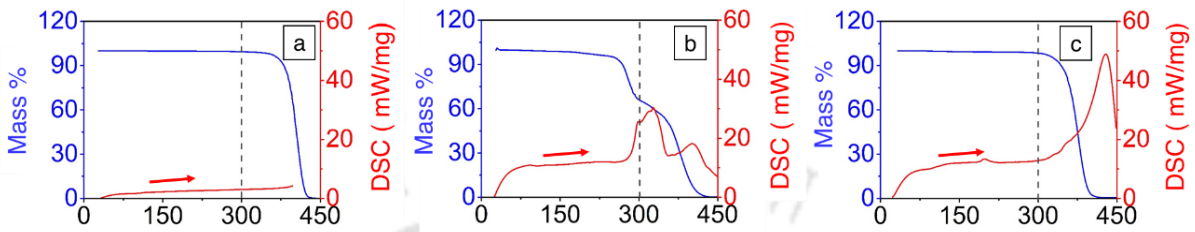

Figure 2.3*. TGA (blue line) and DSC (red line) for (a) PS (b) PMMA and (c) random PS-b-PMMA.*

RAMAN Spectroscopic Analysis: PS contains both aliphatic and aromatic C-H groups in its structure. The characteristic peaks of polystyrene were observed between 3200-2800 cm^{-1} in Raman spectra (**Figure 2.4a**). The peaks at 2900 cm^{-1} and 2852 cm^{-1} belongs to the tertiary CH stretching and CH_2 stretching respectively. The strong peak at 3050 cm^{-1} was attributed to C-H stretching of aromatic ring.[55,56] Raman spectra of PMMA displayed a broad band at 2952 cm^{-1} (**Figure 2.4b**). This band is attributed to CH stretching, which is the most prominent characteristic peak of PMMA.[57]It can be observed from Figure 4(a,b) that both PS and PMMA exhibited a reduced Raman intensity (a.u.) after RTA at the identical peak positions. **Figure 2.4c** shows the mixed characteristic peaks of PS and PMMA at 3050 cm^{-1} and 2952 cm^{-1}, respectively for RCP[58] and the peak positions and intensity did not change after thermal annealing due to the presence of strong covalent bonds among the individual polymer domains and it further confirmed the thermal stability of the polymers during RTA.

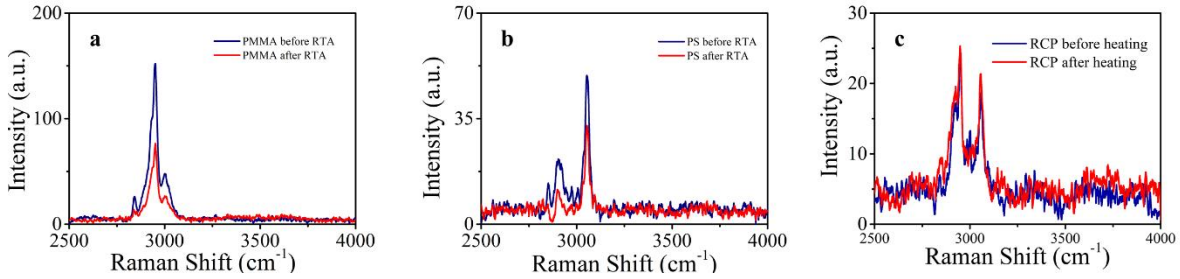

Figure2.4*. Raman Spectra for (a) PS (b) PMMA and (c) random PS-r-PMMA.*

3.3 Blend over PS underlayer

It is important to examine the morphology of the spun-cast film before thermal annealing, to check the stability of the bilayer film. First and second rows of **Figure 2.5** show the topography images from AFM at the different stages (as-cast, thermally annealed, acetic acid treated and cyclohexane treated) of PS/PMMA blend over the thin (~ 17 nm) and thick (~ 54 nm) PS film, respectively. It should be noted that before the spin coating of the second layer, the first PS layer was left for 12 h in a vacuum desiccator to remove the solvent from the film. During spin coating of the PS/PMMA blend solution (upper layer) over the dry PS film, there is a possibility that the toluene from the spin coated polymer blend layer might diffuse through the PS underlayer and soften or dissolve the film. However, the duration of the spin was merely 2 min and within that time span, the diffusion through the underlying polymer layer to reduce the viscosity of that layer was almost negligible. To validate this fact, one experiment was performed with the striped pre-patterned underlying RCP polymer film, on top of which polymer blend solution in toluene was spin coated at identical conditions of all the other experiments. At this stage, AFM revealed the flat morphology of the top PS/PMMA blend film. Upon selective solvent etching of polymer, the underlying directional striped pattern was revealed. This implies that the second spin coating of the polymer blend did not disrupt or dissolve the underlying polymer. That being stated, it is undeniable that there must be some degree of mixing between top and underlying layers, but that might be negligible due to short

duration of spin coating and fast evaporation of solvent from the top layer. A dissolution study in **Section 3.1** revealed that the percentage loss of the polymer is ~ 0.5%/ml, ~1%/ml and ~ 0.2%/ml of toluene within 2 min in stirring condition for PS, PMMA and RCP respectively (**Figure 2.2**).

Table 2.2: Number density (/μm^2), Wavelength (μm) and average diameter (μm) of bilayer system.

	Blend over 17 nm PS under layer		Blend over 53 nm PS under layer	
	After spin coating (PMMA mounds)	After RTA (PS mounds)	After spin coating (PMMA mounds)	After RTA (PS mounds)
Number density(/μm^2)	0.725	0.09	0.96	0.075
Wavelength (μm)	1.27 ± 0.27	3.29 ± 0.67	1.31 ± 0.27	4.25± 0.66
Average diameter (μm)	0.85 ± 0.28	1.58 ± 0.49	0.61 ± 0.18	2.11 ± 0.32

Induced by rapid evaporation of solvent, during spin coating of the upper layer, the polymers phase separated and led to the formation of isolated PMMA islands embedded in the PS matrix. The PMMA islands were protruded out of the PS matrix with height of ~ 20–25 nm (**Figure 2.5 e, e1**). The Hildebrand solubility parameters for PS, PMMA and Toluene are $\delta_{PS} =$ 9.1 $cal^{1/2}$ $cm^{-3/2}$, $\delta_{PMMA} = 9.3$ $cal^{1/2}$ $cm^{-3/2}$, $\delta_{Tol} = 8.9$ $cal^{1/2}$ $cm^{-3/2}$ respectively.[59,60] The relatively close values of the Hildebrand parameters of PS and toluene suggest that PS has more tendency to be solubilised in toluene compared to PMMA. This is corroborated by the macroscopic dissolution study, discussed earlier in **Section 3.1**. The PMMA chains get deprived of toluene due to lesser affinity and get solidified in the form of mounds thereby forming sea-islands like morphology. This PMMA mounds in PS morphology was verified by dissolving the PMMA phase preferentially by immersing the sample in acetic acid for 5 min. The morphology of the PMMA removed sample (**Figure 2.5 e2**) revealed that the continuous matrix of PS comprised of holes having depth of ~ 10 - 20 nm, which were filled with the PMMA before washing with acetic acid.[61–63]

The number density, wavelength and average diameters of the embedded mounds of PMMA were found to be around 0.725/μm^2, 1.27 ± 0.27 μm and 0.85 ± 0.28 μm, respectively on the thinner PS underlayer and almost similar feature characteristics (number density (0.96/μm^2), wavelength (1.31 ± 0.27 μm) and average diameters (0.61 ± 0.18 μm)) were obtained from thicker PS underlayer. PMMA in air has marginally higher surface tension ($\gamma_{PMMA} = 29.2\ mJ/m^2$) compared to PS ($\gamma_{PS} = 28.9\ mJ/m^2$)[64] which leads to the formation of small isolated mounds of PMMA on PS.

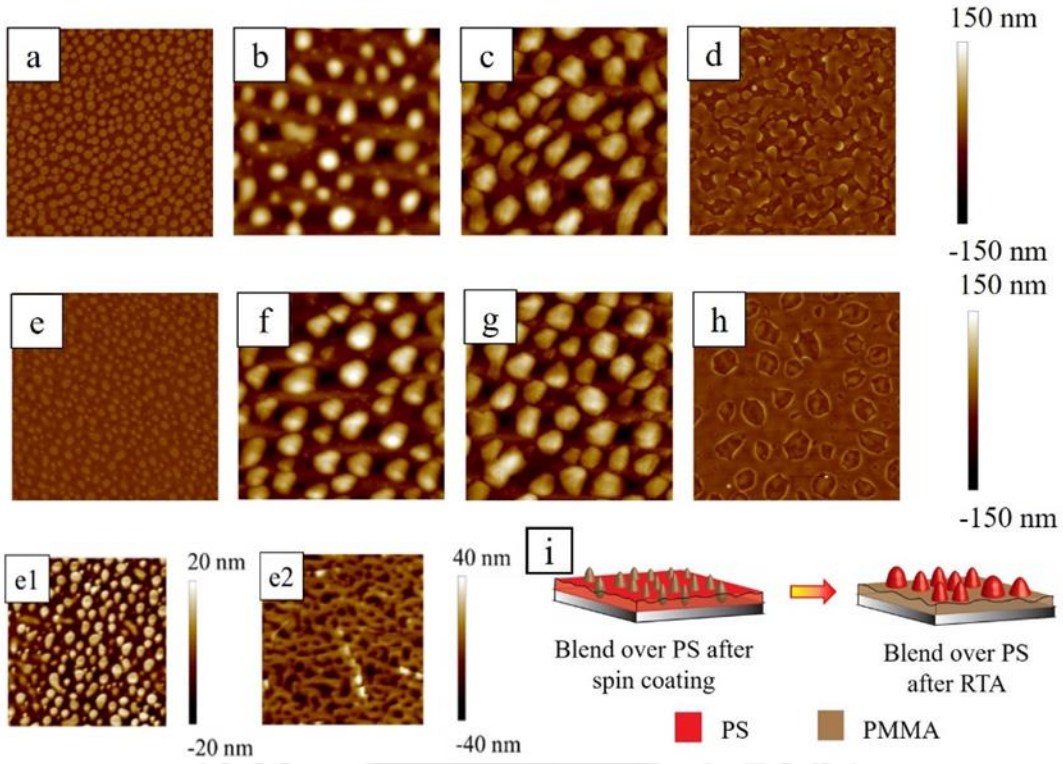

Figure 2.5. *The AFM images for blend over 0.5% PS underlayer after (a) spin coating (b) RTA (c) acetic acid and (d) cyclohexane treatment. Similarly, AFM scans of 20 μm x 20 μm for blend over 1% PS underlayer after (e) spin coating (f) RTA (g) acetic acid and (h) cyclohexane treatment. The e1 and e2 are the AFM images showing morphology after spin coating (similar to e) and after immersion in acetic acid, respectively. A schematic of the morphological evolution of blend over PS underlayer during RTA is shown in (i). The correcponding phase contrast image can be found in Appendix 3.*

During RTA, as both the polymers were in molten state at this high temperature of ~ 300 °C, the PMMA phase preferentially wetted the underlying silicon oxide surface due to its

higher affinity to PMMA compared to PS.[65,66] At this stage, the inversion of the morphology took place and isolated PS mounds were formed and embedded within the PMMA matrix (**Figure 2.5b, 2.5f**). **Figure (2.5c, 2.5g)** and **Figure (2.5d, 2.5h)** shows the preferentially removed PMMA and PS domains from thermally annealed film (**Figure 2.5b, 2.5f**) by washing it in acetic acid and cyclohexane respectively. These figures ascertain that indeed the morphological phase inversion took place. Similar phase inversion behaviour of PS/PMMA system was reported earlier while thermally annealed at ~156°C for more than 85 min in contrast to present work.[61] The number density, wavelength and average diameters of the morphology are summarised in **Table 2.2**. From **Table 2.2**, it is clear that after RTA, the morphological characteristics of the PS mounds although appear similar, but the underlying arrangement of PS domains within PMMA matrix is different in case of thin (**Figure 2.5d**) and thick (**Figure 2.5h**) PS underlayer. The area coverage by the base of the PS mound is ~ 17.41 % and of labyrinth like structure for sample with low PS fraction (relatively thin PS underlayer), whereas, the same for the thick PS underlayer is about 28.11% with irregular circular structure.

Along with that, from the **Table 2.2** it is clear that the number density is slightly higher and the wavelength is smaller for PS domains after RTA in case of thin PS underlayer than its thicker analogue. It is already known that the dewetting wavelength (λ) of a thin polymer film in air is a function of its thickness h as $\lambda \sim h$. Thus with increasing film thickness the λ increases and number density decreases.[47] We suspect that in this bilayer system, similar spinodal decomposition like phase separation took place in case of thin and thick PS underlayer. The wavelength of spinodal decomposition thus smaller for thinner PS underlayer with smaller footprint of the PS domains.

3.4 Blend over PMMA underlayer

Unlike the PS underlayer, PMMA stabilised the uniform film of PS/PMMA blend, irrespective of the underlying PMMA film thickness (**Figure 2.6a, 2.6e**) due to the marginally higher surface energy of PMMA compared to PS. First and second rows of **Figure 2.6** represent thin (~ 20 nm) and thick (~ 47 nm) PMMA underlayer at different stages of treatment of the blend/PMMA bilayer. The uniform bilayer film upon RTA, forms interconnected PS mounds protruded out of PMMA matrix due to the higher affinity of PMMA towards the silicone oxide, PMMA remained adhered with the substrate and allowed PS to reorganise in the PMMA matrix.

These interconnected PS mounds appear as small ribbon-like structures. As the overall fraction of the PMMA is lower for **Figure 2.6b** compared to the **Figure 2.6f**, there are larger numbers of smaller PS mounds observable in the former case. In **Figure 2.6f**, the PS mounds are submerged under the thick PMMA layer except for the few taller structures. The submerged smaller PS structures were revealed when both the samples, with thin and thick PMMA underlayer, were washed with acetic acid (**Figure 2.6c, 2.6g**). In case of thin PMMA underlayer, the smaller PS structures were visible even before washing with the acetic acid. This is evident from the characteristic length scales (average distance between two adjacent features) of the ribbon like structures, estimated from **Figure 2.6b** and **Figure 2.6f**, which are found to be 4.13 ± 1.21 μm and 6.48 ± 0.74 μm respectively. The features of the connected mounds imply that the phase separation was incomplete within this short period of RTA. The base footprints of the PS structures were revealed when washed with cyclohexane and as expected, the percentage coverage of the footprint of PS domain was found to be higher in thin PMMA underlayer compared to the thick PMMA underlayer due to higher PS fraction in the former case (**Figure 2.6d, 2.6h**).

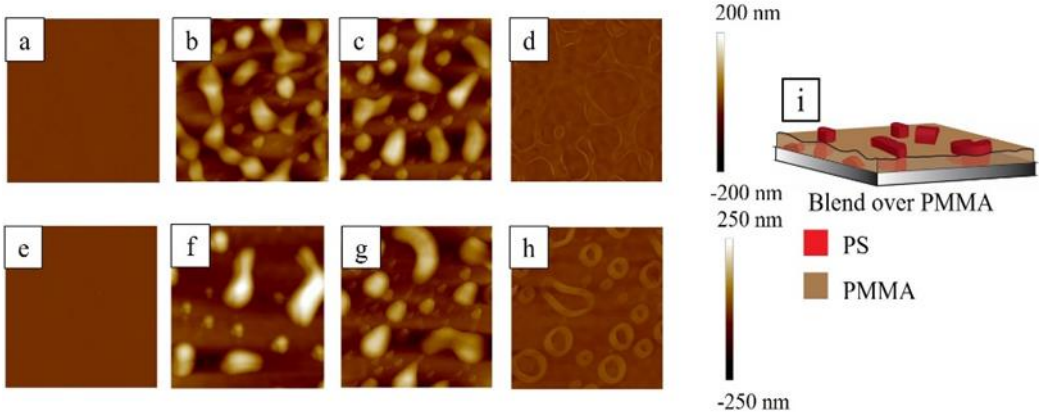

Figure 2.6*. The AFM scans of 20 µm x 20 µm for blend over 0.5% PMMA after (a) spin coating (b) RTA (c) acetic acid and (d) cyclohexane treatment. Similarly, AFM scans of 20 µm x 20 µm for blend over 1% PMMA after (e) spin coating (f) RTA (g) acetic acid and (h) cyclohexane treatment. A schematic of the morphology of PS/PMMA blend over PMMA after RTA is shown in (i). The correcponding phase contrast image can be found in Appendix 3.*

3.5 Blend over blend underlayer

Coating of PS/PMMA blend over the thin (first row, **Figure 2.7**) and thick (second row, **Figure 2.7**) PS/PMMA blend underlayer found topographically uniform (**Figure 2.7a, 2.7e**) with slight undulation of ~ 10 nm. When subjected to RTA, the prominent bicontinuous structure was observed in case of thin blend underlayer (**Figure 2.7b**), whereas somewhat isolated elongated mounds (**Figure 2.7f**) were noticed in case of thick blend underlayer. Washing with cyclohexane (**Figure 2.7d, 2.7h**) revealed that the topographically protruded bicontinuous structures in **Figure 2.7b** and isolated-elongated mounds in **Figure 2.7f** were of PS as depicted in schematic (**Figure 2.7i**). After removal of PMMA from dewetted film, by washing with acetic acid, the extent of continuity of the PS structures in **Figure 2.7c** and **Figure 2.7g** were found more compared to that observed in **Figure 2.7b** and **Figure 2.7f**. This suggests that some fraction of the connected structure of PS was submerged under PMMA after RTA. PMMA has inherent tendency to be adhered to the silicone oxide substrate compared to PS. During RTA, the phase separation of the PS and PMMA was incomplete and formed the bicontinuous phase as far as thin underlayer was concerned. On the other hand, relatively more phase separation

occurred for the thicker underlayer compared to the thinner one. This implies that the apparent viscosity of the polymer blend near the substrate is much reduced in case of thicker underlayer compared to the thinner blend underlayer.[67]

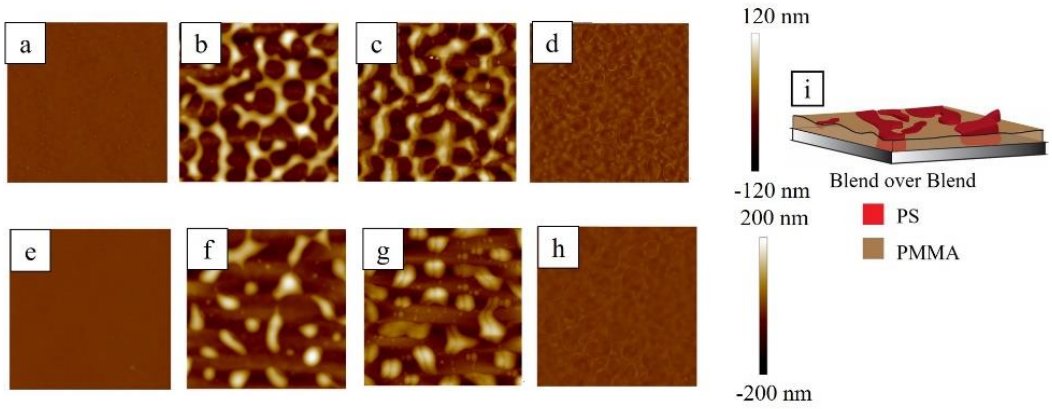

***Figure 2.7**. AFM scans of 20 µm x 20 µm for blend over 0.5% blend after (a) spin coating (b) after RTA (c) acetic acid treatment and (d) cyclohexane treatment. Similarly, AFM scans of 20 µm x 20 µm for blend over 1% blend after (e) spin coating (f) RTA (g) acetic acid treatment and (h) cyclohexane treatment. A schematic of the morphology of PS/PMMA blend over blend after RTA is shown in (i). The correcponding phase contrast image can be found in Appendix 3.*

3.6 Blend over RCP underlayer

In case of PS-r-PMMA (RCP) underlayer, irrespective of the underlayer thickness, the morphology of the upper PS/PMMA blend surface after the spin coating was almost uniform but with small undulation (~ 12 nm) having bicontinuous like structure (not evident from the **Figure 2.8a** or **Figure 2.8c** due to larger depth scale (-250 nm to 250 nm)). This smaller length scale bicontinuous structure also contains some isolated domains of dot like structures. This suggests that the underlayer RCP self-organises with smaller length scale and that influences the upper PS/PMMA blend to phase separate with smaller length scale, i.e. the underlying bicontinuous pattern of RCP bleeds through the upper PS/PMMA blend layer.

The samples when subjected to RTA, the upper blend layer phase separates and forms larger PS droplet like structure in PMMA matrix. Within the underlayer, RCP domains also self-

assemble to form isolated PS dot like structure within PMMA matrix. The smaller length scale of the morphology within this underlayer is attributed to the restrictive movement of the polymers due to tethering between the PS and the PMMA blocks. The self-organisation and phase separation of PS in underlayer with larger domain would cost the fission energy of the covalent bonds. This energy penalty of bond fission is huge compared to the global energy minimisation of the system by the preferential wetting of silicone oxide by PMMA against PS. Thus, underlayer RCP maintained the smaller length scale and optimised reorganisation keeping the bonds among the PS blocks and the PMMA blocks intact.

When the thermally annealed blend/RCP bilayer samples (**Figure 2.8b,2.8f**) were washed with selected solvent to remove particular polymer preferentially, fascinating hierarchical morphology with two different length scales was obtained. Relatively smaller length scale structures emerged from the underlying RCP layer, whereas, morphology with large length scale was dictated by the upper blend layer. Upon selective extraction of PMMA from the blend/RCP bilayer film using acetic acid, the large mound structure (from blend) as well as small tiny droplets of PS (from RCP) remained over the Silicon oxide substrate (**Figure 2.8c, 2.8g**). This itself produce two different length scales of the morphology (L1 ~ 4 μm and L2 ~ 780 nm) for both thin and thick underlayer. Similarly, when selective dissolution of PS was performed by immersing the bilayer sample into cyclohexane, the remnant PMMA morphology revealed a smooth surface with rim enclosed regime. The rim enclosed regime indicates the footprint of the PS droplet, which was present earlier before washing with the cyclohexane. It is also interesting to note that the enclosed rim area contains a few tiny droplets like morphology of PMMA. This intrigued us to examine this surface more closely and we hypothesised that a very thin layer of PMMA (from blend) made a protective layer upon the RCP underlayer. During this process, it might also be possible that PS from blend also remain adhered to some of the PS segments from the RCP. Large mounds of PS, (from blend only),

were residing on top of the protective layer of PMMA and protruded out of the PMMA matrix. This justify the fact that after washing the thermally annealed sample with cyclohexane, inside the rim, tiny droplet like structures were observed. These small droplet-like structures are smaller PS structures from RCP covered with the PMMA protective layer. Outside the rim, thick PMMA layer from the blend forms the matrix. So, at this stage (**Figure 2.8d, 2.8h**), if the sample is treated with acetic acid, to remove the protective PMMA layer, it should reveal the underlying PS morphology from the RCP. We washed the sample with acetic acid and indeed, there exists small PS domains within closed circular trench just in the position of the PMMA rim (**Figure 2.9**) and also outside the rim.

Based on the rich morphology obtained by the combination of the RCP and the blend of the constituent polymers, as discussed above, we opted to fabricate a complex hierarchical ordered morphology by employing soft lithographic technique.

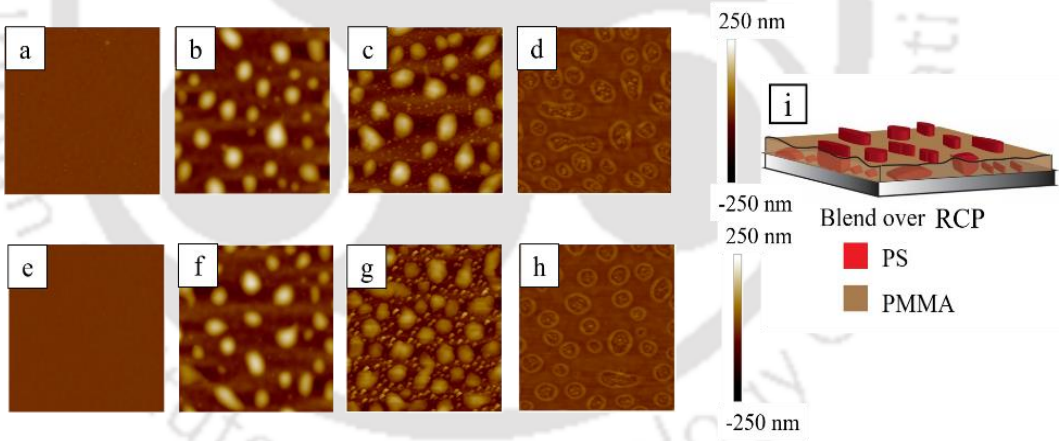

***Figure 2.8**. AFM scans of 20 µm x 20 µm for blend over 0.5% RCP after (a) spin coating (b) RTA (c) acetic acid treatment and (d) cyclohexane treatment. Similarly, AFM scans of 20 µm x 20 µm for blend over 1% RCP after (e) spin coating (f) RTA (g) acetic acid treatment and (h) cyclohexane treatment. A macroscopic schematic of PS/PMMA blend over RCP after RTA is shown in (i). The correcponding phase contrast image can be found in Appendix 3.*

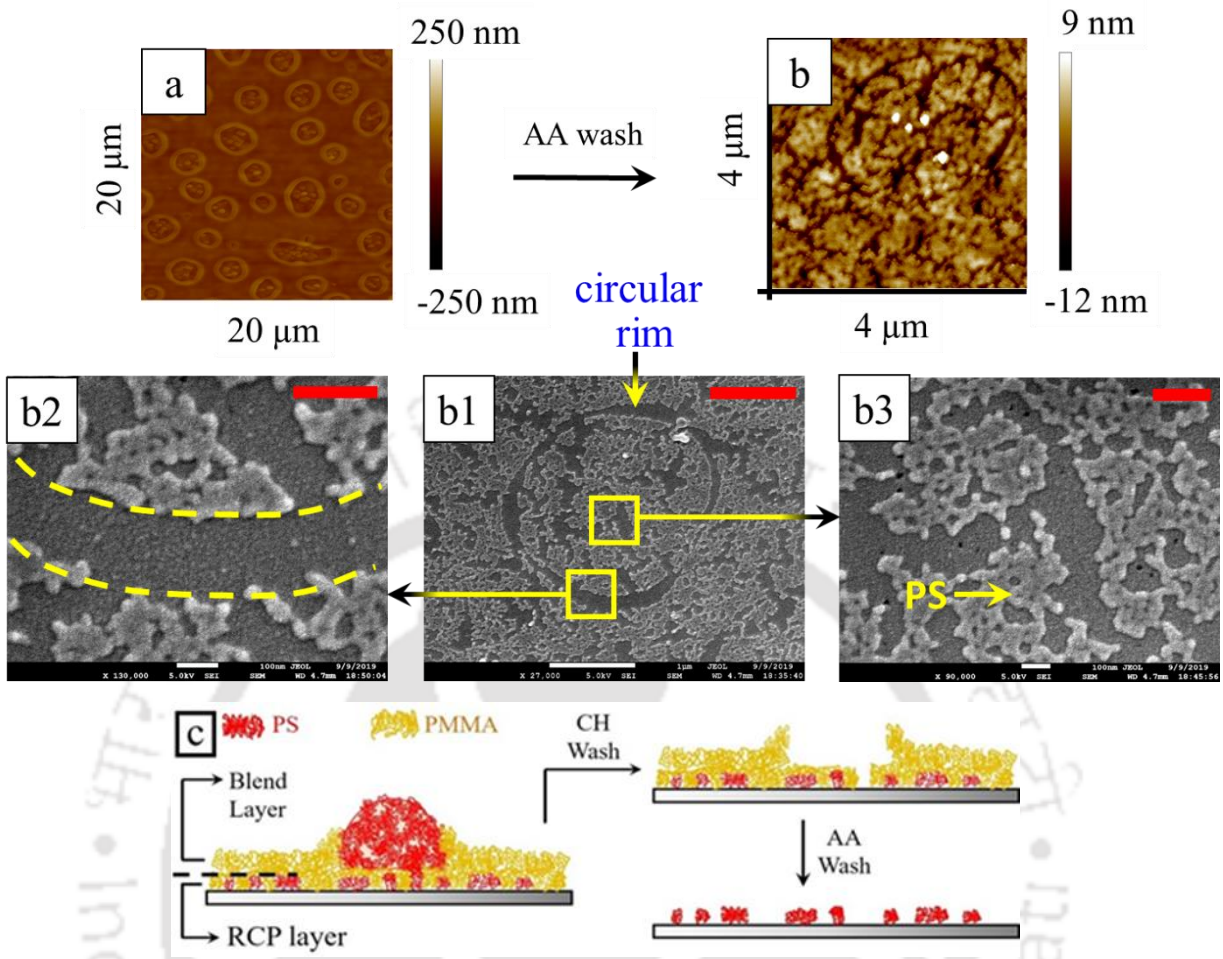

Figure 2.9*. (a) Depicts AFM image of composite thin film of blend over RCP underlayer after RTA and after washing with the cyclohexane (PS removed). This sample was washed with acetic acid (protective layer of PMMA removed) and corresponding AFM image is shown in (b). (b1) is the SEM image showing the PS remnant from RCP, which was protected by the PMMA layer. A circular rim, which gives the impression of the footprint of a PS droplet surrounded by a PMMA rim. A segment of the rim is shown in the magnified image (b2) and the morphology of the PS remnant is portrayed in the magnified image (b3). The red scale bar at the top right corner is 200 nm for b2 and b3 and 1 µm for b1. (c) schematics of the thermally annealed blend/RCP layer, after cyclohexane treatment (CH wash) and after acetic acid wash (AA wash) are depicted.*

3.7 Complex Hierarchical Patterning

A thin RCP film of ~ 49 nm was prepared from 1% (weight percentage) toluene solution on a silicon wafer and kept in a vacuum desiccator for 12 h so that the excess solvent was evaporated. A flexible aluminium stamp having alternate stripe and groove with periodicity of 1.5 µm was placed over the film and sandwiched between two glass slide with a clamp and was kept inside an oven above the glass transition temperature (T_g ~ 96°C) for 16 h. Above T_g,

due to low viscosity and increased mobility, the liquid RCP partially filled the empty space of the groove of the stamp. Depending on the pressure applied and the thickness of the parent RCP film, different patterned morphology can be obtained by this capillary force lithography (CFL) method. Upon cooling to room temperature, the imprinted pattern was solidified in RCP layer (**Figure 2.10a**). On this double stripe patterned RCP, 1% PS/PMMA blend solution in toluene was spun coat. Although premature, but at this stage itself, wherever the film thickness is less, few holes were formed and these holes were vaguely guided by underlying patterned RCP layer (**Figure 2.10b**). Next, RTA of this composite bilayer film-initiated phase separation and morphology revealed that the PS mounds protruded out of the PMMA matrix (**Figure 2.10c**). During RTA, a few phenomena happened almost simultaneously:

- First, the double humped striped structures of RCP merged and formed a single striped pattern of RCP.
- Second, a thin protecting layer of PMMA covers the patterned RCP layers but with ruptures at the protruded ridges, exposing the underlying RCP to the PS and PMMA of the blend.
- Third, on this PMMA, large dewetted PS mounds were formed, surrounded by rims of PMMA.

Washing of PS with cyclohexane leads to the formation of complex multiscale patterns - aligned elongated drop (width ~ 700 nm) like morphology with smaller length scale of ~1.5 µm and ring like structure of diameter ~ 3.5 µm having larger separation distance of ~ 6.4 µm (**Figure 2.10d**). Selective removal of the PMMA from the thermally annealed sample reveals PS droplet of height about 190 nm and diameter of ~ 3.5 µm (**Figure 2.10 e2**) in the background

of aligned and elongated PS droplet (originated from the underlying RCP) of smaller length scale (periodicity ~ 1.5 µm, **Figure 2.7e1**).

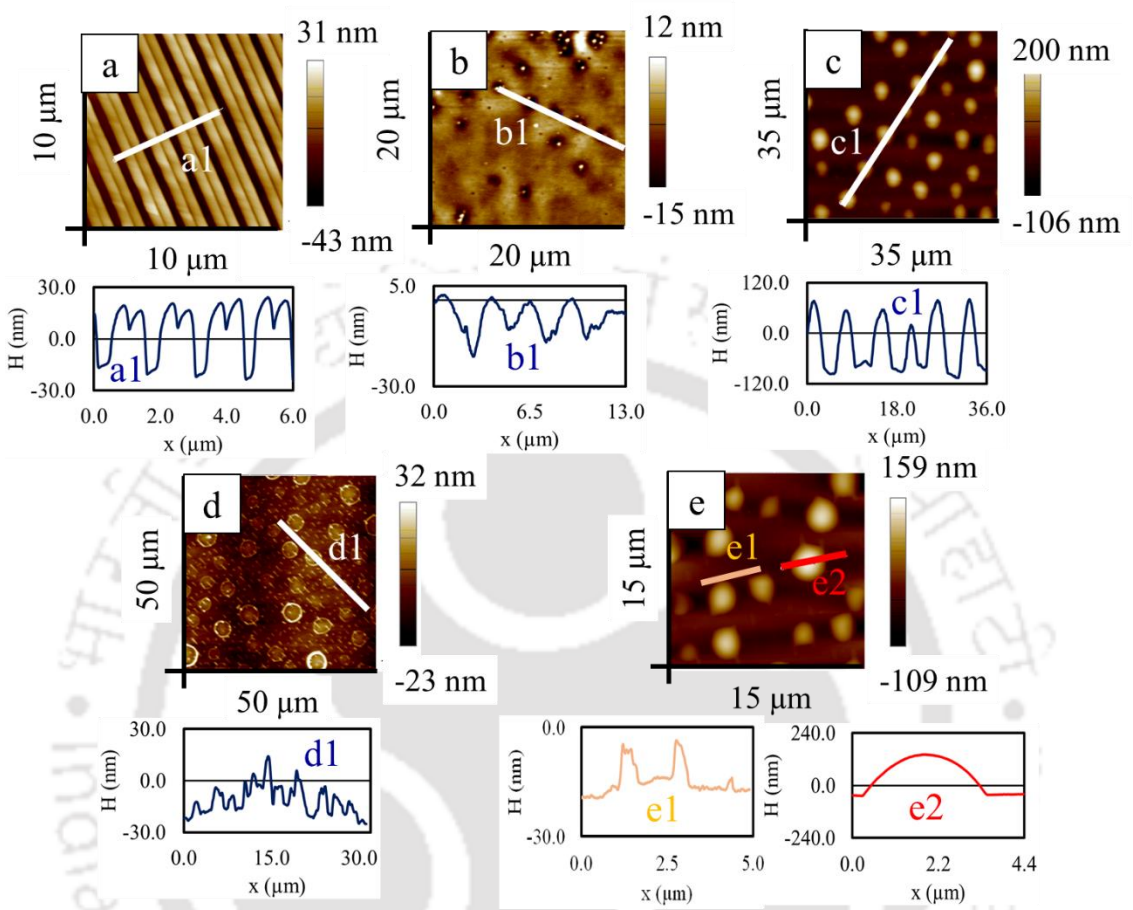

***Figure 2.10**. The AFM scans for (a) patterned RCP under layer (b) coating of blend upper layer (c) after RTA (d) after cyclohexane treatment and (e) after acetic acid treatment. Corresponding line scan is shown in a1, b1, c1, d1, e1 and in e2.*

4. CONCLUSIONS

In this chapter, for the first time we have uncover the rich morphological evolution of PS/PMMA blend polymer on labile PS-r-PMMA up on rapid thermal annealing at high temperature. A thin protective layer of PMMA from blend wets the underlying RCP and on this thin layer, PS from blend forms dewetted mounds like structure. Apart from this important findings, morphology of blend polymer upon spin coating and subsequent RTA was systematically discussed while underlayer is of PS or PMMA or PS/PMMA blend. It is found that while PMMA underlayer stabilise the PS/PMMA blend polymer, PS underlayer promotes

spin dewetting of the blend layer. Upon RTA, the phase inversion took place on PS underlayer system as reported earlier by Li *et.al*.[61] In the present report, however, the annealing temperature was high (~300°C) enough to reduce the morphological evolution time (~12-15 min). Here we probed the kinetically driven fast morphological evolution of the polymer thin film in bilayer settings. Finally, an easy and low-cost fabrication avenue for multi length-scale complex patterns were demonstrated exploiting the fast evolution of PS/PMMA blend over topographically patterned RCP layer while subjected to RTA. From this PS-PMMA combination, only by switching the selective solvent to etch out one polymer component, one can fabricate complementary patterns. The methodology described will be helpful for complex lithography of soft functional polymers with micro/nano scale features that appeal to many industrial and technologically challenging applications.

REFERENCES

[1] L. Chen, W.A. Phillip, E.L. Cussler, M.A. Hillmyer, Robust nanoporous membranes templated by a doubly reactive block copolymer, J. Am. Chem. Soc. 129 (2007) 13786–13787. https://doi.org/10.1021/ja0753041.

[2] S.Y. Yang, I. Ryu, H.Y. Kim, J.K. Kim, S.K. Jang, T.P. Russell, Nanoporous membranes with ultrahigh selectivity and flux for the filtration of viruses, Adv. Mater. 18 (2006) 709–712. https://doi.org/10.1002/adma.200501500.

[3] W.A. Phillip, J. Rzayev, M.A. Hillmyer, E.L. Cussler, Gas and water liquid transport through nanoporous block copolymer membranes, J. Memb. Sci. 286 (2006) 144–152. https://doi.org/10.1016/j.memsci.2006.09.028.

[4] G. Liu, J. Ding, A. Guo, M. Herfort, D. Bazett-Jones, Potential skin layers for membranes with tunable nanochannels, Macromolecules. 30 (1997) 1851–1853.

https://doi.org/10.1021/ma961530b.

[5] R.M. Dorin, W.A. Phillip, H. Sai, J. Werner, M. Elimelech, U. Wiesner, Designing block copolymer architectures for targeted membrane performance, Polymer (Guildf). 55 (2014) 347–353. https://doi.org/10.1016/j.polymer.2013.09.038.

[6] O. Hellwig, J.K. Bosworth, E. Dobisz, D. Kercher, T. Hauet, G. Zeltzer, J.D. Risner-Jamtgaard, D. Yaney, R. Ruiz, Bit patterned media based on block copolymer directed assembly with narrow magnetic switching field distribution, Appl. Phys. Lett. 96 (2010) 052511–052513. https://doi.org/10.1063/1.3293301.

[7] S. Xiao, X. Yang, E.W. Edwards, Y.H. La, P.F. Nealey, Graphoepitaxy of cylinder-forming block copolymers for use as templates to pattern magnetic metal dot arrays, Nanotechnology. 16 (2005) S324–S329. https://doi.org/10.1088/0957-4484/16/7/003.

[8] M. Ma, R.M. Hill, J.L. Lowery, S. V. Fridrikh, G.C. Rutledge, Electrospun poly(styrene-block-dimethylsiloxane) block copolymer fibers exhibiting superhydrophobicity, Langmuir. 21 (2005) 5549–5554. https://doi.org/10.1021/la047064y.

[9] J.T. Han, X. Xu, K. Cho, Diverse access to artificial super-hydrophobic surfaces using block copolymers, Langmuir. 21 (2005) 6662–6665. https://doi.org/10.1021/la051042+.

[10] P. Pareo, G.L. De Gregorio, M. Manca, M.S. Pianesi, L. De Marco, F. Cavallaro, M. Mari, S. Pappadà, G. Ciccarella, G. Gigli, Ultra lightweight PMMA-based composite plates with robust super-hydrophobic surfaces, J. Colloid Interface Sci. 363 (2011) 668–675. https://doi.org/10.1016/j.jcis.2011.07.075.

[11] K. Liu, L. Jiang, Bio-inspired design of multiscale structures for function integration, Nano Today. 6 (2011) 155–175. https://doi.org/10.1016/j.nantod.2011.02.002.

[12] D. Adak, S. Ghosh, P. Chakraborty, K.M.K. Srivatsa, A. Mondal, H. Saha, R. Mukherjee, R. Bhattacharyya, Non lithographic block copolymer directed self-assembled and plasma treated self-cleaning transparent coating for photovoltaic modules and other solar energy devices, Sol. Energy Mater. Sol. Cells. 188 (2018) 127–139. https://doi.org/10.1016/j.solmat.2018.08.011.

[13] N.A. Gengec, U. Cengiz, H.Y. Erbil, Superhydrophobic perfluoropolymer/polystyrene blend films induced by nonsolvent, Appl. Surf. Sci. 383 (2016) 33–41. https://doi.org/10.1016/j.apsusc.2016.04.160.

[14] S. Walheim, E. Schäffer, J. Mlynek, U. Steiner, Nanophase-separated polymer films as high-performance antireflection coatings, Science. 283 (1999) 520–522. https://doi.org/10.1126/science.283.5401.520.

[15] W. Joo, M.S. Park, J.K. Kim, Block copolymer film with sponge-like nanoporous strucutre for anti-reflection coating, Langmuir. 22 (2006) 7960–7963. https://doi.org/10.1021/la061441k.

[16] K. Hur, Y. Francescato, V. Giannini, S.A. Maier, R.G. Hennig, U. Wiesner, Three-dimensionally isotropic negative refractive index materials from block copolymer self-assembled chiral gyroid networks, Angew. Chemie - Int. Ed. 50 (2011) 11985–11989. https://doi.org/10.1002/anie.201104888.

[17] A. del Campo, E. Arzt, Fabrication approaches for generating complex micro- and nanopatterns on polymeric surfaces, Chem. Rev. 108 (2008) 911–945. https://doi.org/10.1021/cr050018y.

[18] M. Altissimo, E-beam lithography for micro-/nanofabrication, Biomicrofluidics. 4 (2010) 026503. https://doi.org/10.1063/1.3437589.

[19] A. Verma, A. Sharma, Self-organized nano-lens arrays by intensified dewetting of electron beam modified polymer thin-films, Soft Matter. 7 (2011) 11119–11124. https://doi.org/10.1039/c1sm06229h.

[20] A.S. Holland, P.W. Leech, G.K. Reeves, Reactive ion etching of organic polymers for application in waveguide trench molds, J. Mater. Sci. 39 (2004) 3505–3508. https://doi.org/10.1023/B:JMSC.0000026962.62088.2f.

[21] A. Asatekin, M.C. Barr, S.H. Baxamusa, K.K.S. Lau, W. Tenhaeff, J. Xu, K.K. Gleason, Designing polymer surfaces via vapor deposition, Mater. Today. 13 (2010) 26–33. https://doi.org/10.1016/S1369-7021(10)70081-X.

[22] A. Biswas, I.S. Bayer, A.S. Biris, T. Wang, E. Dervishi, F. Faupel, Advances in top-down and bottom-up surface nanofabrication: Techniques, applications & future prospects, Adv. Colloid Interface Sci. 170 (2012) 2–27. https://doi.org/10.1016/j.cis.2011.11.001.

[23] S.Y. Chou, P.R. Krauss, P.J. Renstrom, Imprint of sub-25 nm vias and trenches in polymers, Appl. Phys. Lett. 67 (1995) 3114. https://doi.org/10.1063/1.114851.

[24] S.Y. Chou, P.R. Krauss, P.J. Renstrom, Imprint lithography with 25-nanometer resolution, Science. 272 (1996) 85–87. https://doi.org/10.1126/science.272.5258.85.

[25] A. Perl, D.N. Reinhoudt, J. Huskens, Microcontact printing: Limitations and achievements, Adv. Mater. 21 (2009) 2257–2268. https://doi.org/10.1002/adma.200801864.

[26] M. Wang, H.G. Braun, T. Kratzmüller, E. Meyer, Patterning polymers by micro-fluid-contact printing, Adv. Mater. 13 (2001) 1312–1317. https://doi.org/10.1002/1521-4095(200109)13:17<1312::AID-ADMA1312>3.0.CO;2-Z.

[27] W.M. Lackowski, P. Ghosh, R.M. Crooks, Micron-scale patterning of hyperbranched polymer films by micro-contact printing, J. Am. Chem. Soc. 121 (1999) 1419–1420. https://doi.org/10.1021/ja983545q.

[28] Y. Xia, G.M. Whitesides, Soft lithography, Annu. Rev. Mater. Sci. 28 (1998) 153–184. https://doi.org/10.1146/annurev.matsci.28.1.153.

[29] R. Mukherjee, A. Sharma, Creating self-organized submicrometer contact instability patterns in soft elastic bilayers with a topographically patterned stamp, ACS Appl. Mater. Interfaces. 4 (2012) 355–362. https://doi.org/10.1021/am201422h.

[30] P.S.G. Pattader, I. Banerjee, A. Sharma, D. Bandyopadhyay, Multiscale pattern generation in viscoelastic polymer films by spatiotemporal modulation of electric field and control of rheology, Adv. Funct. Mater. 21 (2011) 324–335. https://doi.org/10.1002/adfm.201001206.

[31] S. Srivastava, P.D.S. Reddy, C. Wang, D. Bandyopadhyay, A. Sharma, Electric field induced microstructures in thin films on physicochemically heterogeneous and patterned substrates, J. Chem. Phys. 132 (2010) 174703. https://doi.org/10.1063/1.3400653.

[32] P. Roy, R. Mukherjee, D. Bandyopadhyay, P.S. Gooh Pattader, Electrodynamic-contact-line-lithography with nematic liquid crystals for template-less E-writing of mesopatterns on soft surfaces, Nanoscale. 11 (2019) 16523–16533. https://doi.org/10.1039/c9nr05729c.

[33] N. Arun, A. Sharma, P.S.G. Pattader, I. Banerjee, H.M. Dixit, K.S. Narayan, Electric-field-induced patterns in soft viscoelastic films: From long waves of viscous liquids to short waves of elastic solids, Phys. Rev. Lett. 102 (2009) 254502. https://doi.org/10.1103/PhysRevLett.102.254502.

[34] M.D. Morariu, N.E. Voicu, E. Schäffer, Z. Lin, T.P. Russell, U. Steiner, Hierarchical structure formation and pattern replication induced by an electric field, Nat. Mater. 2 (2003) 48–52. https://doi.org/10.1038/nmat789.

[35] E. Schäffer, T. Thurn-Albrecht, T.P. Russell, U. Steiner, Electrically induced structure formation and pattern transfer, Nature. 403 (2000) 874–877. https://doi.org/10.1038/35002540.

[36] R. Mukherjee, A. Sharma, Instability, self-organization and pattern formation in thin soft films, Soft Matter. 11 (2015) 8717–8740. https://doi.org/10.1039/c5sm01724f.

[37] A. Sharma, G. Reiter, Instability of thin polymer films on coated substrates: Rupture, dewetting, and drop formation, J. Colloid Interface Sci. 178 (1996) 383–399. https://doi.org/10.1006/jcis.1996.0133.

[38] G. Reiter, Dewetting of Thin Polymer Films, Phys. Rev. Lett. 68 (1992) 75–80.

[39] G. Reiter, Unstable Thin Polymer Films: Rupture and Dewetting Processes, Langmuir. 9 (1993) 1344–1351. https://doi.org/10.1021/la00029a031.

[40] L. Xue, J. Zhang, Y. Han, Phase separation induced ordered patterns in thin polymer blend films, Prog. Polym. Sci. 37 (2012) 564–594. https://doi.org/10.1016/j.progpolymsci.2011.09.001.

[41] M.C. Orilall, U. Wiesner, Block copolymer based composition and morphology control in nanostructured hybrid materials for energy conversion and storage: Solar cells, batteries, and fuel cells, Chem. Soc. Rev. 40 (2011) 520–535. https://doi.org/10.1039/c0cs00034e.

[42] F.S. Bates, Polymer-Polymer Phase Behavior, Science. 251 (1991) 898–905.

[43] E. Manias, L.A. Utracki, Polymer Blends Handbook, Second, Springer, 2014.

[44] P.W. Majewski, K.G. Yager, Rapid ordering of block copolymer thin films, J. Phys. Condens. Matter. 28 (2016) 403002-1–37. https://doi.org/10.1088/0953-8984/28/40/403002.

[45] C. Sinturel, M. Vayer, M. Morris, M.A. Hillmyer, Solvent vapor annealing of block polymer thin films, Macromolecules. 46 (2013) 5399–5415. https://doi.org/10.1021/ma400735a.

[46] D.U. Ahn, Z. Wang, I.P. Campbell, M.P. Stoykovich, Y. Ding, Morphological evolution of thin PS/PMMA films: Effects of surface energy and blend composition, Polymer (Guildf). 53 (2012) 4187–4194. https://doi.org/10.1016/j.polymer.2012.07.037.

[47] H. Ogawa, T. Kanaya, K. Nishida, G. Matsuba, Phase separation and dewetting in polystyrene/poly(vinyl methyl ether) blend thin films in a wide thickness range, Polymer (Guildf). 49 (2008) 254–262. https://doi.org/10.1016/j.polymer.2007.11.031.

[48] S. Walheim, M. Bo, G. Krausch, U. Steiner, Structure Formation via Polymer Demixing in Spin-Cast Films, 9297 (1997) 4995–5003.

[49] D.U. Ahn, Z. Wang, I.P. Campbell, M.P. Stoykovich, Y. Ding, Morphological evolution of thin PS/PMMA films: Effects of surface energy and blend composition, Polymer (Guildf). 53 (2012) 4187–4194. https://doi.org/10.1016/j.polymer.2012.07.037.

[50] P. Mansky, Y. Liu, E. Huang, T.P. Russell, C. Hawker, Controlling Polymer-Surface Interactions with Random Copolymer Brushes, Science. 275 (1997) 1458–1461.

[51] R. Mukherjee, A. Sharma, M. Gonuguntla, G.K. Patil, Adhesive Force Assisted Imprinting of Soft Solid Polymer Films by Flexible Foils, J. Nanosci. Nanotechnol. 8

(2008) 3406–3415. https://doi.org/10.1166/jnn.2008.121.

[52] K.Y. Suh, Y. Kim, H.H. Lee, Capillary Force Lithography, Adv. Mater. 13 (2001) 1386–1389.

[53] L.E. Manring, Thermal Degradation of Poly(methyl methacrylate). 2. Vinyl-Terminated Polymer, Macromolecules. 22 (1989) 2673–2677. https://doi.org/10.1021/ma00196a024.

[54] T. Kashiwagi, A. Inaba, J.E. Brown, K. Hatada, T. Kitayama, E. Masuda, Effects of Weak Linkages on the Thermal and Oxidative Degradation of Poly(methyl methacrylates), Macromolecules. 19 (1986) 2160–2168. https://doi.org/10.1021/ma00162a010.

[55] N. Brun, I. Youssef, M. Chevrel, D. Chapron, C. Schrauwen, S. Hoppe, P. Bourson, A. Durand, In situ monitoring of styrene polymerization using Raman spectroscopy . Multiscale approach of homogeneous and heterogeneous polymerization processes, J. Raman Spectrosc. 44 (2013) 909–915. https://doi.org/10.1002/jrs.4279.

[56] A.D. Curtis, A.R. Calchera, M.C. Asplund, J.E. Patterson, Observation of sub-surface phenyl rings in polystyrene with vibrationally resonant sum-frequency generation, Vib. Spectrosc. 68 (2013) 71–81. https://doi.org/10.1016/j.vibspec.2013.05.011.

[57] V.K. Thakur, D. Vennerberg, S.A. Madbouly, M.R. Kessler, Bio-inspired green surface functionalization of PMMA for multifunctional capacitors, RSC Adv. 4 (2014) 6677–6684. https://doi.org/10.1039/c3ra46592f.

[58] C. De Rosa, F. Auriemma, C. Diletto, R. Di Girolamo, A. Malafronte, P. Morvillo, G. Zito, G. Rusciano, G. Pesce, A. Sasso, Toward hyperuniform disordered plasmonic nanostructures for reproducible surface-enhanced Raman spectroscopy, Phys. Chem.

Chem. Phys. 17 (2015) 8061–8069. https://doi.org/10.1039/c4cp06024e.

[59] A.F.M. Barton, Solubility Parameters, Chem. Rev. 75 (1975) 731–753. https://doi.org/10.1021/cr60298a003.

[60] H.J. Vandenburg, A.A. Clifford, K.D. Bartle, R.E. Carlson, J. Carroll, I.D. Newton, A simple solvent selection method for accelerated solvent extraction of additives from polymers, Analyst. 124 (1999) 1707–1710. https://doi.org/10.1039/a904631c.

[61] X. Li, Y. Han, L. An, Annealing effects on the surface morphologies of thin PS/PMMA blend films with different film thickness, Appl. Surf. Sci. 230 (2004) 115–124. https://doi.org/10.1016/j.apsusc.2004.02.046.

[62] S. Walheim, M. Böltau, J. Mlynek, G. Krausch, U. Steiner, Structure formation via polymer demixing in spin-cast films, Macromolecules. 30 (1997) 4995–5003. https://doi.org/10.1021/ma9619288.

[63] S. Roy, A. Sharma, Self-organized morphological evolution and dewetting in solvent vapor annealing of spin coated polymer blend nanostructures, J. Colloid Interface Sci. 449 (2015) 215–225. https://doi.org/10.1016/j.jcis.2014.12.095.

[64] X. Liu, N. Bhandaru, M. Banik, X. Wang, A.M. Al-Enizi, A. Karim, R. Mukherjee, Capillary Force Lithography Pattern-Directed Self-Assembly (CFL-PDSA) of Phase-Separating Polymer Blend Thin Films, ACS Omega. 3 (2018) 2161–2168. https://doi.org/10.1021/acsomega.7b02078.

[65] S. Roy, A. Sharma, Self-organized morphological evolution and dewetting in solvent vapor annealing of spin coated polymer blend nanostructures, J. Colloid Interface Sci. 449 (2015) 215–225. https://doi.org/10.1016/j.jcis.2014.12.095.

[66] L. Kailas, B. Nysten, P. Bertrand, Difference in the annealing behaviour of thin films of PS/PMMA blends and copolymers as revealed by ToF-SIMS and AFM, Surf. Interface Anal. 36 (2004) 1227–1230. https://doi.org/10.1002/sia.1882.

[67] S. Pronk, E. Lindahl, P.M. Kasson, Dynamic heterogeneity controls diffusion and viscosity near biological interfaces, Nat. Commun. 5 (2014) 1–7. https://doi.org/10.1038/ncomms4034.

CHAPTER 3

Chapter 3

Phase separation in polymer bilayer system: role of variation in PS: PMMA Ratio and ordering of phase separated domains

GRAPHICAL ABSTRACT

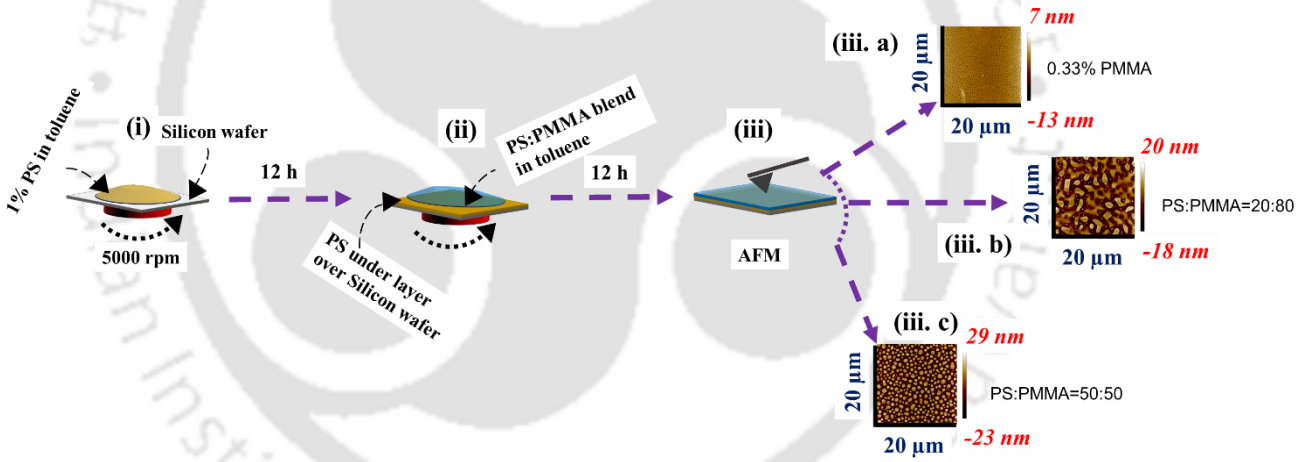

ABSTRACT

The present study focusses on the phase separation of polymer blend over a labile underlayer of homopolymer. The upper layer was a blend of polystyrene (PS) and polymethyl methacrylate (PMMA) and underlayer was polystyrene (PS). The non-equilibrium phase separation was observed due to rapid loss of solvents during the spin coating. The ratio of PS:PMMA ratio was altered in upper layer. The study also focuses on ordering of the phase separated domains. This was successfully achieved by using capillary force lithography (CFL) to pattern the underlayer. Orderly phase separated domains of the blend PS/PMMA was achieved when spun coated over patterned PS underlayer.

Keywords: *polymer blend, polystyrene, polymethyl methacrylate, bilayer, capillary force lithography (CFL)*

1. INTRODUCTION

The phase separation in polymer blend thin films is a thermodynamic process. The final morphologies is dependent upon a lot of factors like polymer solvent interactions,[1] polymer substrate interactions,[1] molecular weight,[2] evaporation rate of solvent,[3,4] etc. For binary polymer blends the relative concentrations of polymers coupled with rapid evaporation give rise to a variety of phase separated domains.[5,6] The final morphologies obtained are far from the equilibrium and generate random patterns.

Many studies have been reported for the generation of orderly patterns of phase separated domains. These reports often utilize a synergistic approach by combining the phase separation in polymer blends with conventional lithographic process like Dip pen lithography, [7] nano imprint lithography (NIL),[8] capillary force lithography (CFL),[9] breadth figure technique. Moreover, chemically [10] or topographically [11] patterned substrates can also be used to create orderly arrangements.

The present study is a detailed report on the phase separation in polymer bilayer system. The upper layer was a blend PS/PMMA and underlayer was polystyrene (PS). The ratio of PS:PMMA was changed in upper layer while keeping the under layer unaltered. The rapid evaporation of solvent, coupled with variation in the concentration of individual polymers engendered a variety of complex morphologies. Next objective of the work was to align the phase separated domains using synergies of capillary force lithography and phase separation in polymer blends.

2. MATERIALS AND METHODS

2.1 Preparation of polymer solutions

Separate solutions of polymers, polystyrene (PS, Sigma Aldrich, Mw = 1,92,000) and polymethyl methacrylate (PMMA, Sigma Aldrich, Mw = 1,20,000) were prepared in toluene. The concentration of polymers solutions was fixed at 1%. These polymers are mixed in various proportions to form a homogenous blend of PS and PMMA.

2.2 Preparation of polymer bilayer

At first, silicon wafers (1 cm x 1 cm) were thoroughly cleaned using various solvents and Piranha solutions (H_2O_2 : H_2SO_4::20: 80). Proper safety protocol was followed while handling the chemicals and reagents. Next, the cleaned and nitrogen dried silicon wafers were firmly placed over a chuck of a spin coater. A copious amount of 1% polymer solution was dispensed over the silicon wafers and rotated at a constant spin speed of 2500 rpm for 2 mins. The samples were placed in a vacuum desiccator and the solvent was allowed to evaporate for 12 h. Next, the previously prepared polystyrene films were spin-coated with pre-prepared blend solutions.The complete process is depicted in **Figure 3.1.**

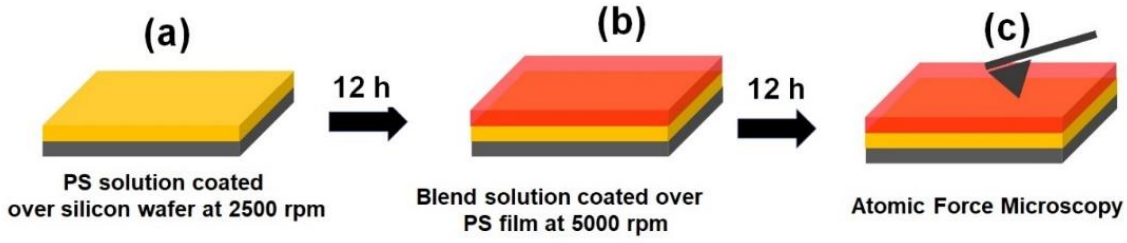

Figure 3.1*. The schematic experimental procedure was shown here. A thin 53 nm polystyrene (PS) film was spun coated over silicon wafer at 5000 rpm for 2 min (a). After 12 h blend PS: PMMA in toluene was next spun coated over previously coated PS layer (b). Next, AFM scans captured (c).*

2.3 Preparation of orderly arrangements

Capillary force lithography was used to fabricate patterned underlayer. Aluminium foils were used as thin flexible molds. These foils have stripes alternate lines of grooves and crests with periodicity, width and height of about 1.6 µm, 800 nm and 120 nm respectively.[12] The aluminium foils were peeled off from the compact disks (CDs) and placed over the cleaned

silicon wafer was spin coated with PS solution as mentioned previously. Before this assembly was heated at 120ºC, it was firmly sandwiched between two glass slides and firmly clamped with binder clips. After 12 h, the whole assembly was cooled to room temperature and later dismantled. [13] The prepared patterned underlayer was then spun coated with a thin layer of blend (PS: PMMA: 50:50) at 2500 rpm for 2 min. The bilayer system prepared was then characterized using atomic force microscopy.

2.4 Characterization

The films surface was characterized using atomic force microscopy (AFM, Bruker, Innova series) using sharp-edged antimony doped silicon tips (TESPA-V2, Bruker) with a resistivity of 0.01-0.025 Ohm-cm, frequency 320 kHz and force constant 42 N/m. The scan rate was maintained at 0.8 Hz in tapping mode. The film thickness was measured using ellipsometer (EP3 Nanofilm, Accurion, Germany) and Cauchy model was used as fitting model.

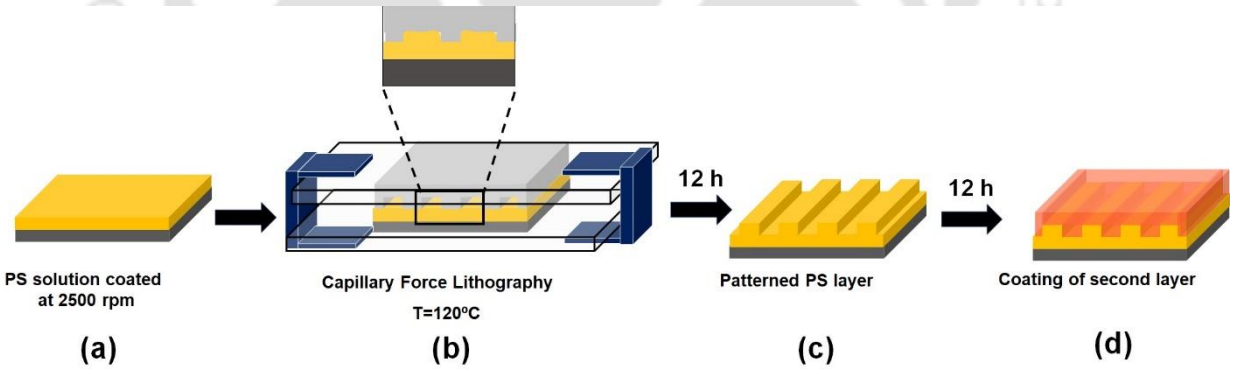

Figure 3.2*. The schematic experimental procedure was shown here to generate orderly arrangement of phase separated structures. A thin 53 nm polystyrene (PS) film was spun coated over silicon wafer at 5000 rpm for 2 min (a). The capillary force lithography was performed at 120°C over the prepared PS underlayer (b-c). Next, the blend PS: PMMA ::50:50 was next spun coated over previously coated patterned PS layer (d).*

3. RESULTS AND DISCUSSIONS

Figure 3.3 shows the AFM images obtained after the spin coating of blend over PS underlayer. Keeping the underlayer intact, in the upper layer the PS:PMMA ratio was altered. For the case

when the PS to PMMA ratio in blend was fixed at 20:80, peculiar patterns exhibiting interconnected ribbons with contorted raised domains were observed as shown in **Figure 3.3 (a)**. The height of the raised protrusions was around ~ 20 nm (**Figure 3.3 (a1)**). Later when immersed in acetic acid for 10 mins, PMMA domains were removed. The irregular protrusions disappeared and the remaining PS layer was found to contain holes. This confirmed that the irregular protrusions were of PMMA and are embedded into the PS matrix (**Figure 3.3 a2**). The toluene dissolves both PS and PMMA. However, toluene shows more affinity towards PS than PMMA. It is evident from the Hildebrand solubility parameters for PS, PMMA and Toluene are δ_{PS} =9.1cal$^{1/2}$ cm$^{-3/2}$, δ_{PMMA} = 9.3 cal$^{1/2}$ cm$^{-3/2}$, δ_{Tol} = 8.9 cal$^{1/2}$ cm$^{-3/2}$ respectively.[14] During local evaporation of the solvent the PS chains are still swelled retained toluene while PMMA chains gets solidified due to rapid loss of solvent. Upon prolonged evaporation, the PS chains lose the solvent. Due to the loss of solvents in PS chains, the swelling of PS chains is also reduced. This resulted in protruded PMMA domains with sharp edges.[1]

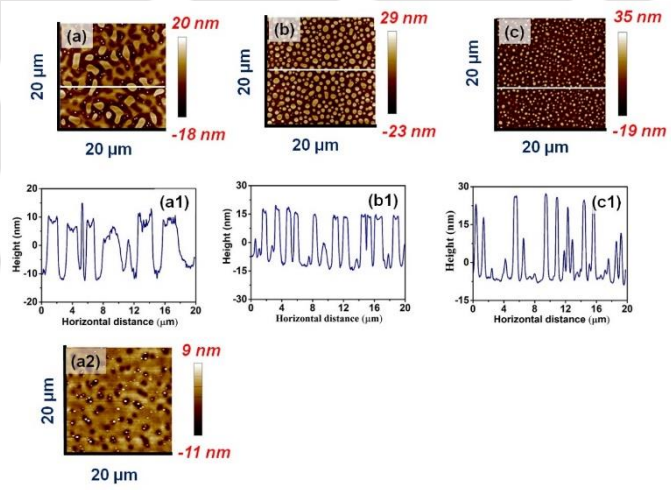

Figure 3.3*. The AFM images obtained after spin coating of blend layer over PS under layer. Three PS:PMMA ratio of blend were (a) 20:80; (b) 50:50 and (c) 80:20. The corresponding line scans are shown in a1-c1. The AFM image obtained after dissolution of PMMA from the bilayer system with PS:PMMA ratio 20:80.*

Next, when the PS:PMMA ratio was increased to 50:50, cylindrical polymeric were obtained. The height, width, wavelength and number density of these domains were ~ 25 nm, ~ 650 nm, 1.3 μm and ~ 0.83 μm^{-2} respectively. When the ratio of PS:PMMA increased to 80:20, the width and wavelength of the cylindrical polymer domains reduced to ~ 450 nm and 0.90 μm. Moreover, the number density increases to ~ 1.45 μm^{-2}. However, there was marginal changes in the height of the polymeric domains and thus engendering spike-like morphologies. This confirms that the individual concentrations of the polymers in the blend have the direct impact on the final morphologies after phase separation.

Next, a synergistic approach was utilized to generate orderly arrangement. For this capillary force lithography was utilized to fabricate a patterned PS underlayer. The flexible mold used here was aluminium foil peeled off from the CD and firmly placed over the thin film of PS. The system was heated to a temperature higher than the glass transition temperature of the polymer. This induces the mobility in the polymer chains and resulted in the filling up of the cavities inside the mold. After the process the system is cooled to room temperature and the whole assembly was dismantled. Through this process stripes were created on the PS underlayer. The height, width and wavelength of the stripes was obtained was ~ 120 nm, ~ 1.5 μm and ~1.5 nm respectively (**Figure 3.4 a1**). The blend (PS: PMMA :: 50:50) was then spin coated over the prepatterned PS underlayer this assisted in the generation of orderly arrangements of PMMA protrusions with height of 30 nm (**Figure 3.4 b**). The corresponding line scans is shown by **Figure 3.4 b1**.

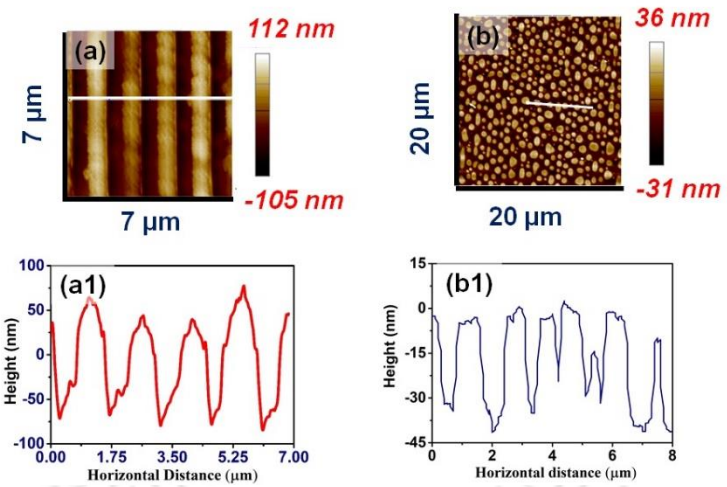

Figure 3.4*. A thin 53 nm polystyrene (PS) film was spun coated over silicon wafer at 5000 rpm for 2 min (a). The capillary force lithography was performed at 120°C over the prepared PS underlayer (b-c). Next, the blend PS:PMMA::50:50 was next spun coated over previously coated patterned PS layer (d).*

4. CONCLUSIONS

Non-equilibrium phase separation occurs due to rapid evaporation of solvent during spin coating. The loss of solvent causes solidification of polymer chains before achieving equilibrium. The blend upper layer tends to phase separate due to rapid evaporation of solvent and presence of marginally low surface energy PS underlayer. Moreover, by altering the ratio PS: PMMA, labyrinthine type or sea-island morphologies. Later, the PS underlayer was patterned using CFL and thus used to generate orderly arrangements of the phase-separated domains.

REFERENCES

[1] S. Walheim, M. Böltau, J. Mlynek, G. Krausch, U. Steiner, Structure formation via polymer demixing in spin-cast films, Macromolecules. 30 (1997) 4995–5003. https://doi.org/10.1021/ma9619288.

[2] K. Tanaka, A. Takahara, T. Kajiyama, Surface molecular aggregation structure and

surface molecular motions of high-molecular-weight polystyrene/low-molecular-weight poly(methyl methacrylate) blend films, Macromolecules. 31 (1998) 863–869. https://doi.org/10.1021/ma9709866.

[3] P. Müller-Buschbaum, J.S. Gutmann, M. Wolkenhauer, J. Kraus, M. Stamm, D. Smilgies, W. Petry, Solvent-induced surface morphology of thin polymer films, Macromolecules. 34 (2001) 1369–1375. https://doi.org/10.1021/ma0009193.

[4] P. Mokarian-Tabari, M. Geoghegan, J.R. Howse, S.Y. Heriot, R.L. Thompson, R.A.L. Jones, Quantitative evaluation of evaporation rate during spin-coating of polymer blend films: Control of film structure through defined-atmosphere solvent-casting, Eur. Phys. J. E. 33 (2010) 283–289. https://doi.org/10.1140/epje/i2010-10670-7.

[5] C. Ton-That, A.G. Shard, D.O.H. Teare, R.H. Bradley, XPS and AFM surface studies of solvent-cast PS/PMMA blends, Polymer (Guildf). 42 (2001) 1121–1129. https://doi.org/10.1016/S0032-3861(00)00448-1.

[6] K. Tanaka, A. Takahara, T. Kajiyama, Film Thickness Dependence of the Surface Structure of Immiscible Polystyrene / Poly (methyl methacrylate) Blends, (1996) 3232–3239.

[7] D.C. Coffey, D.S. Ginger, Patterning Phase Separation in Polymer Films with Dip-Pen Nanolithography, J. Am. Chem. Soc. 69 (2004) 4564. https://doi.org/10.1063/1.347325.

[8] Z. Wang, D.U. Ahn, Y. Ding, Topographically uniform but chemically heterogeneous nanostructures by nanoimprinting demixed polymer blends, Langmuir. 26 (2010) 14909–14914. https://doi.org/10.1021/la102523t.

[9] D. Ho, J. Zou, B. Zdyrko, K.S. Iyer, I. Luzinov, Capillary force lithography: The versatility of this facile approach in developing nanoscale applications, Nanoscale. 7

(2015) 401–414. https://doi.org/10.1039/c4nr03565h.

[10] A. Karim, J.F. Douglas, B.P. Lee, S.C. Glotzer, J.A. Rogers, R.J. Jackman, E.J. Amis, G.M. Whitesides, Phase separation of ultrathin polymer-blend films on patterned substrates, Phys. Rev. E - Stat. Physics, Plasmas, Fluids, Relat. Interdiscip. Top. 57 (1998) 6273–6276. https://doi.org/10.1103/PhysRevE.57.R6273.

[11] X.C. Chen, H.M. Li, F. Fang, Y.W. Wu, M. Wang, G. Bin Ma, Y.Q. Ma, D.J. Shu, R.W. Peng, Confinement-induced ordering in dewetting and phase separation of polymer blend films, Adv. Mater. 24 (2012) 2637–2641. https://doi.org/10.1002/adma.201200089.

[12] R. Mukherjee, M. Gonuguntla, A. Sharma, Meso-patterning of thin polymer films by controlled dewetting: From nano-droplet arrays to membranes, J. Nanosci. Nanotechnol. 7 (2007) 2069–2075. https://doi.org/10.1166/jnn.2007.771.

[13] A. Pandey, K. Murmu, P.S. Gooh Pattader, Non-equilibrium thermal annealing of a polymer blend in bilayer settings for complex micro / nano patterning, RSC Adv. 11 (2021) 10183–10193. https://doi.org/10.1039/d1ra00017a.

[14] A.F.M. Barton, Solubility Parameters, Chem. Rev. 75 (1975) 731–753. https://doi.org/10.1021/cr60298a003.

CHAPTER 4

Chapter 4

Multiple length scale structures formation using synergies of capillary force lithography and polymer bilayer system

GRAPHICAL ABSTRACT

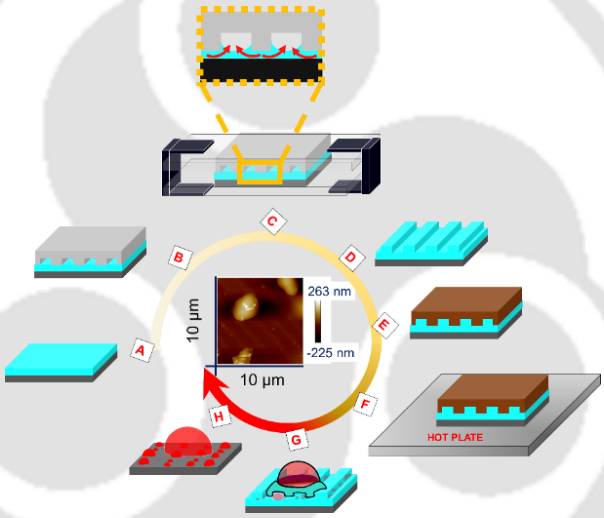

ABSTRACT

Fabrication of multiple-length scale structures is a challenge and the reported methods are often tedious, costlier and time consuming. To overcome these difficulties a facile approach is presented here that uses synergies of phase separation in polymeric bilayer system, capillary force lithography (CFL) and rapid thermal annealing (RTA). The upper layer used here is a blend of polystyrene (PS) and polymethyl methacrylate (PMMA) in toluene, and under layer was patterned random copolymer (RCP) consisting of PS and PMMA blocks. The under-layer RCP was patterned using CFL. It has been found that upon phase separation in blend upper layer, coarser domains were obtained. On the contrary phase separation RCP under layer resulted in smaller structures. Also, in our study we report that, the phase separation rate was enhanced by rapid thermal annealing (RTA) at high temperature of ~300°C. Later, by using selective solvent etching of polymers, complex yet intriguing patterns were obtained. The method offers an inexpensive, faster and straightforward pathway to generate multiple length scale structures.

Keywords: *Hierarchical structures, Blend, Random copolymers, Capillary force lithography, Rapid Thermal Annealing.*

1. INTRODUCTION

The properties of polymers like the interaction of chains with photons/electrons or the or phase separation in blend/copolymer systems open the avenue for numerous patterning techniques. These techniques have been successfully utilized to generate exquisite mico/nanopatterns over the surface. A few examples of such techniques include photolithography,[8,9] electrohydrodynamic (EHD) based patterning,[10] electron beam lithography,[11–13] micro-contact printing,[14–17] dynamic contact line lithography based patterning,[18] phase separation in polymer blends or copolymers,[19–22] etc.

The phase separation in polymer blends and copolymer stands out among all reported techniques in terms of low-cost fabrication of patterns. Phase separation in polymer blend or copolymer films is a thermodynamic process that can be altered on demand to meet the requirement of the micro/ nano fabrication. The fabrication of domains of the order of few nanometres is done by copolymers (a particular class of polymers that is synthesized using more than one monomer).[23,24] The typical morphologies obtained after phase separation copolymers are cylindrical, lamellar, and bicontinuous.[20] For coarser domains , a blend (a homogeneous solution of two or more chemically dissimilar polymers in a common solvent) is used. The morphologies obtained after phase separation in polymer blends are sea-island (droplets of one polymer inside the matrix of another) and labyrinth type (interconnected ribbons of both the polymers lie side by side).[25,26] To achieve orderly polymeric structures in blends, phase separation is often coupled with other techniques like capillary force lithography or by using patterned substrate.[27–30]

However, generating bio-inspired patterns with multiple length scales through conventional methods is challenging, time-consuming, and expensive due to the involvement of sophisticated, costly equipment! It is required to find alternative and innovative fabrication

methods that are simpler than conventional methods. The phase separation in polymer blends and copolymers can be successfully be utilised to generated bio-inspired multiple length scale structures. For instance, Byun et al. introduced PS and PMMA in toluene using sphere-on-flat geometry. The study showed that fused silica lens with a radius of curvature ~ 2 cm to spread a drop of blend in the form of lines. As the solvent is evaporated, phase separation is induced, creating highly ordered domains.[31] Kim et al. reported simultaneous phase separation in copolymer and homopolymer that resulted in orderly patterns with two different length scales. In this system the phase separation in block copolymer results in smaller phase separated domains whereas dewetting in homopolymer results in larger domains.[32] Albeit use of block copolymer still makes the process costlier.

Alternatively, the capillary force lithography (CFL) is a soft lithographic technique that involves firmly placing a flexible stamp or mould over a thin polymer film. The efficacy of CFL lies in the interaction of solid walls of mould and polymer. When mould is placed over the polymer film, and the temperature was raised above the glass transition temperature T_G of the polymer, the polymer fills the cavity in the mould. Later, when the polymer solidifies upon cooling and subsequent mould removal generates a negative replica of the mould. Thus, CFL provides a simple and cost-effective alternative to conventional lithographic techniques. Mukherjee and co-workers, in their studies, reported the use of aluminum foil from compact disks as flexible mould. These aluminum foils contain strips with width, depth, and periodicity 750 nm, 130 nm, and 1500 nm, respectively.[33] Combining top-down and bottom-up techniques, capillary force lithography, and phase separation in the blend, Liu et al. applied a synergistic approach to generate complex patterns. The study incorporated replica moulding to generate a soft PDMS stamp having patterns with negative replica taken from DVD. These PDMS stamps were then firmly placed over the PS and PMMA blend. Subsequently, pattern transfer from

stamps to blend films occurs when a low pressure of 4 kPa and temperature of 180°C was applied for different time intervals. This resulted in strips containing polymer domains of both PS and PMMA.[27]

To fabricate multiple length scale structures synergies of capillary force lithography (CFL), Rapid thermal annealing (RTA) and phase separation in blend and random copolymer (RCP) are used extensively in the present studies. The detailed study presented here is divided into three parts 1) phase separation in blend PS/PMMA over flat surface, 2) phase separation in patterned RCP layer over silicon wafer, and 3) phase separation in bilayer with upper layer being blend and under layer is a patterned RCP layer. The faster phase separation was assisted by rapid thermal annealing (RTA). The phase separation in blend over silicon wafer resulted in random domains. The phase separation in capillary force assisted RCP layer resulted in more order and smaller domains. Multiple length scale structures were fabricated by incorporating a polymeric bilayer system. The underlayer was blend PS/PMMA and underlayer is CFL assisted patterned underlayer. The polymer chain lengths in upper layer were larger as compared to that of under layer. The difference in the polymer chain lengths gives rise to hierarchical patterns. Also, the study present methods to generate orderly complimentary structures by the use of selective solvent etching.

2. MATERIALS AND METHODS

2.1 Preparation of solutions

The solutions of PS and PMMA solutions in toluene were mixed thoroughly to form a homogeneous blend with a ratio of PS: PMMA in solution was maintained at 40:60. The overall polymer concentration was 1%. The solution was further diluted in three different concentrations with blend: toluene viz. 90:10, 50:50 and 10:90. Likewise, a suitable amount of PS-r-PMMA random copolymer (average Mw 1,00,000-1,50,000, styrene 40 mol%, Sigma

Aldrich) was dissolved in toluene to make a homogeneous polymer solution of concentration 1 %.

2.2 Spin coating and rapid thermal annealing in blend films

The prepared solutions were separately spun coated (2500 rpm for 120 s) over thoroughly cleaned silicon wafers (N.J. International, India). The film thickness was measured using ellipsometry, and values are reported in Table 1. The samples were coded as A1, B1, and C1 in the order of decreasing film thickness. The films were then placed in a petri dish at room temperature for 12 h to remove residual solvent. After 12 h, the films were subjected to rapid thermal annealing (RTA). In this step, the films were heated rapidly up to 300°C. The samples were allowed to remain at that temperature for the next 30 s. It might be possible that higher annealing temperature could degrade the polymers. However, due the shorter time duration of the annealing process there was no appreciable degradation of the polymers as confirmed by Thermogravimetric analysis (TGA), differential scanning calorimetry (DSC) and Raman Spectroscopy.[34] After annealing, the samples were allowed to cool by natural convection. Since the sample contains two polymers PS and PMMA, the next step is to remove one of the polymers keeping another polymer intact. One sample from each set was separately dipped in cyclohexane and acetic acid for 10 minutes to remove PS and PMMA, respectively. The residual solvent was removed by using a slow stream of nitrogen. In the final step, the samples were vacuum dried for 6 h at 60°C.

2.3 Patterning and Rapid thermal annealing (RTA) in RCP film

Next, the prepared solution was then spin-coated over thoroughly cleaned silicon wafers at 2500 rpm for 120 s. The thickness of the film was ~78 nm. Aluminum foils from compact disks were peeled and carefully placed over the RCP film prepared earlier. These foils are pre-

patterned with parallel trenches having a width (w_m) ~750 nm, depth (h_m) ~130 nm and wavelength (λ_m) ~1500 nm.[33] This arrangement was tightly sandwiched between two glass slides using binder clips. The whole assembly was placed in a vacuum over at 120°C for 12 h. The system was cooled to room temperature. Thereafter, the whole assembly was dismantled and binder clips, glass slides, and stamps were removed. These steps ensured that pattern transfer had occurred from stamps to the RCP films. The patterned RCP films were rapidly annealed and subsequently cooled down to room temperature. Later, the annealed RCP films were subjected to selective solvent etching.

2.4 Fabrication and subsequent patterning in bilayer system

The blend solutions were separately spin-coated (2500 rpm for 120 s) over the patterned RCP films. It might be possible that toluene from upper layer may damage the protrusions in the underlayer. However, shorter spin coating duration prevents damage to the underlayer.[34] After 12 h, the films were subjected to rapid thermal annealing (RTA). The films were heated rapidly up to 300°C, the samples were allowed to remain at that temperature for the following 30 s. After that, the samples were cooled down to room temperature by natural convection. Selective solvent etching was performed by immersing the samples in cyclohexane and acetic acid for 10 minutes to remove PS and PMMA, respectively. The residual solvent was removed by using slow stream of nitrogen. Finally, the samples were vacuum dried for 6 h at 60°C. The complete process is shown in **Figure 4.1**.

2.5 Characterization

The surface morphology of the samples was analyzed using atomic force microscopy (AFM, Bruker, Innova series) using sharp-edged antimony doped silicon tips (TESPA-V2, Bruker) having a resistivity of 0.01-0.025 Ohm-cm, frequency 320 kHz, and force constant 42 N/m.

The film thickness was measured using ellipsometer EP3 Nanofilm, Accurion, Germany, with Cauchy model for fitting the data.

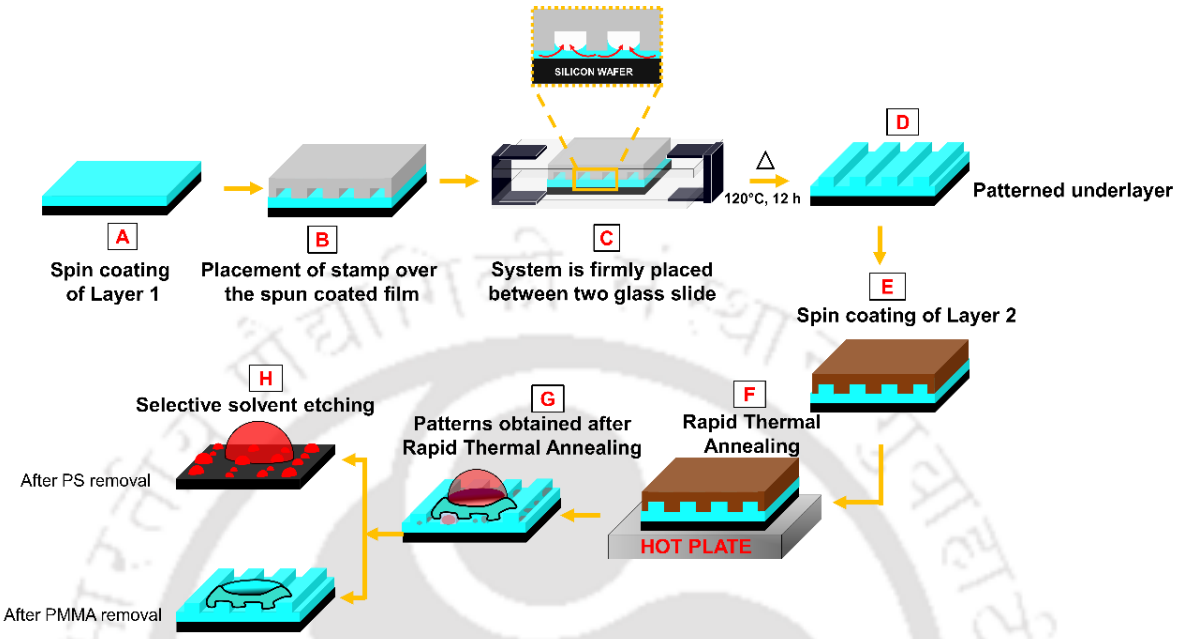

Figure 4.1. *The figure is showing the steps followed during the experiment. The sequence of steps are as follows (A) spin coating of RCP film at 2500 rpm for 120 s (B) placement of aluminium foil stamp over the RCP film (C) the film with flexible mould over it firmly sandwiched between two glass slides and heated over 120℃ for 12 h (D) pattern transfer from mould to RCP films (E) a second coat of blend over pre-patterned RCP layer (F) rapid thermal annealing (RTA) of bilayer films (G) patterns obtained after RTA and (H) selective solvent etching after immersion in acetic acid to remove PMMA and selective solvent etching for PS removal using cyclohexane.*

Table 4.1: *The consolidated characteristics for blend films spun coated upon silicon wafer.*

Sample	Blend:	As cast film				After RTA		
	Toluene	t	Ra	Rq	N	D	H	λ
		(nm)	(nm)	(nm)	(μm^{-2})	(μm)	(nm)	(μm)
A1	90:10	56	1.24	1.62	0.036	2.3 ± 0.92	199.27 ± 62.42	6.16 ± 1.33
B1	50:50	29	0.72	0.92	0.292	0.83 ± 0.24	88.47 ± 20.35	1.96 ± 0.31
C1	10:90	6	0.96	1.21	16.4	0.09 ± 0.02	9.12 ± 2.58	0.27 ± 0.05

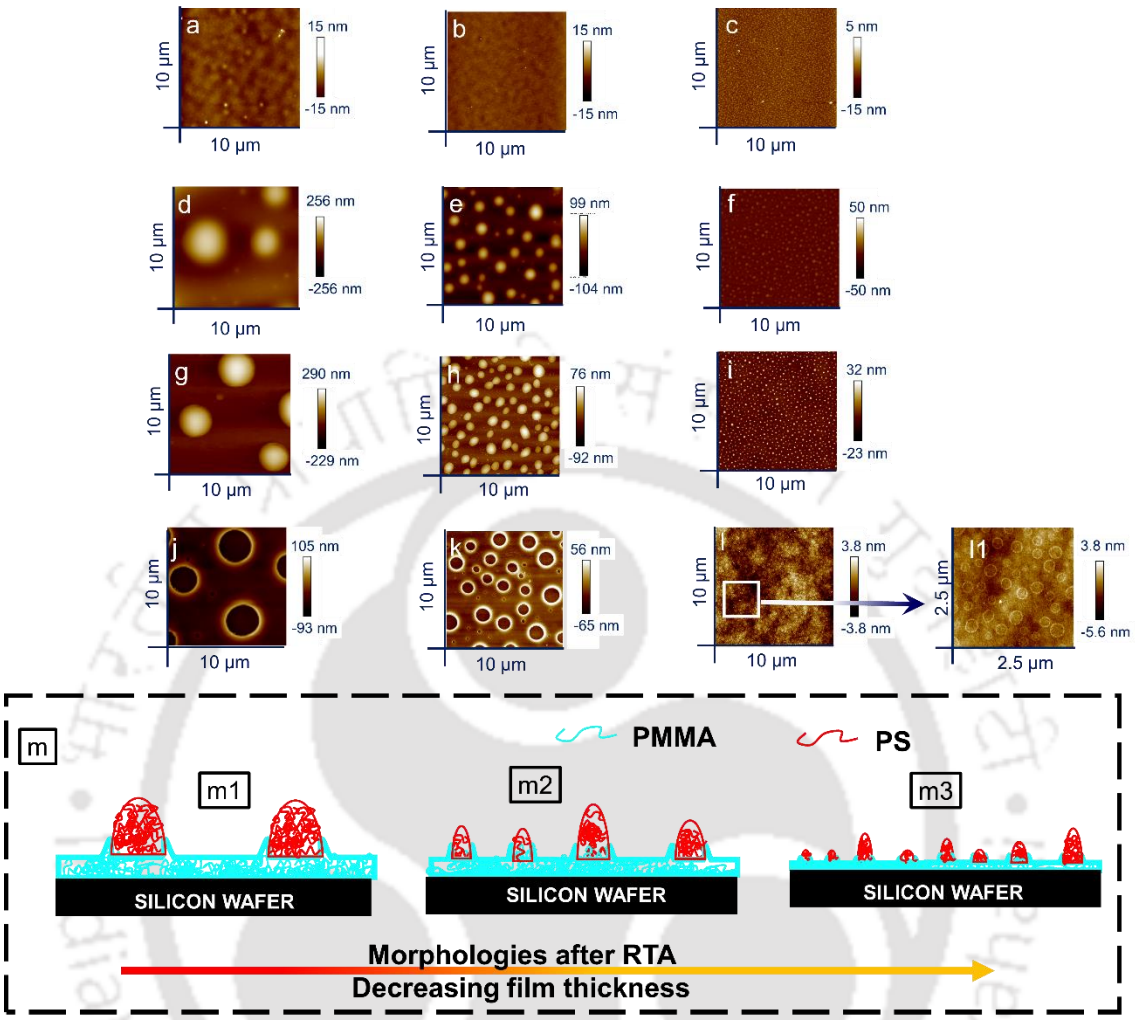

Figure 4.2. *AFM images for blend spun coated over silicon wafer with a blend toluene ratio a) 90:10; b) 50:50 and c) 10:90. The corresponding AFM images captured after RTA were shown in d-f. After acetic acid treatment, the PS mound obtained was shown in g-i. Likewise, after cyclohexane treatment, the PMMA rims were shown in j-l. l1 shows the small area AFM scan for l. The schematic showing PS mounds surrounding by PMMA rims is depicted in m.*

3. RESULTS AND DISCUSSIONS

3.1 Phase separation in polymer blend thin film over flat surface

The blend solutions were spun-coated over silicon wafers without RCP underlayer at fixed rpm. The film thickness was varied by varying the blend to toluene ratio. The high blend to toluene ratio produced the thicker film; likewise, the lower blend to toluene ratio produced thinner films (**Table 4.1**). The AFM images captured were shown in **Figure 4.2 a-c**. The

average roughness values for as-casted samples A1, B1, and C1 were 1.24 nm, 0.716 nm, and 0.96 nm, respectively. The overall polymer concentration and film thickness directly impact the size of the droplets formed after RTA. The diameters, wavelength, height, and number density for the samples are provided in **Table 4.1**. As the film thickness was reduced, the average diameter (D), wavelength (λ), and average height (H) decreased, thereby decreasing the size. On the contrary to this trend, the number density of the droplets was found to increase with decreasing film thickness. After RTA, the samples were separately immersed in acetic acid (to remove PMMA) and cyclohexane (to remove PS). The PS mounds were found to be surrounded by PMMA rims **Figure 4.2 (g-m)**. The size of the structures reduced as the thickness of the blend films reduced.

The spin coating is a batch process and starts with dispensing a copious amount of solution over the substrate, which is firmly placed over the chuck. During spin coating, the centrifugal force generated by rotating substrate forces the liquid to flow radially outwards. Due to this radially outward flow, a large amount of solution is spilled out of the substrate leaving behind a thin layer of PS and PMMA blend is coated over the silicon wafer.[35] The phase separation starts at a critical thickness. Moreover, PMMA has more affinity towards the SiO_2 layer. Hence PMMA forms a layer over the substrate, and a thin PS layer is formed over the PMMA layer.[36] During thermal annealing, the deformable liquid-liquid interface becomes unstable, and PS dewets over the PMMA layer.[37] In the late stage, randomly placed droplets were formed such that the PS mound is surrounded by PMMA rims, as shown by **Figure 4.2 h**.[38] As the temperature used here is much higher than T_G for a shorter time. It is required to analyse the polymers for thermal stability.

3.2 Phase separation in RCP layer

To generate orderly patterns in RCP film, CFL is used as patterning method. As mentioned in the materials and method section, aluminum foil peeled off from compact disks (CD), were used as a soft, flexible mould. This mould was placed over a previously coated RCP film over a silicon wafer (thickness ~ 78 nm). The system was then clamped using two glass slides and binder clips. This capillary rise allows the polymer to fill the cavities inside the mould. When the polymer film thickness is sufficiently large, the cavities were filled by the polymer. However, when the film is thinner, there is not enough polymer to fill up the cavities present inside the mould. This incomplete filling reduces the height of the final morphology. It also leads to the formation of a meniscus inside the cavities of the mould. When annealed for a sufficiently long duration, the meniscus dewets.[39] The complete process is shown schematically by **Figure 4.3**. **Figure 4.4 (a)** shows the AFM image for RCP film with strips after execution of capillary force lithography (CFL). The corresponding line scans (**Figure 4.4 (a1)**), the red line shows the line scans for patterns in CD aluminum foil (AFM image not shown here), and the blue line shows the line scan for RCP films with patterns having a width (w_p), height (h_p) and wavelength (λ_p) as ~750 nm, ~55 nm, and ~750 nm. Upon comparison with the line scan for mould perfect negative replica was not obtained as polymer film was very thin. The reduced height and width further assisted in downsizing of the final patterns. After RTA, the stipes dilate and the height of features considerably reduced to around 35 nm (**Figure 4.4 b**). When the sample was immersed in acetic acid to remove PMMA, the final PS domains dewet due to the solvent-induced dewetting (**Figure 4.4 c**). However, the patterns were found to be intact when immersed in cyclohexane (**Figure 4.4 d**). The line scans for AFM images after solvent etching were shown by **Figure 4.4 c1**. It was found that after RTA, PMMA forms a covering over PS domains. The RTA process in patterned RCP layer is schematically shown by **Figure 4.4 f**.

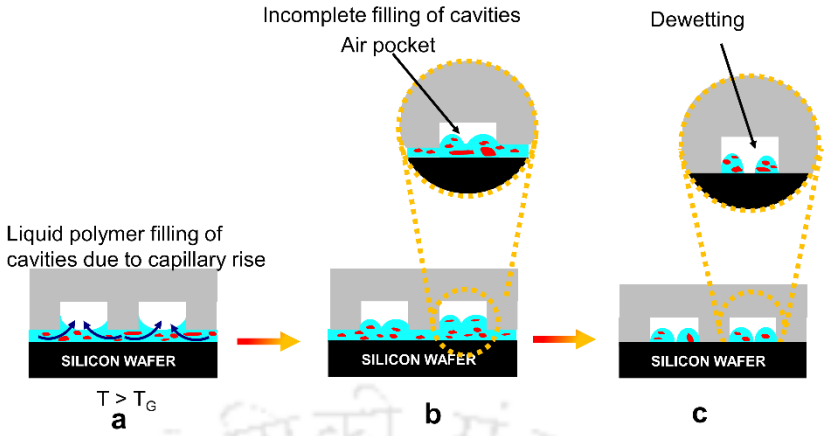

Figure 4.3. *Schematic representation of capillary force lithography (CFL). The sequence of CFL is as follows: (a) as the temperature was kept higher than glass transition temperature allows polymer melt to fill the vacant cavities in the mould, (b) incomplete filling of cavities due to thinner RCP layer, and (c) dewetting of meniscus.*

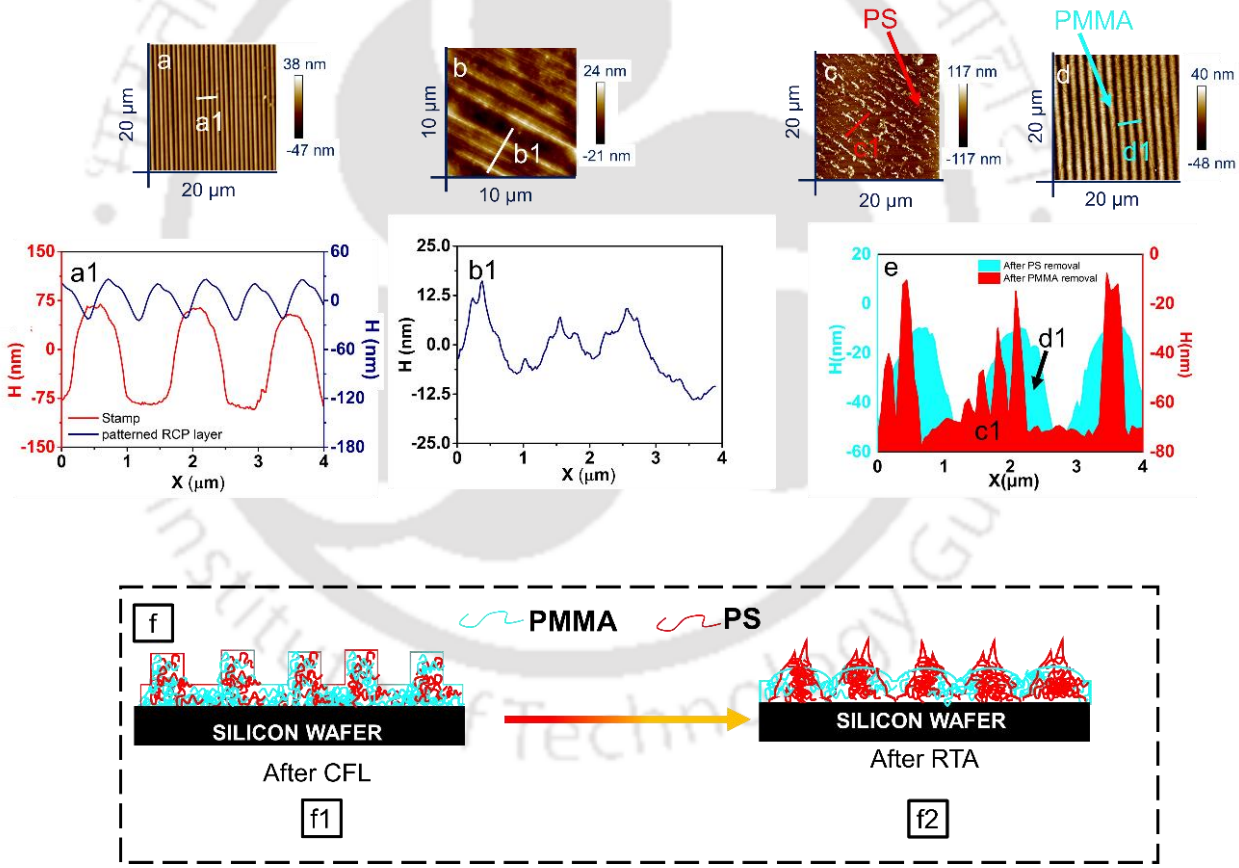

Figure 4.4. *The AFM images for RCP films (a) after capillary force lithography (CFL), (b) the CFL assisted patterned films after subjecting to rapid thermal annealing (RTA) (c) after immersion in acetic acid and (d) after immersion in cyclohexane. The corresponding line scans are shown in a1, b1 and e. Schematically the process is represented by (f).*

3.3 Phase separation in bilayer

Next, the blend solutions were spun coated over CFL-assisted pre-patterned RCP films. The blend solutions spun coated having the blend: toluene ratio as 90:10, 50:50, and 10:90 with sample codes A2, B2, and C2, respectively(**Table 4.2**). There is the negligible dissolution of polymer in the underlayer with the solvent in the upper layer.[34] The corresponding AFM images were shown in **Figure 4.5**. The upper blend layer forms a thin covering over the RCP underlayer with protruded droplets. Also, keeping the spin coating conditions same as case for blend over silicon wafer, it was found that phase separation has occurred immediately after spin coating (**Figure 4.5 a-c**). The PMMA chains present in blend upper layer lose toluene faster than PS chains as the PS chains have more affinity towards toluene than PMMA chains. This allows PMMA domains gets solidified in the form of droplets inside the matrix of PS domains, while PS chains still retained small amount of toluene.[34,40,41] Moreover, the protrusions present in underlayer increases the undulations in upper layer thereby providing more surface area and allowing polymers to rapidly get rid of solvent through evaporation. After solvent evaporation the bilayer system was subjected to RTA, the AFM images that were captured clearly show that the size of the droplets gradually decreased from sample A2 to sample C2 (**Figure 4.5 d-f**). Moreover, for sample A2 and B2, the blend droplets were random and irregular because the wavelength of dewetted blend droplets, λ_b (defined as the center-to-center distance between two droplets) is much greater than the wavelength of the patterned RCP layer, λ_p.The droplets were irregular due to the pinning of droplets with RCP underlayer, as shown in **Figures 4.4 g** and **Figures 4.h**. However, at comparable wavelengths, for sample C2, the blend droplets were beautifully placed between the protrusions present in the RCP film (**Figure 4.5 c**). The results obtained were in line with an existing report by Chen et al.[30]

***Table 4.2**: The data obtained for droplets formed when blend films spun coated upon patterned RCP underlayer were subjected to rapid thermal annealing (RTA).*

Sample	Blend: Toluene	After RTA		
		D (μm)	H (nm)	λ_b (μm)
A2	90:10	3.8 ± 0.11	250 ± 80	5.6 ± 1.22
B2	50:50	2.5± 0.74	200 ± 20	3.8 ± 0.47
C2	10:90	0.76 ± 0.05	55 ± 1.65	1.4 ± 0.22

Since the system under consideration consisted of a blend of homopolymers and random copolymers, it is required to check for the possible domain formation of the polymers after RTA. For that, selective etching of polymers was done using acetic acid and cyclohexane to remove PMMA and PS respectively, the procedure for the selective removal of polymers is described in the materials and method section. The AFM images captured were shown in **Figure 4.5 (g-l)**. As the PMMA chains are removed from the system using acetic acid, the PS chains form intriguing; the two length scale structures one from blend upper layer (diameter, d ~ 3 μm) and another from RCP underlayer (diameter, d ~ 0.5 μm). Likewise, for sample B2 and sample C2, the larger PS domains have a diameter, d~ 1 μm, and 0.77 μm, respectively (**Figure 4.5 j-l**). When PS domains were selectively removed, PMMA domains from the blend formed the ring in the upper layer, while RCP patterned underlayer formed the discontinuous ridges. As the blend concentration was reduced from sample A2 to sample C2, the ring diameter was also reduced, which finally formed an ordered arrangement of rings, as shown in **Figure 4.5 j-l**. The schematic representation is shown by m for bilayer after fabrication (m1) and after RTA (m2).

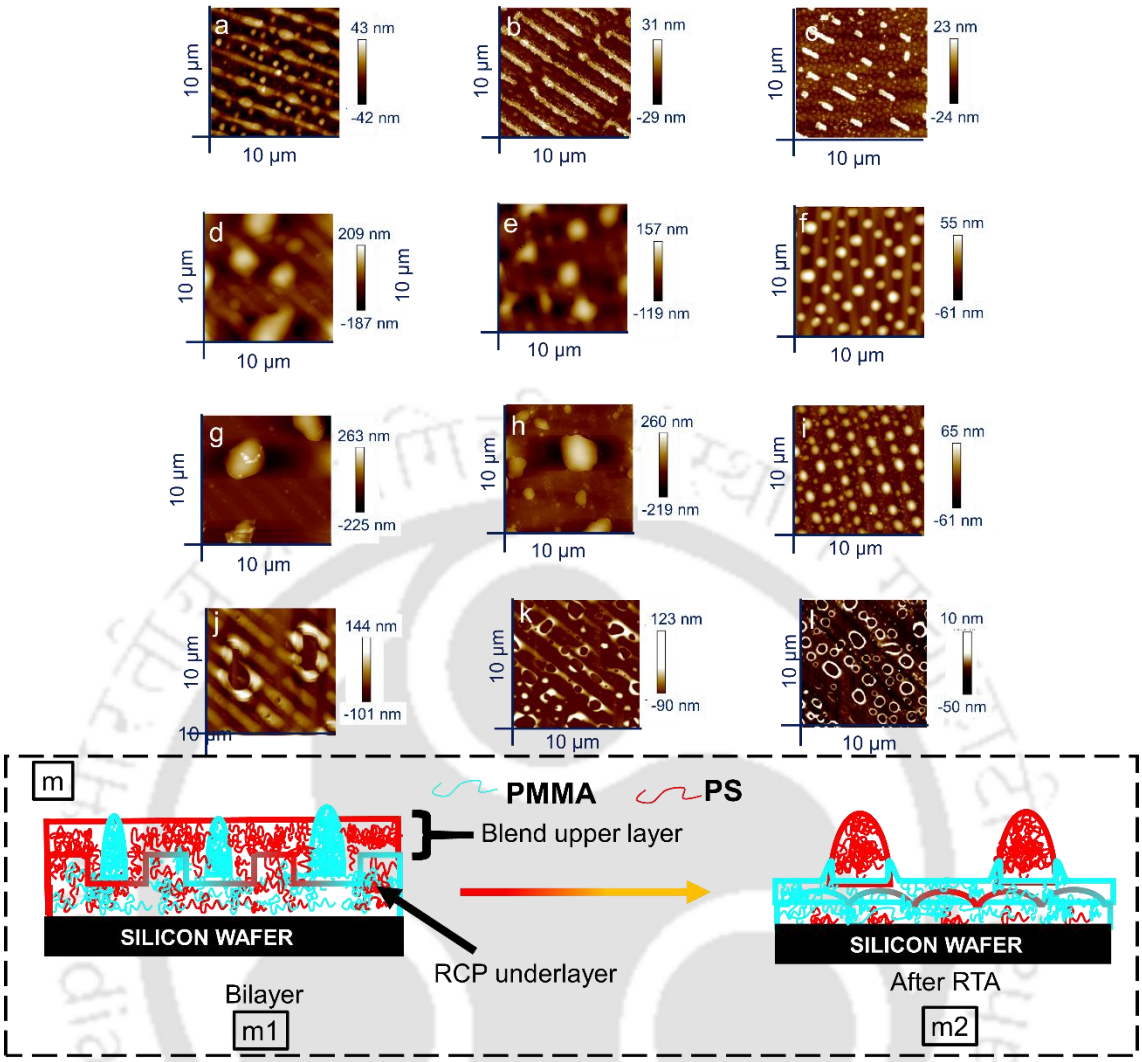

Figure 4.5*. The AFM images for blend spun coated over patterned RCP layer with a blend toluene ratio a) 90:10 (sample A2); b) 50:50 (sample B2) and c) 10:90 (sample C2). The corresponding AFM images captured after RTA were shown in d-f. After acetic acid treatment, the PS mound obtained was shown in g-i. Likewise, after cyclohexane treatment, the PMMA rims were shown in j-l. The schematic representation of the process is shown in m.*

4 CONCLUSIONS

The study presented here successfully demonstrates the facile, inexpensive, faster and generic method to fabricate multiple length scale structures. A polymer bilayer system was carefully designed such that the difference in chain length can give rise to multiple length scale structures. The key highlights of the work are as follows

1. The phase separation in blend of PS and PMMA generated larger domains whereas RCP resulted with smaller domains after phase separation.
2. Using a bilayer system with upper layer blend and under layer RCP can be used to fabricate bimodal phase separated domains
3. To achieve orderly arrangement, the under layer was patterned via. inexpensive capillary force lithography. The aluminium foils peeled off from CDs are used flexible moulds in the experiments.
4. Faster phase separation in polymer blend was achieved by using rapid thermal annealing (RTA).
5. The upper layer film thickness has direct impact on the randomness of the final morphology. When the film thickness was higher, the phase separated structures produced are random and larger in size (D~ 3.5 μm) in comparison to the structures present in the underlayer.
6. At lower film thickness, the wavelength of phase separated droplets matches with the wavelengths of the protrusions present in the under layer (D~ 0.76). Thereby, creating an orderly arrangement.

REFERENCES

(1) Ghasemlou, M.; Daver, F.; Ivanova, E. P.; Adhikari, B. Bio-Inspired Sustainable and Durable Superhydrophobic Materials: From Nature to Market. *J. Mater. Chem. A* **2019**, *7* (28), 16643–16670.

(2) Liu, K.; Jiang, L. Bio-Inspired Design of Multiscale Structures for Function Integration. *Nano Today* **2011**, *6* (2), 155–175.

(3) Desert, N.; Desert, T. N. Water Capture by a Desert Beetle. *Nature* **2001**, *414*

(November), 33–34.

(4) Munch, E.; Launey, M. E.; Alsem, D. H.; Saiz, E.; Tomsia, A. P.; Ritchie, R. O. Tough, Bio-Inspired Hybrid Materials. *Science* **2008**, *322*, 1516–1520.

(5) Muehlberger, M.; Ruttloff, S.; Nees, D.; Moharana, A.; Belegratis, M. R.; Taus, P.; Kopp, S.; Wanzenboeck, H. D.; Prinz, A.; Fechtig, D. Nanoimprint Replication of Biomimetic, Multilevel Undercut Nanostructures. *Nanomaterials* **2021**, *11* (4), 1–10.

(6) Thickett, S. C.; Neto, C.; Harris, A. T. Biomimetic Surface Coatings for Atmospheric Water Capture Prepared by Dewetting of Polymer Films. *Adv. Mater.* **2011**, *23* (32), 3718–3722.

(7) Jeong, H. E.; Kwak, R.; Khademhosseini, A.; Suh, K. Y. UV-Assisted Capillary Force Lithography for Engineering Biomimetic Multiscale Hierarchical Structures: From Lotus Leaf to Gecko Foot Hairs. *Nanoscale* **2009**, *1* (3), 331–338.

(8) Berkowski, K. L.; Plunkett, K. N.; Yu, Q.; Moore, J. S. Introduction to Photolithography: Preparation of Microscale Polymer Silhouettes. *J. Chem. Educ.* **2005**, *82* (9), 1365–1369.

(9) del Campo, A.; Arzt, E. Fabrication Approaches for Generating Complex Micro- and Nanopatterns on Polymeric Surfaces. *Chem. Rev.* **2008**, *108*, 911–945.

(10) Roy, P.; Mukherjee, R.; Bandyopadhyay, D.; Gooh Pattader, P. S. Electrodynamic-Contact-Line-Lithography with Nematic Liquid Crystals for Template-Less E-Writing of Mesopatterns on Soft Surfaces. *Nanoscale* **2019**, *11* (35), 16523–16533.

(11) Altissimo, M. E-Beam Lithography for Micro-/Nanofabrication. *Biomicrofluidics* **2010**, *4* (2), 026503.

(12) Verma, A.; Sharma, A. Self-Organized Nano-Lens Arrays by Intensified Dewetting of Electron Beam Modified Polymer Thin-Films. *Soft Matter* **2011**, *7* (23), 11119–11124.

(13) Pandey, A.; Maity, S.; Murmu, K.; Middya, S.; Bandyopadhyay, D.; Gooh Pattader, P. S. Self-Organization of Random Copolymers to Nanopatterns by Localized e-Beam Dosing. *Nanotechnology* **2021**, *32* (28), 285302.

(14) Perl, A.; Reinhoudt, D. N.; Huskens, J. Microcontact Printing: Limitations and Achievements. *Adv. Mater.* **2009**, *21*, 2257–2268.

(15) Wang, M.; Braun, H. G.; Kratzmüller, T.; Meyer, E. Patterning Polymers by Micro-Fluid-Contact Printing. *Adv. Mater.* **2001**, *13* (17), 1312–1317.

(16) Lackowski, W. M.; Ghosh, P.; Crooks, R. M. Micron-Scale Patterning of Hyperbranched Polymer Films by Micro-Contact Printing. *J. Am. Chem. Soc.* **1999**, *121* (6), 1419–1420.

(17) Xia, Y.; Whitesides, G. M. Soft Lithography. *Annu. Rev. Mater. Sci.* **1998**, *28* (1), 153–184.

(18) Murmu, K.; Burgula, K. P.; Gooh Pattader, P. S. Dynamic Contact Line Lithography: Template-Less Complex Meso-Patterning with Polystyrene and Poly(Methyl Methacrylate). *J. Colloid Interface Sci.* **2021**, *601*, 156–166.

(19) Xue, L.; Zhang, J.; Han, Y. Phase Separation Induced Ordered Patterns in Thin Polymer Blend Films. *Prog. Polym. Sci.* **2012**, *37* (4), 564–594.

(20) Orilall, M. C.; Wiesner, U. Block Copolymer Based Composition and Morphology Control in Nanostructured Hybrid Materials for Energy Conversion and Storage: Solar Cells, Batteries, and Fuel Cells. *Chem. Soc. Rev.* **2011**, *40* (2), 520–535.

(21) Roy, S.; Sharma, A. Self-Organized Morphological Evolution and Dewetting in Solvent Vapor Annealing of Spin Coated Polymer Blend Nanostructures. *J. Colloid Interface Sci.* **2015**, *449*, 215–225.

(22) Walheim, S.; Böltau, M.; Mlynek, J.; Krausch, G.; Steiner, U. Structure Formation via Polymer Demixing in Spin-Cast Films. *Macromolecules* **1997**, *30* (17), 4995–5003.

(23) Manias, E.; Utracki, L. A. *Polymer Blends Handbook*, Second.; Utracki, L. A., Wilkie, C. A., Eds.; Springer, 2014.

(24) Yu, H.; Qiu, X.; Moreno, N.; Ma, Z.; Calo, V. M.; Nunes, S. P.; Peinemann, K. V. Self-Assembled Asymmetric Block Copolymer Membranes: Bridging the Gap from Ultra- to Nanofiltration. *Angew. Chemie - Int. Ed.* **2015**, *54* (47), 13937–13941.

(25) Xue, L.; Zhang, J.; Han, Y. Phase Separation Induced Ordered Patterns in Thin Polymer Blend Films. *Prog. Polym. Sci.* **2012**, *37* (4), 564–594.

(26) Tanaka, K.; Takahara, A.; Kajiyama, T. Film Thickness Dependence of the Surface Structure of Immiscible Polystyrene/Poly(Methyl Methacrylate) Blends. *Macromolecules* **1996**, *29* (9), 3232–3239.

(27) Liu, X.; Bhandaru, N.; Banik, M.; Wang, X.; Al-Enizi, A. M.; Karim, A.; Mukherjee, R. Capillary Force Lithography Pattern-Directed Self-Assembly (CFL-PDSA) of Phase-Separating Polymer Blend Thin Films. *ACS Omega* **2018**, *3* (2), 2161–2168.

(28) Ermi, B. D.; Nisato, G.; Douglas, J. F.; Rogers, J. A.; Karim, A. Coupling between Phase Separation and Surface Deformation Modes in Self-Organizing Polymer Blend Films. *Phys. Rev. Lett.* **1998**, *81* (18), 3900–3903.

(29) Raczkowska, J.; Cyganik, P.; Budkowski, A.; Bernasik, A.; Rysz, J.; Raptis, I.; Czuba,

P.; Kowalski, K. Composition Effects in Polymer Blends Spin-Cast on Patterned Substrates. *Macromolecules* **2005**, *38* (20), 8486–8493.

(30) Chen, X. C.; Li, H. M.; Fang, F.; Wu, Y. W.; Wang, M.; Ma, G. Bin; Ma, Y. Q.; Shu, D. J.; Peng, R. W. Confinement-Induced Ordering in Dewetting and Phase Separation of Polymer Blend Films. *Adv. Mater.* **2012**, *24* (19), 2637–2641.

(31) Byun, M.; Hong, S. W.; Qiu, F.; Zou, Q.; Lin, Z. Evaporative Organization of Hierarchically Structured Polymer Blend Rings. *Macromolecules* **2008**, *41* (23), 9312–9317.

(32) Kim, J. Y.; Jin, H. M.; Jeong, S. J.; Chang, T.; Kim, B. H.; Cha, S. K.; Kim, J. S.; Shin, D. O.; Choi, J. Y.; Kim, J. H.; Yang, G. G.; Jeon, S.; Lee, Y. G.; Kim, K. M.; Shin, J.; Kim, S. O. Bimodal Phase Separated Block Copolymer/Homopolymer Blends Self-Assembly for Hierarchical Porous Metal Nanomesh Electrodes. *Nanoscale* **2018**, *10* (1), 100–108.

(33) Mukherjee, R.; Sharma, A.; Patil, G.; Faruqui, D.; Pattader, P. S. G. Soft Lithography Meets Self-Organization: Some New Developments in Meso-Patterning. *Bull. Mater. Sci.* **2008**, *31* (3), 249–261.

(34) Pandey, A.; Murmu, K.; Gooh Pattader, P. S. Non-Equilibrium Thermal Annealing of a Polymer Blend in Bilayer Settings for Complex Micro/Nano-Patterning. *RSC Adv.* **2021**, *11* (17), 10183–10193.

(35) Norrman, K.; Ghanbari-Siahkali, A.; Larsen, N. B. Studies of Spin-Coated Polymer Films. *Annu. Reports Prog. Chem. - Sect. C* **2005**, *101*, 174–201.

(36) Heriot, S. Y.; Jones, R. A. L. An Interfacial Instability in a Transient Wetting Layer Leads to Lateral Phase Separation in Thin Spin-Cast Polymer-Blend Films. *Nat. Mater.*

2005, *4* (10), 782–786.

(37) Rui, X.; Song, Z.; Jing, S.; Decheng, T. Phase Separation and Dewetting Induced Surface Pattern in PS/PMMA Blend Films. *Polym. J.* **2005**, *37* (8), 560–564.

(38) Li, X.; Han, Y.; An, L. Surface Morphology Control of Immiscible Polymer-Blend Thin Films. *Polymer (Guildf).* **2003**, *44* (26), 8155–8165.

(39) Ho, D.; Zou, J.; Zdyrko, B.; Iyer, K. S.; Luzinov, I. Capillary Force Lithography: The Versatility of This Facile Approach in Developing Nanoscale Applications. *Nanoscale* **2015**, *7* (2), 401–414.

(40) Barton, A. F. M. Solubility Parameters. *Chem. Rev.* **1975**, *75* (6), 731–753.

(41) Vandenburg, H. J.; Clifford, A. A.; Bartle, K. D.; Carlson, R. E.; Carroll, J.; Newton, I. D. A Simple Solvent Selection Method for Accelerated Solvent Extraction of Additives from Polymers. *Analyst* **1999**, *124* (11), 1707–1710.

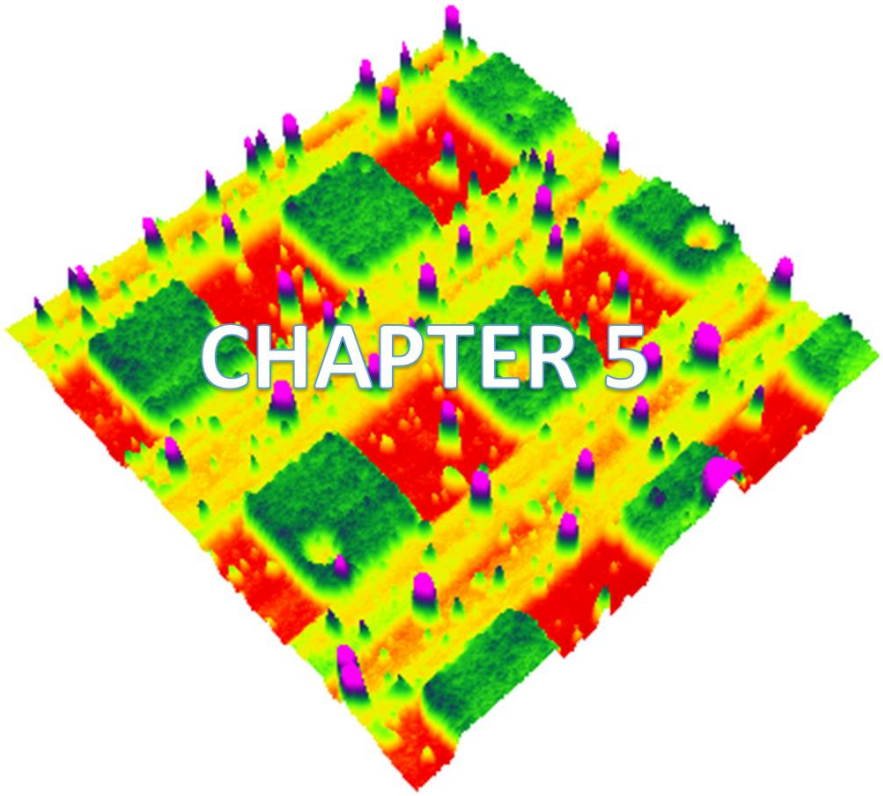

CHAPTER 5

Chapter 5

Complex nanostructure generation by e-beam lithography on a random block copolymer thin-film

GRAPHICAL ABSTRACT

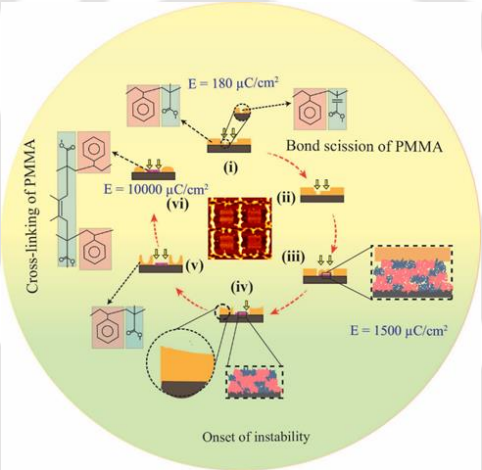

ABSTRACT

A strategic electron beam (e-beam) irradiation on the surface of a PS-PMMA random copolymer ultrathin (< 100 nm) film followed by solvent annealing stimulate a special variety of dewetting, leading to a large-area hierarchical nanoscale patterns. For this purpose, initially, a negative (positive) tone of resist PS (PMMA) under a weak e-beam exposure is exploited to produce an array of sites composed of crosslinked PS (chain-scissioned PMMA). Subsequently, annealing with the help of a developer solvent engenders dewetted patterns in the exposed zones where PMMA blocks are confined by the blocks of cross-linked PS. The e-beam dosage has been systematically varied from 180 μC/cm^2 to 10,000 μC/cm^2 to explore the tone reversal behavior of PMMA on the dewetted patterns. Remarkably, at a relatively higher e-beam dosing, both PMMA and PS blocks act as negative tones in exposed zone. In contrast, the chain-scission of PMMA in the periphery of the exposed regions due to scattered secondary electrons causes confined dewetting upon solvent annealing. Such occurrences eventually leads to an order of magnitude pattern miniaturization than the conventional thermal or solvent vapor annealed dewetting. Selective removal of PMMA blocks of RCP using suitable solvent provide additional 50% size reduction of the dewetted features.

Keywords: *dewetting, random-co-polymer, electron beam lithography, patterning, tone reversal resist*

1. INTRODUCTION

Photoactive polymers can undergo scission or linking of chains under the exposure of an electromagnetic irradiation.[1] Such properties of polymeric materials are very often employed in diverse micro/nano fabrication techniques which include electron beam (EBL), [2] X-ray, [3,4] Deep-UV, UV, [5] or photo-lithography (PL).[6] While the photon or electron induced scission of polymer bonds in a positive-resist, the negative-resist undergoes cross-linking of the chains during its interactions with the electromagnetic waves.[7] Importantly, the chain scission (cross linking) always leads to the reduction (increase) in the molecular weight in the area of electromagnetic exposure, which eventually increase (decrease) the solubility of the polymer in the developer solvent. [7] Thus, upon developing, the irradiated zone of a photo-resist is either removed or retained based on whether it is of positive or negative tone. Exploiting such properties of materials, PL [6] has widely been employed for large-area micro-fabrication while EBL has been employed to decorate ordered nanopatterns. [2] Such micro/nano structured surfaces find extensive applications in the areas involving micro/nano electronics, [8] optoelectronics, [9,10] bioMEMS, [11] membranes, [12] biosensors, [13,14] nanophotonics, [15] or photodetection [16] among others.

Of late, fabrication of large-area nano-patterns using EBL has been scaled-up to the level of the industrial manufacturing of various state-of-art nano-electronic devices such as smart phones, tablets, ipods, ipads, or flexible electronic gadgets, among many others. In general, while fabricating the nanostructures using EBL, the most frequently used positive tone resists are PMMA – poly methyl-methacrylate, [17] ZEP – a co-polymer of chloro-methacrylate and methylstyrene, [17] poly-butene-1-sulfone (PBS) [18] and EBR-9 – a co-polymer of tri-fluoroethyl a-chloro-acrylate and tetra-fluropropyl a-chloroacrylate. [18] On the other hand, HSQ – hydrogen silsesqioaxene,[19] Calixarene – Tokuyama Corp.,[20] SU-8 – Microchem

Corp., [21] mr-L 6000 – Microresist Technology, [21] and PS – poly-styrene [17] have been extensively used as the negative e-beam resists. However, a number of modern mesoscale applications often demand the fabrication of surfaces with complex and hierarchical structures, which are rather difficult to decorate using any of the conventional lithographic techniques. [22,23] In addition, since most of the lithographic processes are costly, they require a large-scale production to meet the economic viability of patterning processes. [24] Such roadblocks kindle the exploration of more economic soft-lithographic pathways to fabricate large-area periodic nanostructures.[25]

In this direction, the self-organized dewetting [26–29] or electric field induced lithography (EFL) [30–33] of thin polymeric films have emerged to be simple but cost-effective techniques of micro/nano fabrication. For example, beyond its glass transition point (T_g), an ultrathin (< 10 nm) polymer film can self-organize into micro/nano patterns under the influence of destabilizing van der Waals interactions, which is also popularly known as *spinodal dewetting*. [34] On the other hand, relatively thicker films (> 40 nm) can self-organize into mesoscale patterns when the physicochemical heterogeneities on the underlying surface trigger the film disintegration, commonly known as *heterogeneous nucleation* or *pattern directed dewetting*.[35] The prior-arts suggest that a typical diameter (D) of the post-dewetted droplets may vary with the film thickness (h) following the correlation, $D \sim h^{1.5}$. This means that the films of thicknesses ranging from 10 nm to 50 nm thickness may form droplets of size ranging from ~ 4 to 15 µm, depending on the variations in properties of the underlying substrates. [36–38] However, as per current technological demands, such feature sizes are quite large and in the past few decades, one of the major goals of such top-down soft-lithography has been the miniaturization of size and periodicity of patterns by a few orders of magnitude.[25]

Intuitively, one of the possible pathways of size reduction can be to increase the number of sites for rupture on the film surface while maintaining periodicity with the help of lateral confinements.[39,40] For example, if we consider a thin film of random or block copolymer (RCP or BCP) composed of polymers with positive and negative tones, a number of nucleation sites for dewetting can be generated in the zones with positive tone upon electromagnetic irradiation. In parallel, the same electromagnetic exposure may also create zone of confinements by cross-linking the polymeric chains of negative tone present in the film. Thus, a strategic exposure of an electromagnetic wave on such a copolymer may generate periodic zones of cross-linking (negative tone) and dewetting (positive tone). In such a scenario, the resolution of the patterns may be controlled simply by tuning the wavelength of the electromagnetic exposure.[41] A preferential removal of a particular block using a selective solvent may also help in the further miniaturization of patterns alongside opening up the possibility of fabricating hierarchical patterns.

In view of background ideation, herein we choose to use a random copolymer (RCP), PS-r-PMMA in which PS acts as the negative tone while PMMA acts as the positive tone to electron beam (e-beam). Under a low intensity e-beam exposure such a RCP film is expected to create a dewetting zone in the PMMA blocks and cross-linking zone in the PS blocks. After the e-beam exposure, we anneal the films with PMMA selective solvents to undergo a room temperature dewetting near the positive tone blocks. In the process, due to reduced interfacial tension at liquid solvent/polymer interface,[42–45] the size reduction is already achieved in the zones of dewetting in between an array of periodic cross-linked PS patterns. The post-dewetted patterns were further miniaturized by ~50% with the help of another set of solvent selective removal of PS (PMMA) using cyclohexane (acetic acid).[46,47] Subsequently, the effects of e-beam dose on the ultrathin PS-r-PMMA film have been systematically explored.

Remarkably, at a higher e-beam dosing, along with the PS blocks, PMMA blocks also switches to the negative tone behavior of crosslinking rather than undergoing chain scission, in the zones of exposure [48,49] (Appendix 4). However, in the adjacent unexposed zones the PMMA blocks start showing the positive tone behavior owing to the scattering effects of the electrons at high e-beam intensities, which we exploit in the fabrication of further miniaturized patterns.

Concisely, harnessing the fundamental chemistry of a RCP, we uncover a novel self-organized soft-lithographic process, which can lead to multi-scale ordered nanopatterns. Along with the individual advantages of the EBL to offer and a co-polymer, for its tendency to ordered self-assembly, this proposed method demonstrate how single copolymer resist can be utilized to generate myriads of micro-nano hierarchical features just by controlling the e-beam dose that modifies the chemistry of one component of the copolymer. The shape, size and periodicity of the nanopatterns obtained from this technique is expected to match any other state-of-art lithography or self-organization techniques.

2. MATERIALS AND METHODS

2.1 Sample preparation

Silicon (Si) wafer was cut into 1 cm × 1 cm pieces and cleaned thoroughly using acetone, isopropanol, and water in sequence before keeping in piranha solution – a mixture of concentrated H_2SO_4 and H_2O_2 in 1:3 volume ratio, for 30 min. Adequate safety protocol was followed while cleaning substrates using piranha solution. The Si wafer pieces were then taken out of piranha solution carefully and after thorough rinsing with copious amount of deionized water, the substrates were dried in nitrogen stream. The PS-r-PMMA random copolymer (RCP) (Sigma Aldrich), having polystyrene (PS) and polymethyl methacrylate (PMMA) blocks in 40:60 ratio (weight average molecular weight, $M_w \sim 100000$-150000), was dissolved in toluene

to have 1% (w/v) RCP solution. The RCP solution was then spin-coated (spin speed 5000 rpm, duration 2 min) over the cleaned silicon wafer pieces and left to dry for 12 h in a vacuum desiccator. The thickness of the film (~ 45 nm) was measured using single wavelength (658 nm) ellipsometer (Nanofilm_ep3-sw, Accurion Gmbh., Germany).

2.2 Patterning with EBL

The line and box patterns were fabricated using an Electron Beam Lithography (EBL) setup (XeDraw 2, XENOS Semiconductor Technologies GmBH, Germany), which was coupled with Field Emission Scanning Electron Microscope (JSM 7610F, JEOL Japan) for the characterization. The 1 µm wide lines having 1 µm spacing in between and 1 µm × 1 µm squares were separately patterned at different exposure doses ranging from 180 µC/cm^2 to 10,000 µC/cm^2. An optimized acceleration potential of 30 kV was chosen for EBL while the beam current was set and maintained at 100 pA. Post exposure, the samples were treated with methyl isobutyl ketone (MIBK) for 3 min before dipping into iso-propanol (IPA). MIBK and IPA are the good solvents for low molecular weight PMMA.[50] After developing, the samples were dried in nitrogen flow.

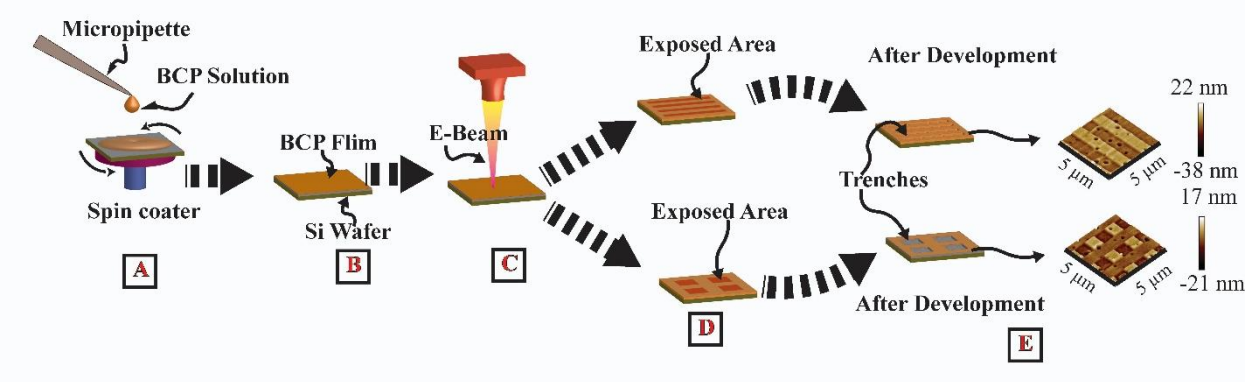

Figure 5.1. *Schematic of the experimental process is depicted. (A) and (B) spin coating of PS-r-PMMA film over silicon wafer, (C) electron beam exposure of the RCP thin film, (D) line and box patterned exposure, and (E) development using solvent to obtain final structures. Typical AFM images showing morphological pattern occurring in random copolymer film.*

2.3 Characterization

After drying in nitrogen stream, the developed patterns were characterized using atomic force microscopy (AFM) (Bruker, Innova series) in tapping mode. A sharp-edged antimony doped silicon tip (TESPA-V2, Bruker) having resistivity of 0.01-0.025 Ohm-cm with resonance frequency of 320 kHz and force constant of 42 N/m was used for imaging the samples. The scan rate was maintained at 0.7-0.8 Hz. All the scans presented here are of fixed dimension (5 μm × 5 μm) unless otherwise mentioned. To determine the possible organization of the polymer, selective good solvents like acetic acid (for PMMA removal) or cyclohexane (for PS removal) were used for wet etching of the respective polymer block by dipping the samples in it for 5 min. The resulted morphology was then characterized by AFM.

3. RESULTS

3.1 Phenomenon

EBL was performed to draw lines on the RCP film of thickness ~45 ± 3 nm in which the width of lines and the spacing in between two lines were 1 μm each. Images (A) – (E) in the **Figure 5.1** schematically show the typical steps to the EBL writing on the RCP film. AFM images (not shown here) at the stage (D) before the solvent was employed to develop the RCP film confirmed that the films were rather undamaged even after the exposure of e-beam. However, the AFM images in the **Figure 5.2** and **Figure 5.3** show the myriad of morphologies, after the solvent treatment stage (E) in the **Figure 5.1**. These figures confirmed that the RCP films underwent a localized room temperature dewetting [42,43] during the solvent annealing after the e-beam exposure. The influence of the progressive increase in the dosage (180 μC/cm^2 to 10,000 μC/cm^2) of e-beam on such dewetted morphologies have also been elaborated in the **Figure 5.2** and **Figure 5.3**.

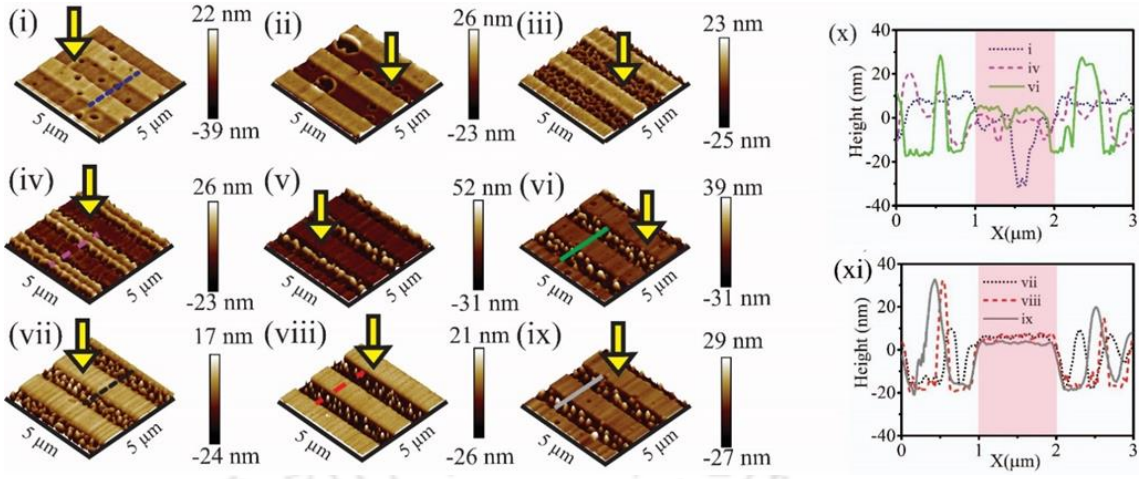

***Figure 5.2**. AFM images showing morphological 1-D patterns on a PS-r-PMMA film when exposed with variable dose of e-beam and subsequent developing in MIBK/IPA. The e-beam dose used were, (i) 180 µC/cm^2 (ii) 700 µC/cm^2 (iii) 1500 µC/cm^2 (iv) 3000 µC/cm^2 (v) 5000 µC/cm^2 (vi) 6000 µC/cm^2 (vii) 10,000 µC/cm^2. The sample (vii) was further treated with acetic acid for selective PMMA removal to obtain (viii) and selective PS removal by cyclohexane to obtain (ix). The line scans on the images (i) – (ix) are shown by plots (x). See section S4 of the Appendix 4 for the representative FESEM images of the 1-D patterns.*

For example, the case associated with the e-beam dose of 180 µC/cm^2 is shown in **Figure 5.2 (i)** and corresponding line scan is shown by (i) in **Figure 5.2 (x)**. The Figure disclosed that after the e-beam dose and solvent methyl isobutyl ketone/iso-propanol (MIBK/IPA) annealing, the depth of the stripe patterns in the zones of exposure, as indicated by the arrow, was ~ 10 nm. This is because, in the zone of exposure the positive tone PMMA underwent chain scission, while the negative tone PS underwent cross-linking under the weak e-beam exposure. Thus, after the solvent treatment, the scissored PMMA part of RCP was removed from the exposed area leading to a 'running trench' of depth 10 nm in between the unexposed 'ridges' of the polymer film. Since MIBK/IPA was expected to remove only exposed PMMA with a very low molecular weight (low-MW), the PMMA in the unexposed part remained intact [51]. Remarkably, during this experiment, we could also observe the formation of an array of randomly placed holes on the surface of the polymer film. The average diameter of the holes was ~400 nm and the depth of the holes was ~28 nm in the exposed area while 38 nm in the

unexposed zones. This experiment gave us the hint of the possibility of solvent induced dewetting of such systems leading to nanostructures, which we explored further with the help of a stronger e-beam exposure.

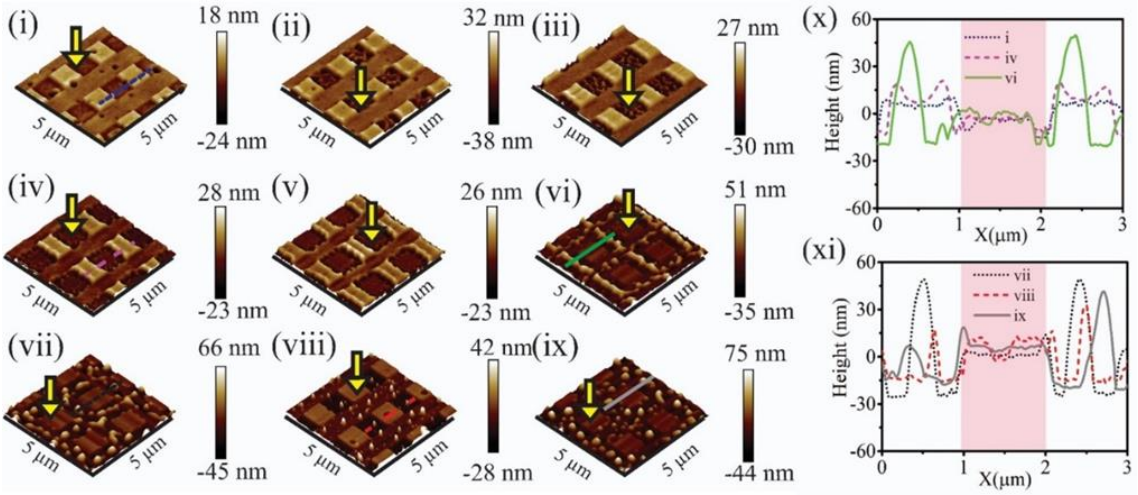

***Figure 5.3**. AFM images showing morphological 2-D patterns occurring on a PS-r-PMMA film when exposed with variable dose of e-beam and subsequent developing in MIBK/IPA. The e-beam dose used were, (i) 180 µC/cm^2 (ii) 700 µC/cm^2 (iii) 1500 µC/cm^2 (iv) 3000 µC/cm^2 (v) 5000 µC/cm^2 (vi) 6000 µC/cm^2 (vii) 10,000 µC/cm^2. Morphology after PMMA removal (viii) and PS removal (ix) using selective solvent washing of sample (vii) is shown. The corresponding line scans are shown by graphs (x), and (xi). The arrow in the AFM image and shaded region in the line scan show the region of e-beam exposure. See section S5 of the Appendix 4 for the representative FESEM images of the 2-D patterns.*

For example, after an e-beam dose of 700 µC/cm^2 followed by MIBK/IPA annealing, the holes became larger (diameter ~ 800 nm) and irregular (**Figure 5.2(ii)**) in shape. This is rather anticipated because the copolymer was PMMA rich and a stronger exposure of e-beam led to a significant chain scission of PMMA, which eventually led to the dewetting of the films at the zones of the exposure upon solvent annealing. On the other hand, the negative tone PS part underwent cross linking under the e-beam exposure, which retained a part of the film at the zone of exposure after solvent treatment. Importantly, the morphologies of the holes at the zone of exposure resembled the onset of dewetting through heterogeneous nucleation.[52] Further, most of the holes were nucleated near the junctions of the zones of exposure and non-exposure, which is another characteristic of pattern directed dewetting. The line scan (Figure S2 of

APPENDIX 4) revealed the presence of mesoscale irregular PS nano-debris with a lateral dimension of ~200 nm inside the nucleated holes after the MIBK treatment [38]. Again, since the MIBK/IPA could only remove the e-beam scissored low-MW PMMA, the PMMA blocks in the unexposed part remained undisturbed during the solvent treatment.

Remarkably, at an e-beam dose to 1500 μC/cm^2 and after the MIBK treatment (**Figure 5.2 (iii)**), the morphologies at the zone of exposure resembled the onset of solvent annealed spinodal dewetting [43]. The height of these interconnected polymer ribbons was found to be of the order of ~17 nm, which was much smaller than the initial film thickness (~45 nm). It is well known that for the low dose of electron, PMMA acts like a positive resist, i.e. the bond scission takes place and the molecular weight of PMMA becomes sufficiently lower to be etched out easily by a good solvent like MIBK/IPA. On the other hand, PS, although not as sensitive as PMMA, acts like a negative resist and cross-linking takes place while exposed to e-beam.[17] However, at a higher dose of electron beam (typically above ~1000 μC/cm^2) both PS and PMMA act like negative tone resists.[53,54] Interestingly, near the borderline of this tone reversal behavior of the copolymer, we observed the spinodal dewetting behavior of the RCP film at the zone of exposure.

It may also be noted here that during the e-beam exposure, the primary electrons could generate the secondary ones in the unexposed RCP matrix due to inelastic scattering within the resist.[55] Subsequently, the scattered electrons penetrated through a larger volume of resist than only the exposed zone, which widened the area of exposure. The range of influence of such scattered electrons were typically of the order of tens of nanometers away from the zone of exposure.[56] The scattered electron also included the back-scattered ones, to enhance the influence of the irradiation in the zones nearby to the exposed area [57–59] and a higher the

dose of e-beam led to a wider area of influence around the exposed area.[60] We exploited these effects for further investigation of the system with an e-beam dose of 3000 μC/cm^2.

In such a scenario, after the e-beam exposure followed by the MIBK/IPA treatment, the expose area underwent cross-linking as both PS and PMMA blocks behaved as negative tones due to the tone reversal of the PMMA in the area of exposure (**Figure 5.2 (iv)** and line scan (iv) in **Figure 5.2 (x)**). However, the effects of the scattered electrons became evident at the edge of the exposed regime by the slight dip in the line scan. The irregular rims at the boundaries of the unexposed and exposed regimes confirmed the chain scission of PMMA blocks in the unexposed regimes due to the scattered electrons. This was also evident by the reduction of the width of the unexposed region to ~650 nm from 1 μm. Subsequently, with solvent annealing, the dewetting phenomena is found to happen in the unexposed zone while the exposed zone remained cross-linked after the tone reversal of PMMA.

Hereafter, upon increasing the dose of the e-beam, the exposed zone started showing the formation of smooth ridges while the unexposed areas started showing dewetted morphologies (**Figure 5.2 (v) – 2 (viii)**). At an e-beam dose of 5000 μC/cm^2 considerable thinning of the unexposed region was observed (**Figure 5.2 (v)**) while the rims at the unexposed zones merged to form a nanothread of width ~ 200 nm and a collection of nanodroplets. The nano threads in the unexposed region underwent capillary instability to form the nanodroplets of polymer at a relatively higher intensity of e-beam (6000 μC/cm^2) (**Figure 5.2 (vi)** and line scan (vi) in **Figure 5.2 (x)**). Finally, at the 10,000 μC/cm^2 the a complete dewetting of the films were observed at the unexposed zones where the droplets had average diameter of ~274 nm (**Figure 5.2 (vii)** with corresponding line scan (vii) in **Figure 5.2 (xi)**). In order to investigate the polymer configuration within a droplet (**Figure 5.2 (vii)**), selective etching of polymer was performed using good solvent for the blocks of the RCP. Subsequently, the average droplet

size diminished to ~160 nm (**Figure 5.2 (viii)**) upon washing with the acetic acid to remove PMMA. Surprisingly, upon washing with cyclohexane, which is a good solvent for PS, the average droplet size did not change much. Thus, the droplets were perhaps composed of a PMMA shell protecting the inside PS core – MIBK/IPA being a better solvent to PMMA than PS facilitates the migration of PMMA blocks to the periphery of the droplets. Importantly, a host of similar experiments were performed with another set of samples of ~45 nm thick RCP films using e-beam wherein an array of periodic two-dimensional (2-D) box patterns were fabricated. Again, as observed in the **Figure 5.2**, depending on the doses of the e-beam, different patterns were achieved after the MIBK/IPA treatment, as shown in the **Figure 5.3**.

Figure 5.3 (i) - (vii) show the occurrence of exact set of events for the 2-D patterns, which was previously described with **Figure 5.2** with the variation in the e-beam dose. Ultimately, at a very high dose (10,000 μC/cm^2), a flat square plateau (exposed area) surrounded by dewetted droplets of polymer blocks were obtained (**Figure 5.3 (vii)**). All the line scan of the AFM images of **Figure 5.3** have been included in the Figure S3 of the APPENDIX 4 section. The images suggest that we could generate 2-D patterns of similar variety with the variation in the strength of e-beam exposure, as observed in the **Figure 5.2**. The experiments in the **Figure 5.2** and **Figure 5.3** together suggest that the proposed soft-lithographic process was rather repeatable.

4. DISCUSSIONS

4.1 Characteristics of Dewetting

In what follows, we investigate three parameters associated with the sub-micron structures formed in the unexposed region of the samples after irradiation with 10,000 μC/cm^2: (i) the number density, N, which is defined as the number of sub-micron features per unit area; (ii) characteristic length scale or wavelength of the pattern, λ, which is the average center-to-center

distance of the features; and (iii) feature size, *D*, the diameter of a droplet or the width of minor axis for an elongated droplet. The summary of these parameters for both the line and box patterns are depicted in **Figure 5.4**. In case of line pattern, the number density, wavelength and average diameter was found to be ~ 2.88 μm^{-2}, ~0.37 μm and ~ 170 nm, respectively. The length scale and the drop diameter were much smaller than the periodicity (~40 μm) and size (~5-15 μm) of drops generated from the thermally or solvent vapor assisted dewetted morphology of a ~45 nm flat PS film.[28,43] The comparison suggests a reduction of more than one order of magnitude in feature dimension employing the proposed methodology of e-beam dosing followed by solvent annealing. Polymer thin films undergoing physical [29] or chemical [61] patterns have already been known for miniaturization of the length scale of dewetting. However, the methodology proposed in this work simultaneously hits a couple of targets that are perhaps unique: (i) the e-beam dosing on a copolymer film with positive and negative tones generate numerous localized sites in the film matrix, especially in the blocks of positive tone, suitable for solvent annealed dewetting; and (ii) in parallel, the negative tones under exposure generate cross-linked boundaries to maintain periodicity of the quarantined patterns, which is perhaps unique.[62,63] It may be noted here that, although the experiments reported here employed an EBL for the strategic e-beam dosing, the same is possible even with a low resource setup composed of an electron gun and a beam blanker. Thus, overall, the proposed soft-lithography technique can generate nanoscale features with a large-area ordering at a much lower resource setting.

The use of PS-r-PMMA as the ultrathin film offered an opportunity for further reduction in the feature size. After selective washing of PS with cyclohexane, the feature size and other parameters remained nearly similar to that of unwashed sample. Whereas, by selective removal of PMMA, the average feature size was reduced to *D* ~114 nm, which was nearly of 50%

reduction, as compared to the unwashed sample (**Figure 5.4(c)**). The number density of the sub-micron features for the box-pattern was nearly similar to that of the line patterns. However, the periodicity of such high-density patterns generated, λ, remained rather unchanged after selective removal of the PMMA or PS (**Figure 5.4(b)**), which was rather obvious. Only reduction of the diameter of the droplets suggested the formation of the droplet with PMMA-shell and PS-core, as shown in the **Figure 5.4(d)**. The results shown here indicate that the ordering, size and periodicity of the morphologies can be tuned further by simply modulating the RCP film thickness, e-beam dosage, and the pattern of e-beam exposure. Of course, composition and molecular weight of the blocks of the copolymer has an important role to play in deciding the sensitivity of the chain scissions, crosslinking during the e-beam exposure, and response towards the solvent annealing.[64]

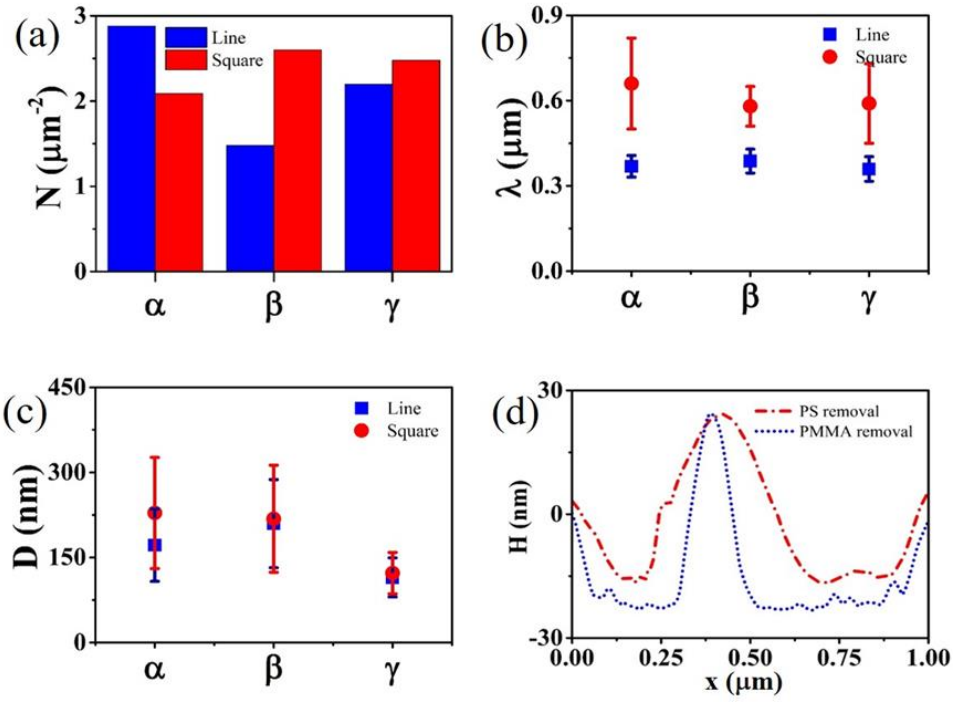

Figure 5.4*. The plots showing variations in (a) number density, N; (b) wavelength, λ and (c) average characteristic length scale (diameter of droplet or width of rims), D, for line and box patterns generated after exposing with e-beam with dose of 10,000 μC/cm^2. The α, β and γ represents condition after e-beam lithography with e-dose of 10,000 μC/cm^2, after PS removal from state α using cyclohexane and finally PMMA removal using acetic acid from state α,*

respectively. (d) represents typical line scan of the polymer droplet after selective removal of a component polymer.

4.2 Scientific basis

Polymer resists upon irradiation with e-beam can undergo several simultaneous processes. Irradiation electron can excite the polymer molecules and/or ionize the polymer and generate secondary electrons, ions, or free radicals while penetrating through the polymer matrix. Secondary electrons can also be generated due to the back scattering from the substrate. Much like primary electrons, the secondary electrons are also capable of transferring energy by excitation and subsequent thermal stabilization along with ionization or free radical formation. The fate of polymer materials under an electromagnetic irradiation depends on several factors such as linear energy transfer (LET), dose rate, or temperature.[65] In presence of oxygen, these polymers may also undergo oxidative degradation.[66] The bond scission and crosslinking are the two competing processes within polymer when irradiated with e-beam.

Different polymers demonstrate different level of sensitivity towards e-beam and prone to follow one of the two processes mentioned, based on which chemical yield is decided. Chemical yield (G) is defined as the number of molecules reacted per 100 eV of absorbed energy. G value for crosslinking, G(X), chain scission, G(S), and the ratio of these two parameters, i.e. G(S):G(X) are three important parameters for a particular polymer. At a lower dose of e-beam, it is reported that the ratio G(S):G(X) is >2 for PMMA and < 0.4 for PS along with very low G(X) value for PS. These values indicate that PMMA is more prone to bond scission (positive tone behavior), whereas, PS is likely to undergo crosslinking of the chain (negative tone behavior), however, with much less sensitivity to the e-beam as compared to PMMA.[66] Thus, the overall process is largely dominated by the response of the PMMA block to the e-beam. Further, operating condition dependent tone reversal behavior of a few polymers are well known. For example, temperature dependent tone switching behavior of

PTFE is reported in literature.[66] Here, the positive tone behavior of PMMA resist at low electron dose switches to negative tone at a higher dose of electrons.[53] Previously, this unique behavior of PMMA was exploited to improve the resolution of e-beam lithography.[48] At a lower e-dose, a simplistic reaction scheme for PMMA chain scission is depicted in **Scheme 5.1(a)**,[67] and at a higher e-beam dose the crosslinking scheme is shown in **Scheme 5.1(b)**.[4]

In this present study, at a lower dose of 180 μC/cm^2 to 1000 μC/cm^2, the trenches were formed in the exposed region due to the bond scission of PMMA during the e-beam exposure and subsequent removal of the broken PMMA chains at developing stage.[68] At a relatively higher e-beam dosage (1500 μC/cm^2 to 10,000 μC/cm^2), the crosslinking of PS and PMMA increased the molecular weight polymer blocks in the exposed regime to generate the periodic confinements. Subsequently, the effects of the secondary electrons started breaking down of the PMMA in the unexposed areas to engender solvent induced dewetting. The sequences of the events process including the, (i) hole formation and bond-scission in the exposed zone at a weaker exposure; (ii) tone reversal in the exposed zone to form the crosslinked PS-PMMA; (iii) instability in the unexposed area due to the effects of scattered electrons on the PMMA blocks; and (iv) drop formation in the unexposed area and crosslinking in the exposed area at a higher e-beam exposure, have been depicted in a step wise manner in the **Figure 5.5**.

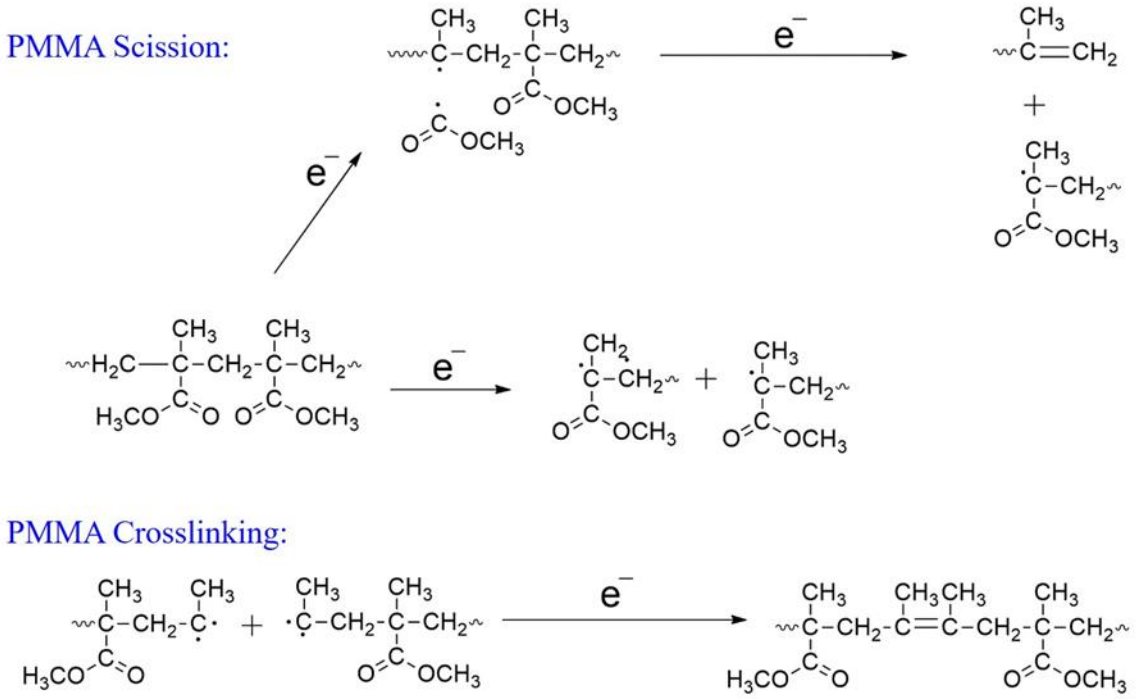

***Scheme 5.1**. Chain scission (a) and crosslinking (b) of PMMA blocks at lower and higher e-beam doses respectively.*

***Table 5.1**: Summary of polymer behavior with e-dose.*

e-dose	Exposed Area		Unexposed area	
	PMMA	**PS**	**PMMA**	**PS**
Low	Scission	Cross-linking	Unaltered	Unaltered
Medium	Partial Cross-linking	Cross Linking	Partial scission	Unaltered
High	Cross-linking	Cross Linking	Scission	Partial Cross-linking

Importantly, as the e-beam dosage increased, the exposed spot also attained higher mean temperature with expanding standard deviation of the Gaussian thermal profile. The Exposure Intensity Distribution (EID) of the e-beam follows an additive Gaussian pattern for primary and secondary backscattered electrons as [59], $I_p = C_p \exp\left[-\left(\frac{r}{B_p}\right)^2\right]$ and $I_s = C_s \exp\left[-\left(\frac{r}{B_s}\right)^2\right]$, respectively where r is the distance from the center of the e-beam while C_p, C_s, B_p, and B_s are the constants, which depend on the e-beam dose, type of polymer or resists, or substrate materials, among others. The energy distribution of an e-beam also follows the additive Gaussian distribution [69] similar to EID (see section S6 of the APPENDIX 4). The lateral resolution of EBL reduced with relatively thicker film and with a higher e-beam dose due to the formation of secondary electrons.[70] This double Gaussian exposure to the RCP film at a higher e-beam dose resulted in core cross-linked zone and a peripheral scission zone for PMMA, which in turn resulted a narrow polymer free zone, removed at the developing stage. Beyond this exposed zone, due to expanded thermal profile induced by a higher e-beam dosage, the RCP underwent chain scission, which was suitable for the solvent annealed dewetting during the development stage.

The profile at the top of **Figure 5.6** shows a schematic of the typical intensity distribution (black line) of a double Gaussian exposure alongside the possible thermal profile (green line) as a function of, *r*, from the center of the e-beam exposure. The profile in the middle depicts the extent of crosslinked (1, brown) and degraded (2, light blue) and dewetted (3, light green) zones under such an e-beam exposure. A typical line scale with an AFM image at the bottom of **Figure 5.6** provides an experimental evidence against the theoretical predictions.

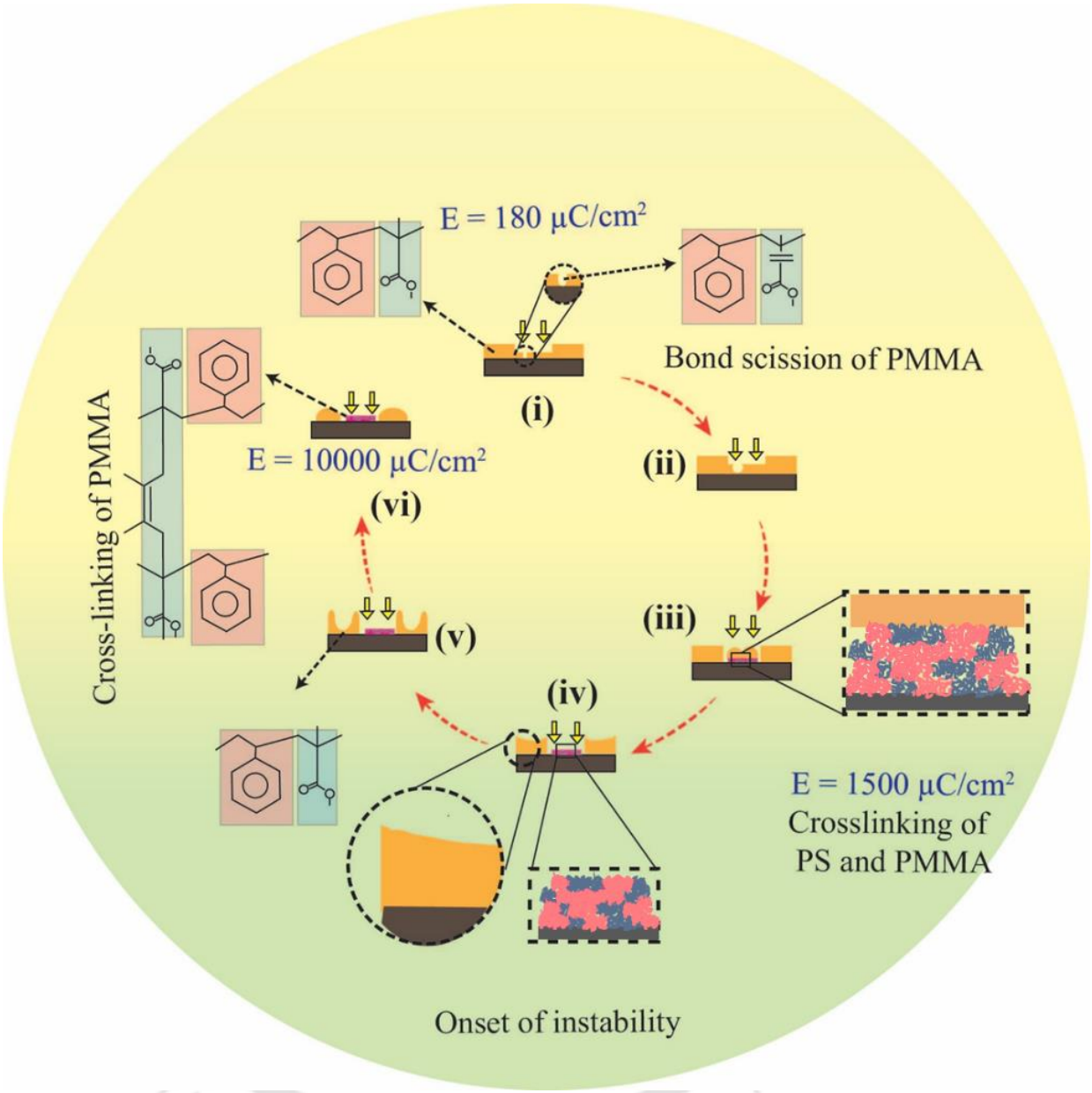

***Figure 5.5**. The schematic representation showing the mechanism for morphological changes occurring at varying dose of e-beam viz. (i) 180 µC/cm² (ii) 300-700 µC/cm² (iii) 1500 µC/cm² (iv) 2000 µC/cm² (v) 3000 µC/cm² and (vi) 6000-10000 µC/cm².*

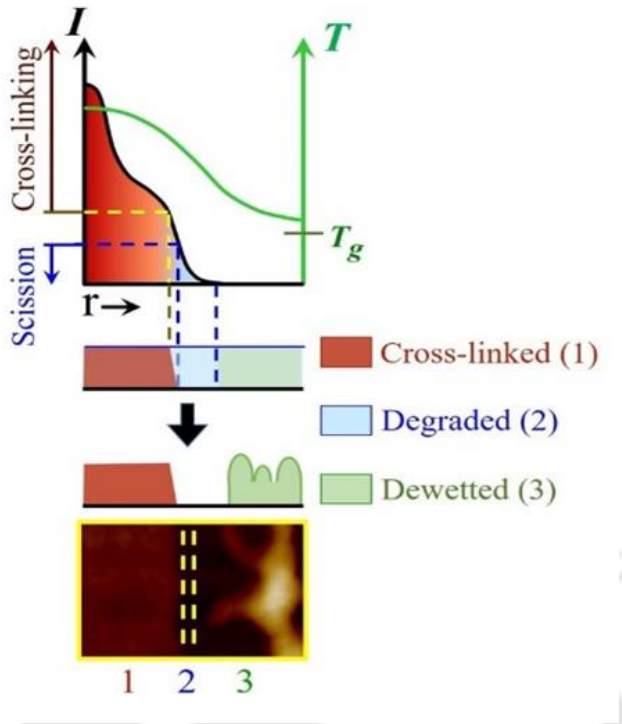

Figure 5.6*. A schematic of the double Gaussian exposure intensity distribution (black line) and thermal profile (green line) as a function of distance r from the center of the exposure. Crosslinked (1, brown) and degraded (2, light blue) zone for PMMA and dewetted zone (3, light green) are shown. A typical scan of the irradiated sample is shown in figure with identified zones. The schematic is not in scale.*

5. CONCLUSIONS

In summary, we have extensively studied the behavior of a PS-r-PMMA film exposed to wide range of e-beam exposure from 180 μC/cm^2 to 10,000 μC/cm^2. At a weaker exposure, the e-beam dissociates the PMMA segments in the exposed zone while PS blocks are cross-linked. Subsequently, the exposed PMMA blocks undergo dewetting to form nanopatterns at room temperature when annealed with selective solvents. The crosslinked PS blocks in the exposed area provide periodic lateral confinements to the dewetted nanopatterns thus fabricated. In comparison, at a high intensity e-beam exposure, the tone reversal of PMMA induce a higher degree of crosslinking in the area of exposure whereas the scattering of electrons in the unexposed area engender a positive tone behavior to the PMMA blocks. Subsequently, the scissored PMMA blocks in the unexposed domain undergoes dewetting

under a suitable solvent annealing to develop large-area nanopatterns. In such a scenario, while the exposed blocks maintain the periodicity of the patterns by creating the quarantine zones, the unexposed area develops the nanopatterns with a very high surface-to-volume ratio. The behavior of the PS and PMMA segments can be summarized as follows:

The patterns thus fabricated, exploiting the polymer behavior mentioned above, show the reduction in size and periodicity by at least an order of magnitude, as compared to any conventional dewetting process. Further miniaturization of feature size by ~50% has been achieved by the selective removal of a particular polymer from the RCP using suitable solvents. Using specific BCP instead of RCP, one can achieve well-ordered hierarchical nano-scale features. The proposed soft-lithography technique is also unique in a sense that it opens up a wide range of future possibilities in the area of micro/nano fabrication with the variations in film thickness (see section S8 of APPENDIX 4), e-beam dosage and pattern, or composition/MW of RCP. There is a possibility that the method described here can be used for deep UV photolithography as well if a photo-initiator such as Irgacure 379 is mixed with the PS-r-PMMA RCP.[71] Further, such explorations can help in the fabrication of a variety of mesoscale patterns with the complex hierarchical arrangement, which has been among many of the real challenges so far.

REFERENCES

[1] A. Charlesby, Atomic radiation and polymers, Pergamon Press, 1960.

[2] C. Vieu, F. Carcenac, A. Pépin, Y. Chen, M. Mejias, A. Lebib, L. Manin-Ferlazzo, L. Couraud, H. Launois, Electron beam lithography: Resolution limits and applications, Appl. Surf. Sci. 164 (2000) 111–117. https://doi.org/10.1016/S0169-4332(00)00352-4.

[3] D.J.D. Carter, A. Pepnin, M.R. Schweizer, H.I. Smith, L.E. Ocola, Direct measurement of the effect of substrate photoelectrons in x-ray nanolithography, J. Vac. Sci. Technol.

B. 15 (1997) 2509. https://doi.org/10.1116/1.589675.

[4] E.M. Lehockey, I. Reid, I. Hill, The radiation chemistry of poly(methyl methacrylate) polymer resists, J. Vac. Sci. Technol. A. 6 (1988) 2221–2225. https://doi.org/10.1116/1.575014.

[5] V. Bakshi, ed., EUV Lithography, SPIE Press Bellingham, USA, 2009.

[6] A. del Campo, E. Arzt, Fabrication approaches for generating complex micro- and nanopatterns on polymeric surfaces, Chem. Rev. 108 (2008) 911–945. https://doi.org/10.1021/cr050018y.

[7] S.R. Turner, R.C. Daly, The Chemistry of Photoresists, in: N.S. Allen (Ed.), Photopolymerisation Photoimaging Sci. Technol., Elsevier science publishers, 1989: pp. 75–113.

[8] Y. Li, L. Huang, M. Zhong, Z. Wei, J. Li, An Efficient and Low-Cost Photolithographic-Pattern- Transfer Technique to Fabricate Electrode Arrays for Micro- / Nanoelectronics, Adv. Mater. Technol. 1 (2016) 1600001. https://doi.org/10.1002/admt.201600001.

[9] D.M. Tennant, T.L. Koch, P.. Mulgrew, R.P. Gnall, F. Ostermeyer, J. Verdiell, Characterization of near-field holography grating masks for optoelectronics fabricated by electron beam lithography, J. Vac. Sci. Technol. B. 10 (1992) 2530. https://doi.org/10.1116/1.586052.

[10] C. Dix, P.F. Mckee, High accuracy electronbeam grating lithography for optical and optoelectronic devices, J. Vac. Sci. Technol. B. 10 (1992) 2667. https://doi.org/10.1116/1.586022.

[11] K. Scholten, E. Meng, Electron-beam lithography for polymer bioMEMS with submicron features, Microsystems Nanoeng. 2 (2016) 1–7. https://doi.org/10.1038/micronano.2016.53.

[12] M. Neklyudova, A.K. Erdamar, L. Vicarelli, S.J. Heerema, T. Rehfeldt, G. Pandraud, Z. Kolahdouz, C. Dekker, H.W. Zandbergen, Through-membrane electron-beam lithography for ultrathin membrane applications, Appl. Phys. Lett. 111 (2017) 063105.

[13] L. Petti, R. Capasso, M. Rippa, M. Pannico, P. La Manna, G. Peluso, A. Calarco, E. Bobeico, P. Musto, A plasmonic nanostructure fabricated by electron beam lithography as a sensitive and highly homogeneous SERS substrate for bio-sensing applications, Vib. Spectrosc. 82 (2016) 22–30. https://doi.org/10.1016/j.vibspec.2015.11.007.

[14] F. Virgilio, M. Prasciolu, P. Ugo, M. Tormen, Microelectronic Engineering Development of electrochemical biosensors by e-beam lithography for medical diagnostics, Microelectron. Eng. 111 (2013) 320–324. https://doi.org/10.1016/j.mee.2013.02.026.

[15] D.B. Dement, M.K. Quan, V.E. Ferry, Nanoscale Patterning of Colloidal Nanocrystal Films for Nanophotonic Applications Using Direct Write Electron Beam Lithography, ACS Appl. Mater. Interfaces. 11 (2019) 14970–14979. https://doi.org/10.1021/acsami.9b01159.

[16] A. Gin, J.R. Wendt, Electron Beam Lithography for the Nanofabrication of Optical Devices, in: S.A. Kemme (Ed.), Microoptics Nanooptics Fabr., CRC Press, 2010: pp. 109–126.

[17] S. Ma, C. Con, M. Yavuz, B. Cui, Polystyrene negative resist for high-resolution electron beam lithography, Nanoscale Res. Lett. 6 (2011) 1–6. https://doi.org/10.1186/1556-276X-6-446.

[18] A.A. Tseng, K. Chen, C.D. Chen, K.J. Ma, Electron beam lithography in nanoscale fabrication: Recent development, IEEE Trans. Electron. Packag. Manuf. 26 (2003) 141–149. https://doi.org/10.1109/TEPM.2003.817714.

[19] M.J. Word, I. Adesida, P.R. Berger, Nanometer-period gratings in hydrogen silsesquioxane fabricated by electron beam lithography, J. Vac. Sci. Technol. B. 21 (2003) L12. https://doi.org/10.1116/1.1629711.

[20] S. Manako, Y. Ochiai, H. Yamamoto, T. Teshima, J. Fujita, E. Nomura, High-purity, ultrahigh-resolution calixarene electron-beam negative resist, J. Vac. Sci. Technol. B. 18 (2000) 3424. https://doi.org/10.1116/1.1321274.

[21] B. Bilenberg, M. Schøler, P. Shi, M.S. Schmidt, P. Bøggild, M. Fink, C. Schuster, F. Reuther, C. Gruetzner, A. Kristensen, Comparison of high resolution negative electron beam resists, J. Vac. Sci. Technol. B. 24 (2006) 1776–1779. https://doi.org/10.1116/1.2210002.

[22] J. Feng, M.T. Tuominen, J.P. Rothstein, Hierarchical superhydrophobic surfaces fabricated by dual-scale electron-beam-lithography with well-ordered secondary nanostructures, Adv. Funct. Mater. 21 (2011) 3715–3722. https://doi.org/10.1002/adfm.201100665.

[23] Y. Chen, Nanofabrication by electron beam lithography and its applications: A review, Microelectron. Eng. 135 (2015) 57–72. https://doi.org/10.1016/j.mee.2015.02.042.

[24] R.M.M. Hasan, X. Luo, Promising Lithography Techniques for Next-Generation Logic Devices, Nanomanufacturing Metrol. 1 (2018) 67–81. https://doi.org/10.1007/s41871-018-0016-9.

[25] Y. Xia, G.M. Whitesides, Soft-lithography, Angew. Chemie - Int. Ed. 37 (1998) 550. https://doi.org/10.1039/c1lc20189a.

[26] S. Roy, K.J. Ansari, S.S.K. Jampa, P. Vutukuri, R. Mukherjee, Influence of substrate wettability on the morphology of thin polymer films spin-coated on topographically patterned substrates, ACS Appl. Mater. Interfaces. 4 (2012) 1887–1896.

https://doi.org/10.1021/am300201a.

[27] N. Bhandaru, A. Karim, R. Mukherjee, Directed ordering of phase separated domains and dewetting of thin polymer blend films on a topographically patterned substrate, Soft Matter. 13 (2017) 4709–4719. https://doi.org/10.1039/c7sm00799j.

[28] R. Mukherjee, D. Bandyopadhyay, A. Sharma, Control of morphology in pattern directed dewetting of thin polymer films, Soft Matter. 4 (2008) 2086–2097. https://doi.org/10.1039/b806925e.

[29] N. Bhandaru, P.S. Goohpattader, D. Faruqui, R. Mukherjee, A. Sharma, Solvent-Vapor-Assisted Dewetting of Prepatterned Thin Polymer Films: Control of Morphology, Order, and Pattern Miniaturization, Langmuir. 31 (2015) 3203–3214. https://doi.org/10.1021/la5045738.

[30] M.D. Morariu, N.E. Voicu, E. Schäffer, Z. Lin, T.P. Russell, U. Steiner, Hierarchical structure formation and pattern replication induced by an electric field, Nat. Mater. 2 (2003) 48–52. https://doi.org/10.1038/nmat789.

[31] N.E. Voicu, S. Harkema, U. Steiner, Electric-field-induced pattern morphologies in thin liquid films, Adv. Funct. Mater. 16 (2006) 926–934. https://doi.org/10.1002/adfm.200500470.

[32] P. Roy, R. Mukherjee, D. Bandyopadhyay, P.S. Gooh Pattader, Electrodynamic-contact-line-lithography with nematic liquid crystals for template-less E-writing of mesopatterns on soft surfaces, Nanoscale. 11 (2019) 16523–16533. https://doi.org/10.1039/c9nr05729c.

[33] P.S.G. Pattader, I. Banerjee, A. Sharma, D. Bandyopadhyay, Multiscale pattern generation in viscoelastic polymer films by spatiotemporal modulation of electric field and control of rheology, Adv. Funct. Mater. 21 (2011) 324–335.

https://doi.org/10.1002/adfm.201001206.

[34] R. Xie, A. Karim, J.F. Douglas, C.C. Han, R.A. Weiss, Spinodal dewetting of thin polymer films, Phys. Rev. Lett. 81 (1998) 1251–1254. https://doi.org/10.1103/PhysRevLett.81.1251.

[35] R. Mukherjee, A. Sharma, Instability, self-organization and pattern formation in thin soft films, Soft Matter. 11 (2015) 8717–8740. https://doi.org/10.1039/c5sm01724f.

[36] G. Reiter, Dewetting of Thin Polymer Films, Phys. Rev. Lett. 68 (1992) 75–80.

[37] G. Reiter, Unstable Thin Polymer Films: Rupture and Dewetting Processes, Langmuir. 9 (1993) 1344–1351. https://doi.org/10.1021/la00029a031.

[38] A. Sharma, G. Reiter, Instability of thin polymer films on coated substrates: Rupture, dewetting, and drop formation, J. Colloid Interface Sci. 178 (1996) 383–399. https://doi.org/10.1006/jcis.1996.0133.

[39] B. Yoon, H. Acharya, G. Lee, H.C. Kim, J. Huh, C. Park, Nanopatterning of thin polymer films by controlled dewetting on a topographic pre-pattern, Soft Matter. 4 (2008) 1467–1472. https://doi.org/10.1039/b800121a.

[40] A. Sehgal, D. Bandyopadhyay, K. Kargupta, A. Sharma, A. Karim, From finite-amplitude equilibrium structures to dewetting in thin polymer films on chemically patterned substrates, Soft Matter. 8 (2012) 10394–10402. https://doi.org/10.1039/c2sm26369f.

[41] S. Okazaki, Resolution limits of optical lithography, J. Vac. Sci. Technol. B Microelectron. Nanom. Struct. 9 (1991) 2829. https://doi.org/10.1116/1.585650.

[42] A. Verma, A. Sharma, Enhanced self-organized dewetting of ultrathin polymer films under water-organic solutions: fabrication of sub-micrometer spherical lens arrays., Adv. Mater. 22 (2010) 5306–5309. https://doi.org/10.1002/adma.201002768.

[43] A. Verma, A. Sharma, Submicrometer pattern fabrication by intensification of instability in ultrathin polymer films under a water-solvent mix, Macromolecules. 44 (2011) 4928–4935. https://doi.org/10.1021/ma200113w.

[44] G. Reiter, R. Khanna, A. Sharma, Enhanced instability in thin liquid films by improved compatibility, Phys. Rev. Lett. 85 (2000) 1432–1435. https://doi.org/10.1103/PhysRevLett.85.1432.

[45] D. Bandyopadhyay, R. Gulabani, A. Sharma, Instability and dynamics of thin liquid bilayers, Ind. Eng. Chem. Res. 44 (2005) 1259–1272. https://doi.org/10.1021/ie049640r.

[46] K. Brassat, D. Kool, C.G.A. Nallet, J.K.N. Lindner, Understanding Film Thickness-Dependent Block Copolymer Self-Assembly by Controlled Polymer Dewetting on Prepatterned Surfaces, Adv. Mater. Interfaces. 7 (2019) 1901605. https://doi.org/10.1002/admi.201901605.

[47] D.U. Ahn, Z. Wang, I.P. Campbell, M.P. Stoykovich, Y. Ding, Morphological evolution of thin PS/PMMA films: Effects of surface energy and blend composition, Polymer (Guildf). 53 (2012) 4187–4194. https://doi.org/10.1016/j.polymer.2012.07.037.

[48] I. Zailer, J.E.F. Frost, V. Chabasseur-Molyneux, C.J.B. Ford, M. Pepper, Crosslinked PMMA as a high-resolution negative resist for electron beam lithography and applications for physics of low-dimensional structures, Semicond. Sci. Technol. 11 (1996) 1235–1238. https://doi.org/10.1088/0268-1242/11/8/021.

[49] A.C.F. Hoole, M.E. Welland, A.N. Broers, Negative PMMA as a high-resolution resist : the limits and possibilities, Semicond. Sci. Technol. 12 (1997) 1166–1170.

[50] J. Brandrup, E.H. Immergut, E.A. Grulke, eds., Polymer Handbook, 4th ed., Wiley, New York, 1999.

[51] J.S. Greeneich, Solubility Rate of Poly-(Methyl Methacrylate), PMMA, Electron-Resist, J. Electrochem. Soc. SOLID-STATE Sci. Technol. 121 (1974) 1669. https://doi.org/10.1149/1.2401767.

[52] R. Seemann, S. Herminghaus, K. Jacobs, Gaining control of pattern formation of dewetting liquid films, J. Phys. Condens. Matter. 13 (2001) 4925–4938. https://doi.org/10.1088/0953-8984/13/21/319.

[53] W.H. Teh, C. Te Liang, M. Graham, C.G. Smith, Cross-linked PMMA as a low-dimensional dielectric sacrificial layer, J. Microelectromechanical Syst. 12 (2003) 641–648. https://doi.org/10.1109/JMEMS.2003.817891.

[54] T. Tada, T. Kanayama, Fabrication of silicon nanostructures with a poly(methylmethacrylate) single-layer process, J. Vac. Sci. Technol. B. 13 (1995) 2801. https://doi.org/10.1116/1.588269.

[55] V.R. Manfrinato, J. Wen, L. Zhang, Y. Yang, R.G. Hobbs, B. Baker, D. Su, D. Zakharov, N.J. Zaluzec, D.J. Miller, E.A. Stach, K.K. Berggren, Determining the resolution limits of electron-beam lithography: Direct measurement of the point-spread function, Nano Lett. 14 (2014) 4406–4412. https://doi.org/10.1021/nl5013773.

[56] N. Samoto, R. Shimizu, Theoretical study of the ultimate resolution in electron beam lithography by Monte Carlo simulation, including secondary electron generation: Energy dissipation profile in polymethylmethacrylate, J. Appl. Phys. 54 (1983) 3855–3859. https://doi.org/10.1063/1.332610.

[57] F. Hubenthal, Noble Metal Nanoparticles : Synthesis and Optical Properties, Elsevier Ltd., 2016. https://doi.org/10.1016/B978-0-12-803581-8.00585-3.

[58] F. Emoto, K. Gamo, S. Namba, N. Samoto, R. Shimizu, 8 nm Wide Line Fabrication in PMMA on Si Wafers by Electron Beam Exposure, Jpn. J. Appl. Phys. 24 (1985) L809–

L811. https://doi.org/10.1143/JJAP.25.L92.

[59] T.H.. Chang, Proximity effect in electron-beam lithography, J. Vac. Sci. Technol. 12 (1975) 1271.

[60] A. Olkhovets, H.G. Craighead, Low voltage electron beam lithography in PMMA, J. Vac. Sci. Technol. B. 17 (1999) 1366–1370. https://doi.org/10.1116/1.590762.

[61] B. Ravi, S. Chakraborty, M. Bhattacharjee, S. Mitra, A. Ghosh, P.S.G. Pattader, D. Bandyopadhyay, Pattern Directed Ordering of Spin-dewetted Liquid Crystal Micro or Nanodroplets as Pixelated Light Reflectors and Locomotives Pattern Directed Ordering of Spin-dewetted Liquid Crystal Micro or Nanodroplets as Pixelated Light Reflectors and Locomotives, Appl. Mater. Interfaces. 9 (2017) 1066–1076. https://doi.org/10.1021/acsami.6b12182.

[62] D. Chu, D.T. Bilir, R.F.W. Pease, K.E. Goodson, Submicron thermocouple measurements of electron-beam resist heating, J. Vac. Sci. Technol. B. 20 (2002) 3044. https://doi.org/10.1116/1.1523023.

[63] T. Abe, K. Ohta, H. Wada, T. Takigawa, Resist heating effect in direct electron beam writing, J. Vac. Sci. Technol. B. 6 (1988) 853. https://doi.org/10.1116/1.584309.

[64] H.Y. Ku, L.C. Scala, Polymeric Electron Beam Resists, J. Electrochem. Soc.Solid State Sci. 116 (1969) 980.

[65] H. Kudoh, M. Celina, G.M. Malone, R.J. Kaye, K.T. Gillen, R.L. Clough, Pulsed e-beam irradiation of polymers - A comparison of dose rate effects and LET effects, Radiat. Phys. Chem. 48 (1996) 555–562. https://doi.org/10.1016/0969-806X(96)00076-X.

[66] K. Makuuchi, S. Cheng, Radiation Processing of Polymer Materials and its Industrial Applications, John Wiley & Sons, Inc., 2012. https://doi.org/10.1002/9781118162798.

[67] V.M. Bermudez, Low-energy electron-beam effects on poly(methyl methacrylate) resist films, J. Vac. Sci. Technol. B. 17 (1999) 2512–2518. https://doi.org/10.1116/1.591134.

[68] B.K. Yoon, W. Hwang, Y.J. Park, J. Hwang, C. Park, J. Chang, Direct patterning of self assembled nano-structures of block copolymers via electron beam lithography, Macromol. Res. 13 (2005) 435–440. https://doi.org/10.1007/bf03218477.

[69] M. Gentili, L. Grella, A. Lucchesini, L. Luciani, L. Mastrogiacomo, P. Musumeci, Energy density function determination in very-high-resolution electron-beam lithography, J. Vac. Sci. Technol. B Microelectron. Process. Phenom. 8 (1990) 1867. https://doi.org/10.1116/1.585175.

[70] M. Aktary, M. Stepanova, S.K. Dew, Simulation of the spatial distribution and molecular weight of polymethylmethacrylate fragments in electron beam lithography exposures Simulation of the spatial distribution and molecular weight of polymethylmethacrylate fragments in electron beam, J. Vac. Sci. Technol. B. 24 (2006) 768. https://doi.org/10.1116/1.2181580.

[71] D.J. Carbaugh, S. Kaya, F. Rahman, Transparent and visible light-insensitive acrylic photoresist for negative tone optical lithography, J. Vac. Sci. Technol. B,. 35 (2017) 011601. https://doi.org/10.1116/1.4971198.

Chapter 6

Conclusions and Future Scope of the work

The study presented here provides a detailed framework for fabricating complex, intricate polymeric patterns over a flat surface like silicon wafers. These patterns are otherwise challenging to fabricate using conventionally available techniques. The study adopts a synergistic approach in which the amalgamation of simple techniques makes pattern formation straightforward, faster and simpler.

Chapter 1 forms the foundation for the subsequent chapters. The chapter gives a detailed account of the fabrication methods reported worldwide for polymeric pattern generation. For the sake of simplicity, the available methods are broadly classified into *Top-down* and *Bottom-up* approaches. According to available literatures, subsequent experiments were meticulously planned and carried out.

In **Chapter 2,** a study is presented that involves phase separation in a polymer bilayer system. The critical findings of the study show that the morphology of a thin film of a polymer blend strongly depends on the properties of the labile polymer underlayer. For example, phase separation occurs in PS/PMMA polymer blend when spun cast on a PS underlayer. The scenario changes when the underlayer is either PMMA, blend PS/PMMA, or RCP (PS-r-

PMMA). The study also presents the effect of rapid thermal annealing (RTA) on the phase separation in the bilayer system. It was found that the equilibrium morphology is achieved faster than conventional techniques like thermal and solvent vapour annealing. Interestingly, when blend PS/PMMA is coated over RCP underlayer, the RTA-induced phase separation resulted in a hierarchical pattern with multiple length scales. Furthermore, a more orderly arrangement of polymeric domains is achieved by patterning the RCP underlayer using capillary force lithography (CFL).

Chapter 3 highlights the phase separation phenomenon occurring in the thin film of blend PS/PMMA coated over PS underlayer. Low surface energy labile PS underlayer induces phase separation in the blend PS/PMMA upper layer. The study successfully establishes the dependency of the phase separated morphologies on the PS: PMMA ratio in the blend upper layer. A low PS: PMMA ratio resulted in labyrinthine type patterns, while a high PS: PMMA ratio gives rise to sea-islands type morphologies. The more orderly arrangement of the patterns is achieved by using CFL-assisted patterning of the PS underlayer.

A detailed fabrication method for multiple length scale structures using phase separation in a polymeric bilayer system is discussed in **Chapter 4**. The phase separation occurring in polymeric bilayer system consisting of PS/PMMA blend upper layer and PS-r-PMMA random copolymer underlayer can give rise to multiple length scale structures. The RCP underlayer was patterned using CFL. Furthermore, by varying the concentration of blend solution in the upper layer, excellent control over the orderly arrangement of the patterns is achieved.

Chapter 5 is an extensive study that deals with the pattern generation by e-beam lithography using the PS-r-PMMA random copolymer as the resist. The previously spun coated random copolymer thin film was exposed to a wide range of e-dose from 180 $\mu C/cm^2$ to 10000

$\mu C/cm^2$. Polymer chains' crosslinking occurs in polystyrene blocks (negative resist) at lower doses, while chain scission occurs in the PMMA blocks (positive resist). Interestingly, with moderate to high dose e-beam exposure, PMMA blocks demonstrate tone reversal from positive to negative resist upon increasing dose with e-beam dose. Moreover, the interaction of secondary electrons with PMMA blocks in unexposed regions engendered bond scission in PMMA blocks, resulting in solvent-induced dewetting.

The study is focused on simple and straightforward methods for pattern generation. The study also provides a generic framework and may be implemented for other polymer combinations too. Moreover, the experiments presented opens up the avenue for interdisciplinary scientific explorations that primarily focus on applications of fabricated complex patterns. Further studies may take up the following directions:

1. The complex pattern fabricated can be utilized as a SERS substrate. This may be done by sputter coating a thin layer of metals like gold or silver over the polymeric structures and analyzed using Raman spectroscopy for surface plasmon resonance Moreover, a thin biological matter like DNA can be placed over these sputter coated samples and can be analyzed for Raman signals. Therefore,these SERS active surfaces may be utilized as an alternative to TERS.
2. Extensive studies can be undertaken in which fabricated patterns can be utilized in bio-inspired applications like fabrication of superhydrophobic / superoleophobic surfaces, dew harvesting, Bio-MEMS, etc.
3. Polymer-polymer bilayer studies can be extended for a trilayer system consisting of three polymeric layers and can expect new exciting phenomenon.This may lead to fabrication of more complex patterns with characteristics of all the three polymers.

4. The study also forms a fundamental basis for a detailed theoretical study with respect to the phase separation in polymer bilayer system. Moreover, using simulation tools predicting the effect of polymer concentrations, rapid thermal annealing over the phase separation can be taken up in future scope of work.

Appendix 1

Flory Huggins Theory

The polymer solutions deviate from classical Raoult's Law. That states that for an ideal solution ($\Delta H_{mix} = 0$), the partial pressure, $p_i$is equal to the product of equilibrium vapor pressure, p_i^* and mole fraction, x_i i.e. $p_i = x_i p_i^*$. To account for this non-ideality Flory and Huggins independently put forward the relation for entropy change of mixing for polymer solutions, which later became the successful tool that explains the phase behavior of polymers in solutions. The derivation from scratch is presented here. It is divided into three parts accounting the terms for 1) Entropy change of mixing of ideal solutions which contains non polymeric solute, 2) Entropy change of mixing for ideal polymeric solutions and 3) Expression for the system with, $\Delta H_{mix} \neq 0$, later combining everything to account for ΔG_{mix}, while putting everything into, $\Delta G_{mix} = \Delta H - T\Delta S$. The theory considers lattice model to derive the expressions for entropy, enthalpy and free energy change of mixing.

1.1 Entropy change of mixing of ideal solutions (solute is not polymer).

Consider a solution with B as solute dissolved in solvent A. The solution is considered as ideal solution ($\Delta H_{mix} = 0$) and all interactions are identical. The system is represented in the form of a lattice in which solute and solvent molecules are represented by red and blue dots respectively Figure A1. Each molecule occupies single lattice site.

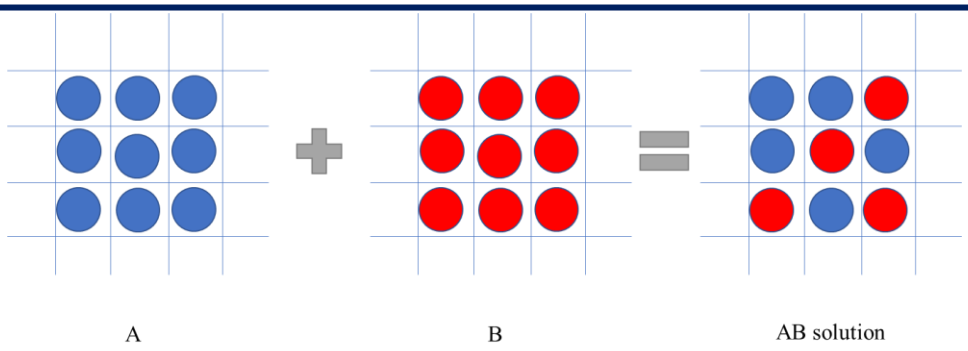

Figure A1 Lattice model for non-polymeric ideal solutions A: solvent (represented by blue) and B: solute (represented by red).

$$\Delta G_{mix} = -T\Delta S; \qquad \Delta H = 0 \qquad (1)$$

The expression for the change in entropy due to the formation of the mixture is given by

$$\Delta S_{mix} = S_{12} - (S_1 + S_2) \qquad (2)$$

According to Boltzmann entropy relation

$$S = k_B \ln \Omega \qquad (3)$$

Where S is entropy, k_B is Boltzmann constant and Ω is the total number of indistinguishable equal energy arrangements of the molecules.

So, the expressions for S_1, S_2 and S_{12} are as follows:

$$S_1 = k_B \ln \Omega_1; S_2 = k_B \ln \Omega_2 \text{ and } S_{12} = k_B \ln \Omega_{12}$$

From equation 2 it follows that

$$\Delta S_{mix} = S_{12} - (S_1 + S_2)$$

$$\Delta S_{mix} = k_B \ln \Omega_{12} - (k_B \ln \Omega_1 + k_B \ln \Omega_2)$$

$$\Delta S_{mix} = k_B \left[\ln \frac{\Omega_{12}}{\Omega_1 . \Omega_2}\right] \qquad (4)$$

Ω_1: is the number of ways of placing N_1 indistinguishable particles or molecules of pure solvent in N_1 lattice site.

Ω_2: is the number of ways of placing N_2 indistinguishable particles or molecules of pure solute in N_2 lattice site.

Likewise, Ω_{12}: is the number of ways of placing $N_1 + N_2$ indistinguishable particles or molecules of pure solute in $N_1 + N_2$ lattice site.

For pure component $\Omega_1 = \Omega_2 = 1$ and for a mixture of 1 and 2; Ω_{12} is given by

$$\Omega_{12} = \left[\frac{(N_1 + N_2)!}{N_1!\ N_2!}\right]$$

From equation (4) we have

$$\Delta S_{mix} = k_B \left[\ln\left[\frac{(N_1 + N_2)!}{N_1!\ N_2!}\right]\right]$$

$$\Delta S_{mix} = k_B[\ln(N_1 + N_2)! - [\ln(N_1!) + \ln(N_2!)]] \qquad (5)$$

According to Sterling's approximation

$$\ln(N)! = N \ln N - N$$

$$\Delta S_{mix} = k_B[[(N_1 + N_2)\ln(N_1 + N_2) - (N_1 + N_2)] - [N_1\ln(N_1) - N_1 + N_2\ln(N_2) - N_2]]$$

After cancellation of the terms the equation reduces to

$$\Delta S_{mix} = k_B[[(N_1 + N_2)\ln(N_1 + N_2)] - [N_1\ln(N_1) + N_2\ln(N_2)]]$$

Upon rearranging the terms

$$\Delta S_{mix} = k_B[N_1(\ln(N_1 + N_2) - N_1\ln(N_1) + N_2(\ln(N_1 + N_2) - N_2\ln(N_2))]$$

$$\Delta S_{mix} = k_B[N_1(\ln(N_1 + N_2) - N_1\ln(N_1) + N_2(\ln(N_1 + N_2) - N_2\ln(N_2))]$$

$$\Delta S_{mix} = -k_B \left[\left(\mathrm{N}_1 \left(\ln \frac{\mathrm{N}_1}{\mathrm{N}_1+\mathrm{N}_2} \right) \right) + \left(\mathrm{N}_2 \left(\ln \frac{\mathrm{N}_2}{\mathrm{N}_1+\mathrm{N}_2} \right) \right) \right] \quad (6)$$

$$\Delta S_{mix} = -k_B \left[\left(\mathrm{N}_1 (\ln X_1) \right) + \left(\mathrm{N}_2 (\ln X_2) \right) \right] \quad (7)$$

Where, X_1 and X_2 are mole fraction

$$\Delta S_{mix} = -k_B \mathrm{N}_{Av} \left[\left(\mathrm{n}_1 (\ln X_1) \right) + \left(\mathrm{n}_2 (\ln X_2) \right) \right] \quad (8)$$

Where, N_{Av} is Avogadro's number and n_1 and n_2 are number of moles

$$\Delta S_{mix} = -R \left[\left(\mathrm{n}_1 (\ln X_1) \right) + \left(\mathrm{n}_2 (\ln X_2) \right) \right] \quad (9)$$

Since we know R is universal gas constant is product of Boltzmann constant and Avogadro's number.

So, from equation (1)

$$\Delta G_{mix} = RT \left[\left(\mathrm{n}_1 (\ln X_1) \right) + \left(\mathrm{n}_2 (\ln X_2) \right) \right] \quad (10)$$

It follows from equation (10) that X_1 and X_2 are less than one so $\Delta S_{mix} > 0;\ \Delta G_{mix} < 0$.

1.2 Entropy change of mixing of ideal polymeric solutions.

Assumptions made here are as follows

1. Same lattice describes the solvent, polymer and the solution.
2. There is no volume change of mixing.
3. All polymer molecule contains same number of segments.
4. Self-interaction within the polymer is allowed.
5. The volume occupied by one polymer segment is equal to that occupied by one solvent molecule.
6. **Mean Field Approximation**: The segments are uniformly distributed throughout the lattice.

Considering athermal mixing i.e. $\Delta H_{mix} = 0$

So, it follows again

$$\Delta G_{mix} = -T\Delta S$$

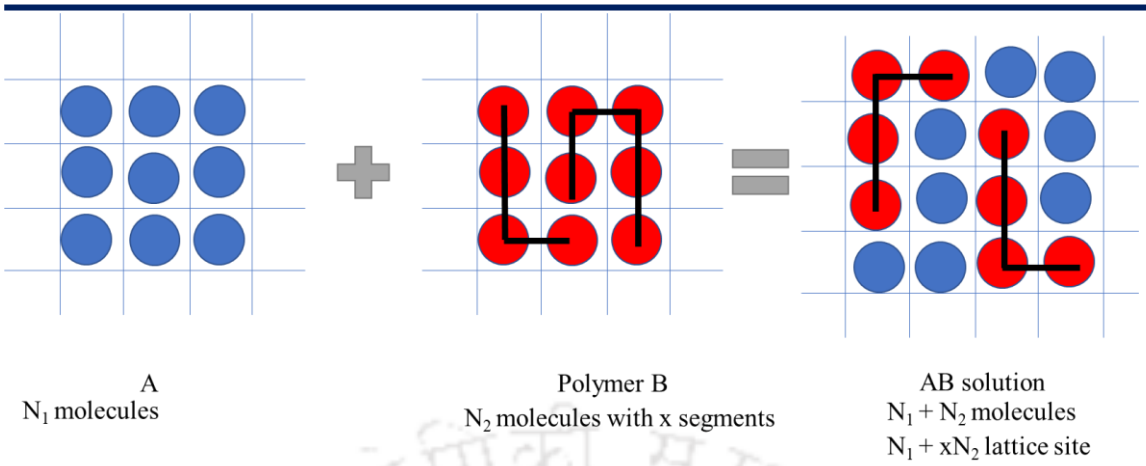

Figure A2 Lattice model for non-polymeric ideal solutions A: solvent (represented by blue) and Polymer B: solute (represented by interconnected red circles).

Total number of molecules in the polymer solution = $N_1 + N_2$

Or, total number of lattice site occupied in polymer solution = $N_1 + xN_2$, where is x segment per molecule.

From equation (3) Boltzmann entropy relation

$$S = k_B \ln \Omega$$

For pure solvent $\Omega_1 = 1$

But unlike earlier case Ω_2 and Ω_{12} are not equal to one as interconnectivity of polymer chains can lead to multiple distinguishable arrangements.

The first polymer segment can be placed anywhere in the empty lattice. For the next segment due to connectivity with the first segment the second segment can be placed in the neighboring lattice cells in the remaining x-1 lattice sites. Individual arrangement for each segment is calculated and number of possible conformations of polymer chain, ν , calculated by multiplying together the number of possible placements of all segments in the chain. The calculation is carried out for each molecule added successively. After the polymer molecules

added to the lattice cell, N_1 solvent molecule are added to remaining N_1 lattice site and only one distinguishable arrangement possible for solvent molecules as they are identical.

So,

$$\Omega_{12} = \frac{1}{N_2!}\prod_{\zeta=1}^{N_2} \nu_\zeta$$

Using mean field approximation

$$\nu_\zeta = [N - x(\zeta - 1)]\left\{z\frac{N - x(\zeta - 1)}{N}\right\}\left\{(z-1)\frac{N - x(\zeta - 1)}{N}\right\}^{x-2}$$

Where z is the coordination number of the lattice.

The above expression can be rearranged to

$$\nu_\zeta = z(z-1)^{x-2}N^{1-x}[N - x(\zeta - 1)]^x$$

So Ω_{12} can be expressed as

$$\Omega_{12} = \frac{1}{N_2!}\prod_{\zeta=1}^{N_2}(z-1)^{x-2}N^{1-x}[N - x(\zeta - 1)]^x$$

$$\Omega_{12} = \frac{1}{N_2!}((z-1)^{x-2}N^{1-x})^{N_2}\prod_{\zeta=1}^{N_2}[N - x(\zeta - 1)]^x$$

For the pure polymer, Ω_2 corresponds to the different arrangements of the xN_2 polymer segments in xN_2 lattice cells. We substitute in expression of Ω_{12} with xN_2 we get,

$$\Omega_2 = \frac{1}{N_2!}((z-1)^{x-2}(xN_2)^{1-x})^{N_2}\prod_{\zeta=1}^{N_2}[xN_2 - x(\zeta - 1)]^x$$

$$\prod_{\zeta=1}^{N_2}[x\mathrm{N}_2 - x(\zeta-1)]^x = \frac{1}{\mathrm{N}_2!}(x\mathrm{N}_2)^{(1-x)N_2}(x)^{xN_2}(\mathrm{N}_2!)^x = (\mathrm{N}_2)^{(1-x)N_2}(x)^{N_2}(\mathrm{N}_2!)^{x-1}$$

taking natural log and applying Sterling's approximation

we get

$$(\mathrm{N}_2)^{(1-x)N_2}(x)^{N_2}(\mathrm{N}_2!)^{x-1} = \left[\frac{x}{e^{x-1}}\right]^{\mathrm{N}_2}$$

So

$$\Omega_2 = \frac{1}{\mathrm{N}_2!}((z-1)^{x-2}(x\mathrm{N}_2)^{1-x})^{N_2}\prod_{\zeta=1}^{N_2}[x\mathrm{N}_2 - x(\zeta-1)]^x = (z(z-1)^{x-2})^{N_2}\left[\frac{x}{e^{x-1}}\right]^{\mathrm{N}_2}$$

$$\Omega_{12} = \Omega_2\left[\left(\frac{N}{x\mathrm{N}_2}\right)^{\mathrm{N}_2}\left(\frac{N}{\mathrm{N}_1}\right)^{\mathrm{N}_1}\right]$$

So combining the expressions we get

$$\Delta S_{mix} = k_B \ln\left(\frac{\Omega_{12}}{\Omega_2\Omega_1}\right) = k_B \ln\left[\left(\frac{N}{x\mathrm{N}_2}\right)^{\mathrm{N}_2}\left(\frac{N}{\mathrm{N}_1}\right)^{\mathrm{N}_1}\right] = k_B\,\mathrm{N}_2 \ln\left(\frac{N}{x\mathrm{N}_2}\right) + \mathrm{N}_1 \ln\left(\frac{N}{\mathrm{N}_1}\right)$$

So,

$$\Delta S_{mix} = -k_B[\mathrm{N}_2 \ln\left(\frac{x\mathrm{N}_2}{N}\right) + \mathrm{N}_1 \ln\left(\frac{\mathrm{N}_1}{N}\right)]$$

Where, ϕ_1 and ϕ_2 are volume fraction.

$$\Delta S_{mix} = -k_B\,[\mathrm{N}_2 \ln(\phi_2) + \mathrm{N}_1 \ln(\phi_1)]$$

$$\Delta S_{mix} = -k_B[\mathrm{N}_2 \ln(\phi_2) + \mathrm{N}_1 \ln(\phi_1)]$$

$$\Delta S_{mix} = -k_B \mathrm{N}_{Av}[\mathrm{n}_2 \ln(\phi_2) + \mathrm{n}_1 \ln(\phi_1)]$$

$$\Delta S_{mix} = -R[\mathrm{n}_2 \ln(\phi_2) + \mathrm{n}_1 \ln(\phi_1)]$$

1.3 Enthalpy change of mixing for polymeric solutions

The key assumptions that are made are as follows:

1. Only first neighboring terms are considered.
2. Only contacts allowed are between solvent solvent, solvent-segment, and segment-segment contact and corresponding Gibbs free energies of interaction are g_{11}, g_{22} and g_{12} respectively.

Gibbs free energy change for formation of solvent-segment contact is

$$\Delta g_{solvent-segment} = g_{12} - \frac{1}{2}(g_{11} + g_{22})$$

$$\Delta G_{mix}{}^{contact} = p_{12}\, \Delta g_{solvent-segment}$$

Where, p_{12} total number of solvent-segment interactions

Number of lattice cells adjacent to each polymer molecule = $[(z-1)(x-2)] + [(z-1) \times 2]$

Where,

$[(z-1)(x-2)]$ accounts for the segments not presents in chain ends.

$[(z-1) \times 2]$ accounts for the segments presents in chain ends.

Or in other terms

Number of lattice cells adjacent to each polymer molecule = $[(z-2)(x)] + 2$

For large x the expression is approximated to $[(z-2)(x)]$

Total number of lattice cells adjacent to all polymer molecule in the solution =$\mathrm{N}_2[(z-2)(x)]$

Using mean field approximation,

Total number of solvent-segment interactions, $p_{12} = \mathrm{N}_2[(z-2)(x)]\phi_1$

So

$$\Delta G_{mix}{}^{contact} = \mathrm{N}_2[(z-2)(x)]\phi_1\,\Delta g_{12}$$

We now define Flory Huggins interaction parameter as

$$\chi = \frac{(z-2)\,\Delta g_{12}}{k_B T}$$

$$\Delta G_{mix}{}^{contact} = k_B T \mathrm{N}_1\,\phi_2\,\chi = RT\mathrm{n}_1\,\phi_2\,\chi$$

$$\chi = a + \frac{b}{T}$$

Where, a and b are constant independent of temperature.

So Gibbs free energy change of mixing

$$\Delta G_m = \Delta G_{mix}{}^{contact} - T\Delta S$$

So

$$\Delta G_m = RT\mathrm{n}_1\,\phi_2\,\chi + RT[\mathrm{n}_2\ln(\phi_2) + \mathrm{n}_1\ln(\phi_1)]$$

$$\Delta G_m = RT[\mathrm{n}_1\,\phi_2\,\chi + \mathrm{n}_2\ln(\phi_2) + \mathrm{n}_1\ln(\phi_1)]$$

This is the expression for Flory Huggins equation for Gibbs free energy change of mixing.

Flory Huggins equation can quantitatively account for:

1. Equilibrium thermodynamic properties of polymer solution.
2. Phase separation and fractionation behavior.
3. Swelling of network polymer.

Limitations

1. Mean field approximation is not suitable for dilute polymer solutions.
2. χ is not a simple parameter.

**The derivation is taken from NPTEL course titled as "Introduction to Polymer physics" by Dr. Amit Kumar, Associate Professor, Department of Chemical Engineering IIT Guwahati.

Appendix 2

Background theories and tools

1. Polymer

Polymer combines two Greek words, "poly" and "mers"; the former means many while the latter means repeating units. Hence, the Oxford dictionary defines polymers as "A natural or artificial substance consisting of large molecules (or groups of atoms) that are made from combinations of small, simple molecules." These simple repeating subunits are known as *monomers*. The covalent bonding of monomers forms the polymers through the *polymerization* process. The number of units present in polymer chains is known as the *degree of polymerization, N*. Among various classifications, the polymers are broadly classified based on nature of origin, thermal behavior, molecular architecture, etc. Based on the type of monomers present, a polymer can be further classified as homopolymer and copolymer. A homopolymer is constituted of only one type of monomer unit bonded together either in a linear or crosslinked manner.

On the contrary, a copolymer is a particular class of polymer in which two or more different repeated units covalently bonded to each other. Moreover, a solution of homopolymers in a common solvent is known as a polymer blend. The peculiar property of polymer blends and

copolymers is phase behavior. To account for the phase behavior Flory and Huggins independently put forward the relation for entropy change of mixing for polymer solutions,

which is popularly known as Flory Huggins theory. The theory is discussed in detail in Chapter 1 and Appendix 1.

2. Thin films preparation through Spin coating

Based on the desired application and type of material to be deposited, coatings can be deposited in the vapor or liquid phase. The present discussion is restricted to the film coating using the *Spin coating* technique. The spin coating is one of the most widely used techniques for preparing uniform film over a flat surface. The widespread applicability of spin coating is attributed to the deposition of a variety of materials like colloidal particles,[1–3] polymers,[4–18] inorganic materials,[19] lipids,[20], etc. It is one of the best techniques to be utilized in the microelectronic industry for uniform coating resist over the substrates like silicon wafers with a thickness of a few nanometers.[21,22] It is a batch process that involves four steps 1) deposition, 2) spin-up, 3) spin-off, and 4) evaporation. In the first step, a copious amount of liquid is dispensed over the substrate, either at rest or rotating at constant rpm. The substrate can be as large as 30 cm.[13] In the spin-up step, the centrifugal force generated by the rotating substrate forces the liquid to flow radially outwards. Due to this radially outward flow, a large amount of solution is spun off (step 3), the substrate leaving behind a very thin layer of the liquid. Next, the solvent is evaporated from the deposited liquid, resulting in forming a thin coat over the substrate. The complete process is described in the report by Scriven.[23] The complete process is described in Figure S1. The factors that affect the film thickness are the concentration of the solution and rotation speed.[24] Moreover, the volatility of solvents used determines the roughness of the prepared films.[25]

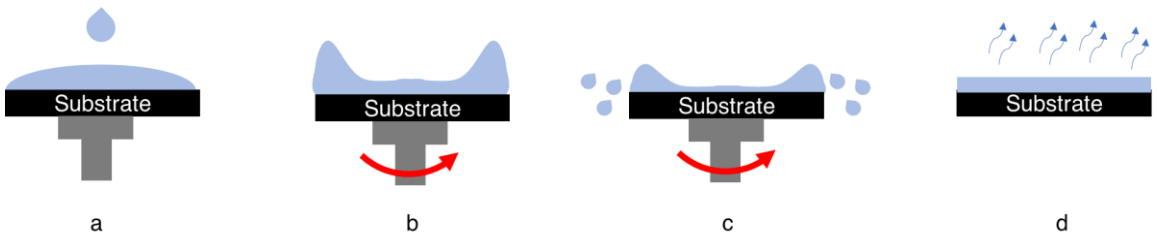

Figure S1. The figure shows steps involved in spin coating (a) deposition, (b) spin-up, (c) spin-off, (d) evaporation of the residual solvent.

3. Rapid thermal annealing (RTA)

Most of the polymers degrade when annealed to high temperatures. Albeit when the annealing of the polymer was done at a very short period, the degradation of the chains can be prevented. Moreover, in the present work (Chapter 2 and Chapter 4) it has been demonstrated that it enhances the rate of phase separation in polymer blend films without affecting the molecular structures of the polymers. In our work, the RTA process has been extensively used to generate faster phase-separated domains in polymeric bilayer systems using a hot plate. A temperature of 300°C was carefully chosen as a set-point for the RTA process. The whole RTA process is divided into three parts: the samples were heated up to 300°C from the ambient temperature. When the set-point is achieved, the samples were allowed to remain at 300°C for the following 30 s. After that, the temperature is suddenly reduced to allow samples to cool through natural convection. The temperature profile is shown in Figure S2.

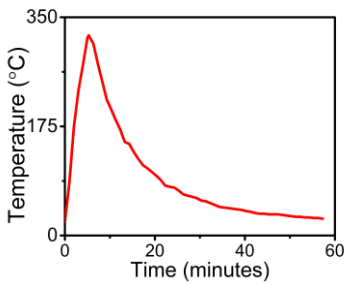

Figure S2. The figure shows the temperature profile during the rapid thermal annealing process.

4. Capillary force lithography

The *Capillary Force Lithography* (CFL) is a facile and low-cost combination of nanoimprint lithography (NIL) and soft lithography.[26] Owing to its simplicity and cost-effectiveness, CFL finds broad applicability in various fields such as gas sensing, drug delivery systems, biomimetics, etc.[27] It is a patterning technique very similar to NIL; however, it utilizes a key feature of soft lithography by incorporating soft mold for pattern generation. Also, it is a low-pressure process, unlike conventional NIL.

The process involves the spin coating of a thin layer of polymer over a substrate (mostly silicon wafers). Next, a soft mold is firmly placed over the previously coated polymer film. In most cases, the soft elastomeric poly dimethyl siloxane (PDMS) mold is utilized. The system is then heated to a temperature higher than that of the glass transition temperature (T_G) of the polymer. At a temperature $T > T_G$ the mobility of the polymer chains increases. This allows the cavities inside the mold to be filled up with the polymer through capillary force. After cooling to room temperature, the mold can be removed and a negative replica of the cavities in the mold is created over the substrate. In our work, aluminium foil peeled off the compact disks is utilized as the soft mold for the experiments involving CFL (Chapter 2, Chapter 3, and Chapter 4).

5. Electron beam lithography (EBL)

The *electron beam lithography* (EBL) is a sophisticated and advanced technique that utilizes focussed electron beam to draw features over polymeric films. A schematic represented EBL set-up is shown in Figure S3. The efficacy of EBL to draw features of the order of few nanometres allows its use in intricate nanoscopic pattern generation. The polymer on which direct writing is done is broadly classified into two viz. positive resists (for example,

polymethyl methacrylate) and negative resists (for example, polystyrene). The former type resist is exposed with a focussed beam the bonds between the polymer units break down in the exposed area. These broken chains are removed using a suitable solvent. This process is known as development. On the contrary to this, in the negative type resist, the crosslinking of the polymer occurs in the exposed area. Subsequently, the unexposed polymer is removed in development process. For further reading on lithographic techniques one can refer review article by del Campo and Arzt.[28] The combinations of EBL and random copolymers (RCP), can be utilized for complex pattern generation (Chapter 5). The study shows the morphological changes occurring when RCP is exposed with variable dose of e-beam.

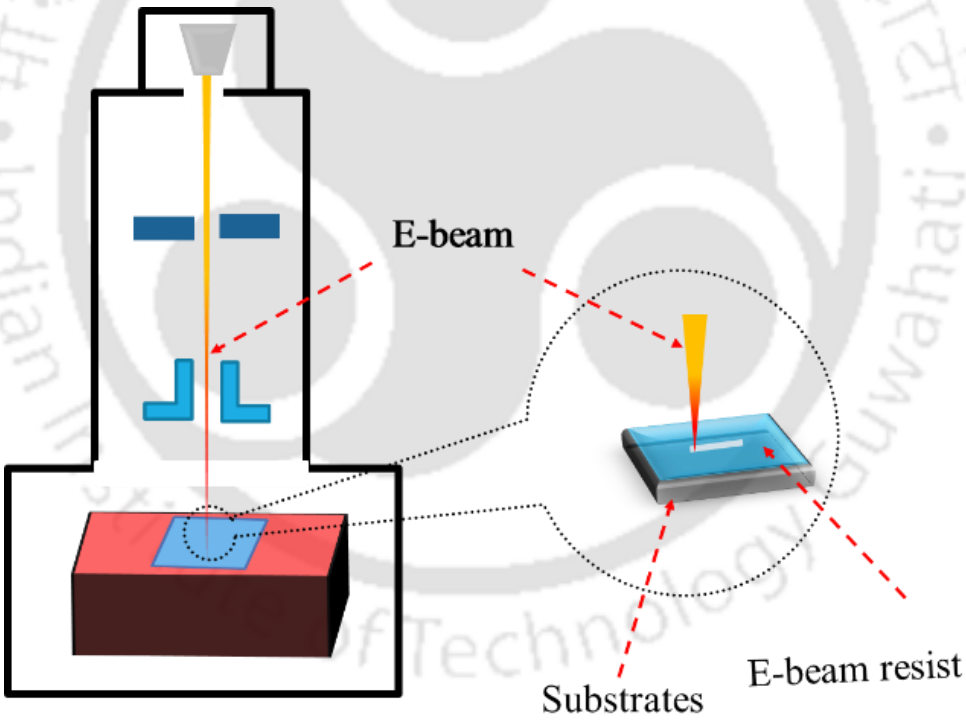

Figure S3. The figure shows the schematic represented electron beam lithography set-up.

6. Characterization techniques

6.1 Atomic force microscopy

In mid-80s, scientists invented *Atomic Force Microscopy* (AFM) to study the surface characteristics of non-conducting samples.[29] The technique was a variation of Scanning

Tunnelling Microscopy (STM) in which only conducting samples were characterized using tunneling current. The resolution limit of AFM is of the order of few nanometres that enables users to study the samples' surface properties. The versatility of the AFM can be seen from the fact that a wide variety of samples can be analyzed. These include biological, polymeric, nanoparticles. The set-up consists of a sharp, probing tip attached to a cantilever that scans the sample's surface. The interaction between the probing tip and the samples enables user to measure local properties like height, surface roughness, magnetic properties, surface potential etc. Usually, three types of mode are used to measure the surface properties, namely contact mode, intermittent contact mode (also known as tapping mode), and non-contact modes.[30] In the presented work, AFM is extensively used to determine the surface properties of the samples.

6.2 Raman Spectroscopy

Raman Spectroscopy is a unique characterization technique that is used to identify vibrational, rotational or other low frequency modes of a sample. These information is unique for a given material. Thus raman spectroscopy is a reliable characterization technique that provides information about molecular and crystal symmetry, bond strengths of the substrates, phase identification purposes, structural disorders, etc.[30,31]

6.3 Ellipsometry

The ellipsometry is a non destructive optical technique used to characterize thin films for properties like film thickness, refractive index, composition etc. It works on the principle of change in the polarization of light after reflection from a surface as a ratio of two perpendicularly polarized beams. The light emmited from a light source is linearly polarized used polarizer. The light is then passe through a compensator. Thereafter, it is incendented over

a surface with angle of incident, ϕ. The light is reflected and passed through detector via analyzer. The whole set-up is schematically represented by Figure S4. The polarization state of the light consist of *s* which oscillates orthogonally to the plane of incidence and parallel to the sample surface. However, the *p* component oscillates parallel to the plane of incidence. The complex reflectance ratio , which is the ratio of amplictude of p and s components is calculated as:

$$\rho = \frac{r_p}{r_q} = \tan(\Psi)\, e^{i\Delta}$$

Where, The amplitude ratio is represented by $\tan(\Psi)$ and phase difference is represented by Δ. Optical properties are calcutated based on models applied on the values of Ψ and Δ. [31]

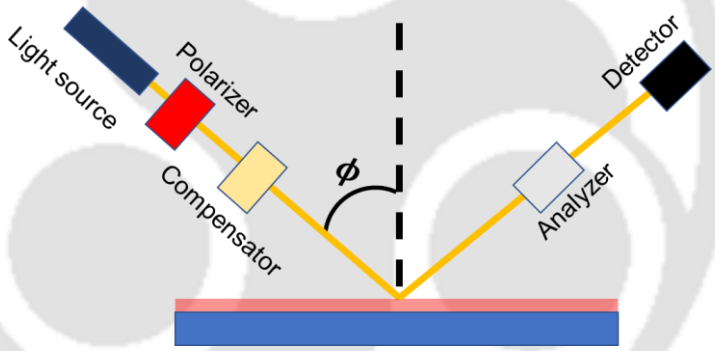

Figure S4. The figure shows the schematic represented ellipsometry set-up.

6.4 Field Emission Scaning electron Microscopy (FESEM)

The scaning electron microscopy (SEM) involves the raster scaning of the samples by high energy focussed electron beams. The technology exploits the interaction of eletrons with the material, which produces various signals. These signals when detected reveals properties of the surface like morphologies and composition. The advanced version of conventional convetional SEM is FESEM.The main difference between SEM and FESEM is the emission source. In conventional SEM the emission source is thermionic type and in FESEM is the field

emission type. The field emission type emitter is better than conventional thermionic type emitter as it is capable of providing extremely focused high and low-energy electron beams. This enhances the resolution and also reduces the working potentials lesser thab 5 kV.

6.5 Differential Scaning Calorimentry (DSC) and Thermo Gravimetric Aanlysis (TGA)

The changes in properties of material with variations in temperature is characterized by TGA and DSC analysis. The changes in heat flow in the sample as the sample is heated or cooled, is monitored by DSC. In the analysis the sample and the reference are heated to same temperature.When thermal transition occurs in the sample, the heat flow to the sample with respect to the reference also changes. This is done to maintain the sample at the set temperature. A schematic DSC curve is shown by Figure S5.[32]

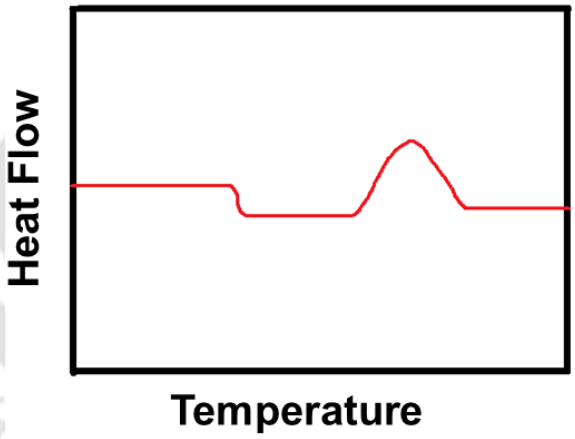

Figure S5. The schematic represented DSC curve.

The TGA analysis also provides information about the changes occurring in the material with changes in the temperature. Unlike DSC, the TGA measures the changes in the weight of the sample with time at a set the temperature. The typical TGA graph is shown by Figure S6. [32]

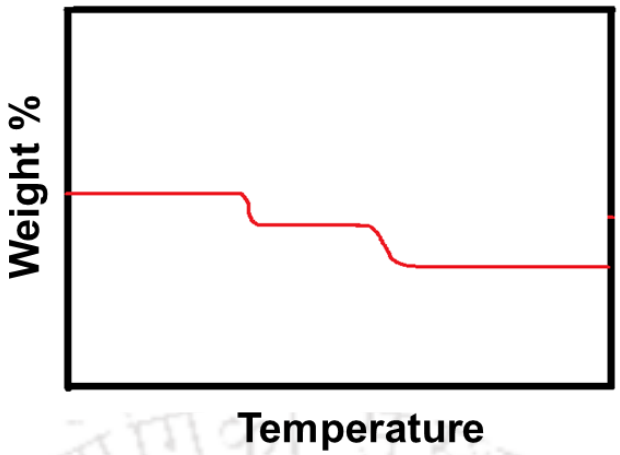

Figure S6. The schematic represented TGA curve.

7. Sources of errors

The intrinsic nature of the system under consideration is itself random and even the smallest of the fluctuations can lead to completely different results. Hence, all the experiments are performed multiple times to ensure the concordant results.

Moreover, the image analysis softwares like ImageJ and Nanoscope Analysis are used for the calculations of parameters like diameters, number density and wavelength of the patterns. The alogorithm of such softwares identifies the features based on image analysis. However, many a times the to user is required to manually identify the features. This step can be a source of manual error if this step is not meticulously performed.

While samples being analysed using AFM, the operator of the instrument must ensure that the tip used to scan the sample is in good condition as a contaiminated or blunt tip may lead to poor quality of image. This will lead to the error in calculations of parameters like diameters and height of the features.

REFERENCES

[1] Y. Zhao, J.S. Marshall, Spin coating of a colloidal suspension, Phys. Fluids. 20 (2008). https://doi.org/10.1063/1.2896601.

[2] T.J. Rehg, G. Higgins, Spin coating of colloidal suspensions, AIChE J. 38 (1992) 489–501. https://doi.org/10.1002/aic.690380403.

[3] D.T.W. Toolan, S. Fujii, S.J. Ebbens, Y. Nakamura, J.R. Howse, On the mechanisms of colloidal self-assembly during spin-coating, Soft Matter. 10 (2014) 8804–8812. https://doi.org/10.1039/c4sm01711k.

[4] S. Walheim, M. Böltau, J. Mlynek, G. Krausch, U. Steiner, Structure formation via polymer demixing in spin-cast films, Macromolecules. 30 (1997) 4995–5003. https://doi.org/10.1021/ma9619288.

[5] Q. Zong, Z. Li, X. Xie, Inversion of phase morphology in polymer-blend thin films on glass substrates, Macromol. Chem. Phys. 205 (2004) 1116–1124. https://doi.org/10.1002/macp.200300235.

[6] H. Zhang, S. Takeoka, Morphological evolution within spin-cast ultrathin polymer blend films clarified by a freestanding method, Macromolecules. 45 (2012) 4315–4321. https://doi.org/10.1021/ma3005394.

[7] J. Raczkowska, P. Cyganik, A. Budkowski, A. Bernasik, J. Rysz, I. Raptis, P. Czuba, K. Kowalski, Composition effects in polymer blends spin-cast on patterned substrates, Macromolecules. 38 (2005) 8486–8493. https://doi.org/10.1021/ma051242s.

[8] S.Y. Heriot, R.A.L. Jones, An interfacial instability in a transient wetting layer leads to lateral phase separation in thin spin-cast polymer-blend films, Nat. Mater. 4 (2005) 782–786. https://doi.org/10.1038/nmat1476.

[9] P.G. de Gennes, Solvent evaporation of spin cast films :“crust” effects, Eur. Phys. J. E. 7 (2002) 31–34. https://doi.org/10.1140/epje/i200101169.

[10] S. Walheim, M. Bo, G. Krausch, U. Steiner, Structure Formation via Polymer Demixing in Spin-Cast Films, 9297 (1997) 4995–5003.

[11] S. Walheim, M. Ramstein, U. Steiner, Morphologies in ternary polymer blends after spin-coating, Langmuir. 15 (1999) 4828–4836. https://doi.org/10.1021/la981467e.

[12] C. Ton-That, A.G. Shard, R.H. Bradley, Surface feature size of spin cast PS/PMMA blends, Polymer (Guildf). 43 (2002) 4973–4977. https://doi.org/10.1016/S0032-3861(02)00333-6.

[13] K. Norrman, A. Ghanbari-Siahkali, N.B. Larsen, Studies of spin-coated polymer films, Annu. Reports Prog. Chem. - Sect. C. 101 (2005) 174–201. https://doi.org/10.1039/b408857n.

[14] P. Mokarian-Tabari, M. Geoghegan, J.R. Howse, S.Y. Heriot, R.L. Thompson, R.A.L. Jones, Quantitative evaluation of evaporation rate during spin-coating of polymer blend films: Control of film structure through defined-atmosphere solvent-casting, Eur. Phys. J. E. 33 (2010) 283–289. https://doi.org/10.1140/epje/i2010-10670-7.

[15] A. Budkowski, A. Bernasik, P. Cyganik, J. Raczkowska, B. Penc, B. Bergues, K. Kowalski, J. Rysz, J. Janik, Substrate-determined shape of free surface profiles in spin-cast polymer blend films, Macromolecules. 36 (2003) 4060–4067. https://doi.org/10.1021/ma0208943.

[16] S. Roy, A. Sharma, Self-organized morphological evolution and dewetting in solvent vapor annealing of spin coated polymer blend nanostructures, J. Colloid Interface Sci. 449 (2015) 215–225. https://doi.org/10.1016/j.jcis.2014.12.095.

[17] X. Li, Y. Han, L. An, Surface morphology control of immiscible polymer-blend thin films, Polymer (Guildf). 44 (2003) 8155–8165.

https://doi.org/10.1016/j.polymer.2003.10.012.

[18] K.E. Strawhecker, S.K. Kumar, J.F. Douglas, A. Karim, The critical role of solvent evaporation on the roughness of spin-cast polymer films, Macromolecules. 34 (2001) 4669–4672. https://doi.org/10.1021/ma001440d.

[19] X. Xu, C. Xia, S. Huang, D. Peng, YSZ thin films deposited by spin-coating for IT-SOFCs, Ceram. Int. 31 (2005) 1061–1064. https://doi.org/10.1016/j.ceramint.2004.11.005.

[20] U. Mennicke, T. Salditt, Preparation of solid-supported lipid bilayers by spin-coating, Langmuir. 18 (2002) 8172–8177. https://doi.org/10.1021/la025863f.

[21] D.J. Carbaugh, S. Kaya, F. Rahman, Transparent and visible light-insensitive acrylic photoresist for negative tone optical lithography, J. Vac. Sci. Technol. B,. 35 (2017) 011601. https://doi.org/10.1116/1.4971198.

[22] W.H. Teh, C. Te Liang, M. Graham, C.G. Smith, Cross-linked PMMA as a low-dimensional dielectric sacrificial layer, J. Microelectromechanical Syst. 12 (2003) 641–648. https://doi.org/10.1109/JMEMS.2003.817891.

[23] L.E. Scriven, Physics and Applications of DIP Coating and Spin Coating, MRS Proc. 121 (1988) 717–729. https://doi.org/10.1557/proc-121-717.

[24] C.J. Lawrence, The mechanics of spin coating of polymer films, Phys. Fluids. 31 (1988) 2786–2795. https://doi.org/10.1063/1.866986.

[25] L. Weh, Surface structures in thin polymer layers caused by coupling of diffusion-controlled Marangoni instability and local horizontal temperature gradient, Macromol. Mater. Eng. 290 (2005) 976–986. https://doi.org/10.1002/mame.200500165.

[26] J. Kong, M.G. Chapline, H. Dai, Capillary force lithography, Adv. Mater. 13 (2001) 1386–1389. https://doi.org/10.1002/1521-4095(200109)13:18<1386::AID-ADMA1386>3.0.CO;2-X.

[27] D. Ho, J. Zou, B. Zdyrko, K.S. Iyer, I. Luzinov, Capillary force lithography: The versatility of this facile approach in developing nanoscale applications, Nanoscale. 7 (2015) 401–414. https://doi.org/10.1039/c4nr03565h.

[28] A. del Campo, E. Arzt, Fabrication approaches for generating complex micro- and nanopatterns on polymeric surfaces, Chem. Rev. 108 (2008) 911–945. https://doi.org/10.1021/cr050018y.

[29] E. Meyer, Atomic force microscopy, Prog. Surf. Sci. 41 (1992) 2–49. https://doi.org/10.1093/oso/9780198856559.003.0016.

[30] R. Asmatulu, W.S. Khan, eds., Synthesis and applications of electrospun nanofibers, Elsevier, 2019.

[31] V.-M. Airaksinen, HANDBOOK OF SILICON BASED MEMS MATERIALS AND TECHNOLOGIES, Second, Elsevier Inc., 2015.

[32] S.R. Byrn, G. Zografi, X.S. Chen, Differential Scanning Calorimetry and Thermogravimetric Analysis, Solid State Prop. Pharm. Mater. (2017) 124–141. https://doi.org/10.1002/9781119264408.ch10.

Appendix 3

Supplementary information: Effect of Labile Underlayer on the Morphology of Thermally Annealed Polymer Blend

Section S1: TGA of the polymers at aerial condition

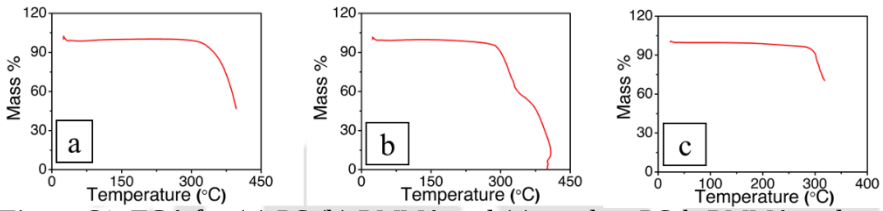

Figure S1. TGA for (a) PS (b) PMMA and (c) random PS-b-PMMA under aerial condition.

Section S2: AFM phase images

S2.1 ***Phase Images for blend over PS underlayer***

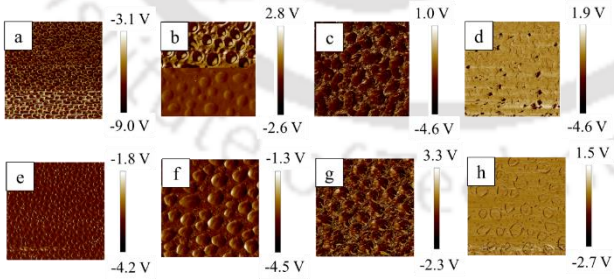

Figure S2.1 The AFM phase images for blend over 0.5% PS underlayer after (a) spin coating (b) RTA (c) acetic acid and (d) cyclohexane treatment. Similarly, AFM phase scans of 20 µm x 20 µm for blend over 1 % PS underlayer after (e) spin coating (f) RTA (g) acetic acid and (h) cyclohexane treatment.

S2.2 Phase Images for blend over PMMA underlayer

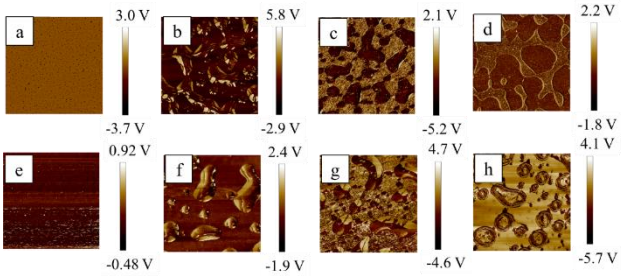

Figure S2.2 The AFM phase scans of 20 µm x 20 µm for blend over 0.5% PMMA after (a) spin coating (b) RTA (c) acetic acid and (d) cyclohexane treatment. Similarly, AFM phase scans of 20 µm x 20 µm for blend over 1% PMMA after (e) spin coating (f) RTA (g) acetic acid and (h) cyclohexane treatment.

S2.3 Phase Images for blend over blend underlayer

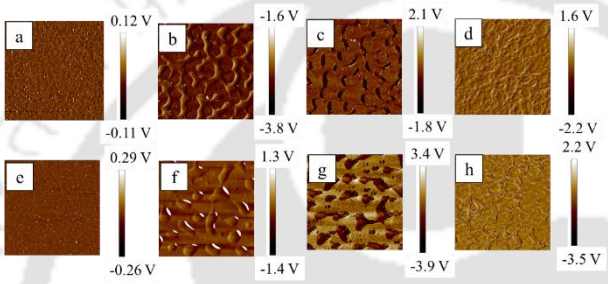

Figure S2.3 AFM phase scans of 20 µm x 20 µm for blend over 0.5% blend after (a) spin coating (b) after RTA (c) acetic acid treatment and (d) cyclohexane treatment. Similarly, AFM phase scans of 20 µm x 20 µm for blend over 1% blend after (e) spin coating (f) RTA (g) acetic acid treatment and (h) cyclohexane treatment.

S2.4 Phase Images for blend over RCP underlayer

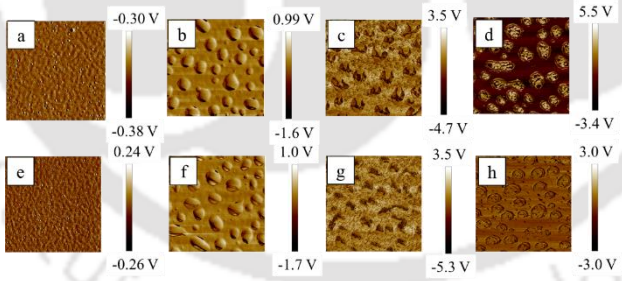

Figure S2.4 AFM phase scans of 20 µm x 20 µm for blend over 0.5% RCP after (a) spin coating (b) RTA (c) acetic acid treatment and (d) cyclohexane treatment. Similarly, AFM phase scans of 20 µm x 20 µm for blend over 1% RCP after (e) spin coating (f) RTA (g) acetic acid treatment and (h) cyclohexane treatment.

Appendix 4

Supplementary information: Complex nanostructure generation by e-beam lithography on a random block copolymer thin-film

S1. Tone reversal behavior of PMMA with e-beam dose:

Upon irradiation with electron beam, Poly methyl methacrylate (PMMA) exhibits tone reversal beahvior. This phenomenon is already demonstrated by Hoole et al.[1] If a PMMA thin film is irradiated with varying e-beam dose and subsequently developed with MIBK/IPA, the remnant film thickness can be schematically depicted as shown in figure S1 below:

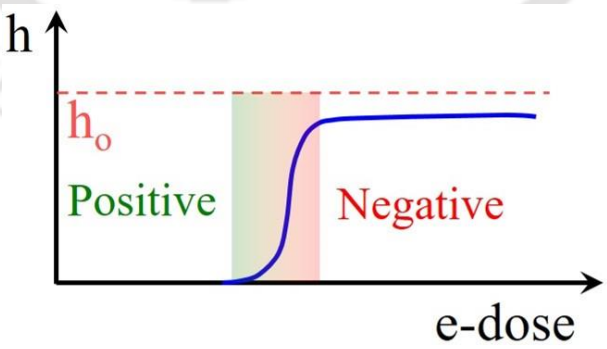

Figure S1. Schematic depicts PMMA film thickness h as a function of e-dose of e-beam exposure and subsequent developing with MIBK/IPA. The pink dotted line shows the initial film thickness h_o and the shaded region shows the transition zone from positive to negative resist behavior with e-dose.

S2. All the AFM images and line scan of the Figure 2 of the main text.

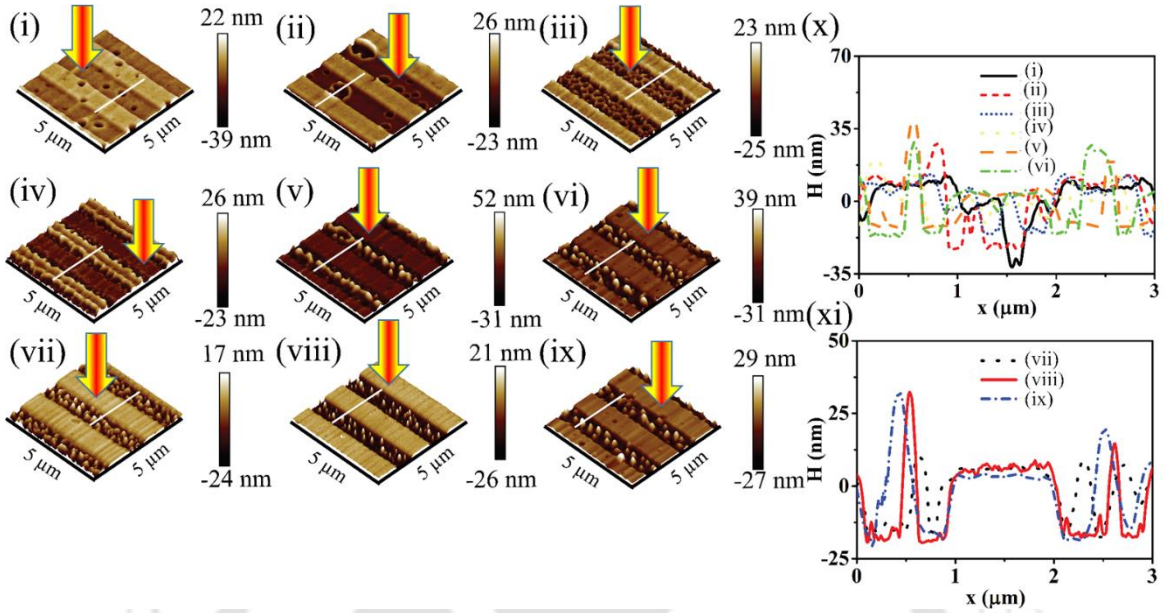

Figure S2. AFM images showing morphological pattern of PS-r-PMMA film when exposed with variable dose of e-beam creating 1-D confinement. The e-beam doses used are (i) 180 µC/cm^2, (ii) 700 µC/cm^2, (iii) 1500 µC/cm^2, (iv) 3000 µC/cm^2, (v) 5000 µC/cm^2, (vi) 6000 µC/cm^2, (vii) 10000 µC/cm^2. After selective solvent etching. (viii) PMMA removal and (ix) PS removal from (vii). The corresponding line scans are shown by graphs (x), and (xi). The arrow shows the region of e-beam exposure.

S3. All the AFM images and line scan of the Figure 3 of the main text:

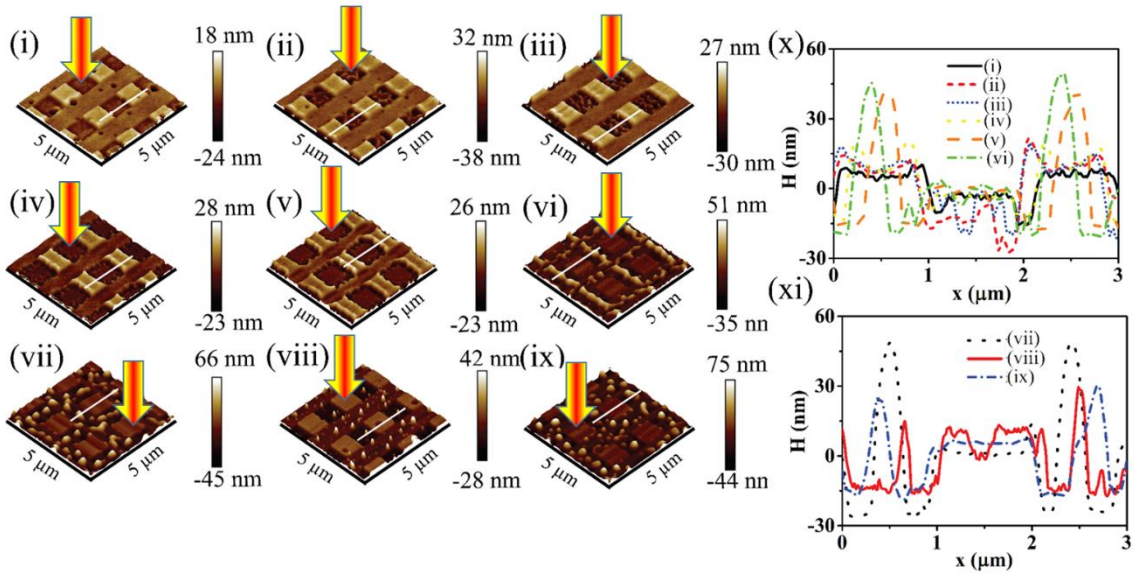

Figure S3. AFM images showing morphological pattern of PS-r-PMMA film when exposed with variable dose of e-beam creating 2-D confinement. The e-beam doses used are (i) 180 µC/cm^2, (ii) 700 µC/cm^2, (iii) 1500 µC/cm^2, (iv) 3000 µC/cm^2, (v) 5000 µC/cm^2, (vi) 6000 µC/cm^2, (vii) 10000 µC/cm^2. After selective solvent etching (viii) PMMA removal and (ix) PS

removal. The corresponding line scans are shown by graphs (x), and (xi). The arrow shows the region of e-beam exposure.

S4. Representative FESEM images of 1D stripe pattern:

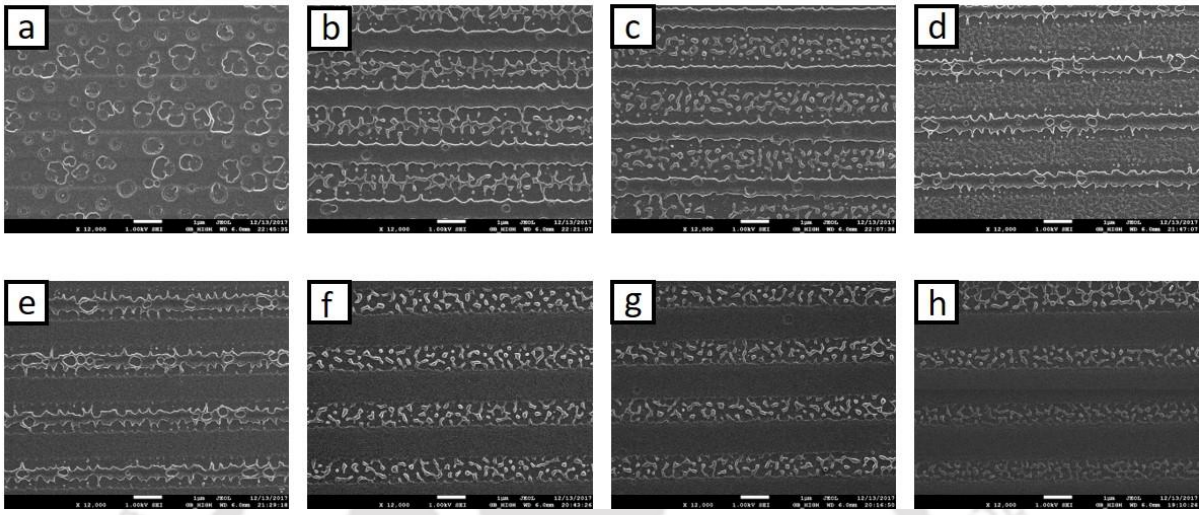

Figure S4. FESEM images showing morphological pattern of PS-r-PMMA film when exposed with variable dose of e-beam creating 1-D confinement. The e-beam doses used are (a) 900 μC/cm^2, (b) 1500 μC/cm^2, (c) 2000 μC/cm^2, (d) 3000 μC/cm^2, (e) 5000 μC/cm^2, (f) 7000 μC/cm^2, (g) 8500 μC/cm^2, (h) 10000 μC/cm^2. Scale bars represent 1 μm.

S5. Representative FESEM images of 2D square pattern:

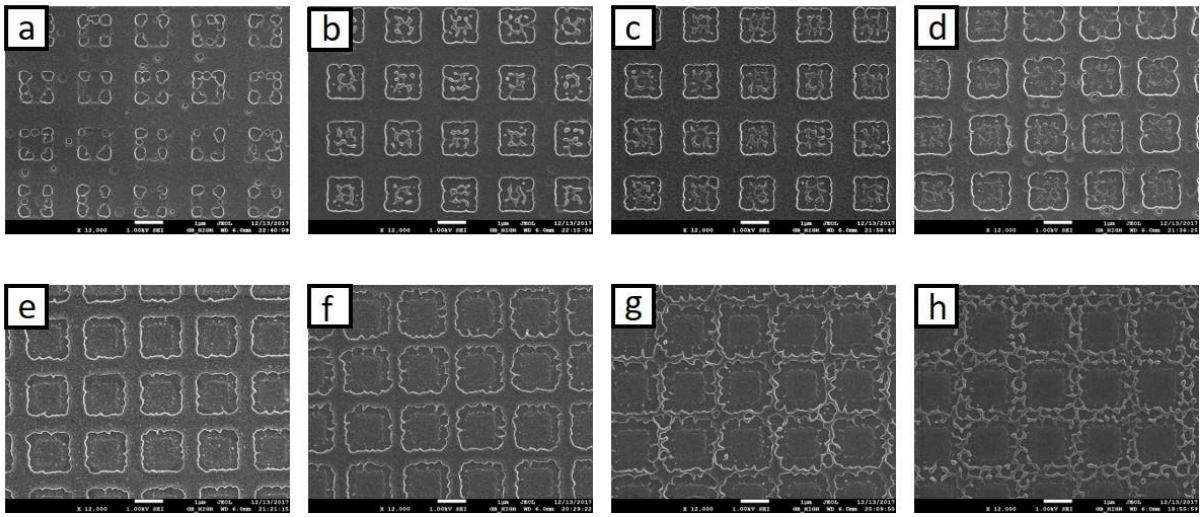

Figure S5. FESEM images showing morphological pattern of PS-r-PMMA film when exposed with variable dose of e-beam creating 2-D confinement. The e-beam doses used are (a) 900 μC/cm^2, (b) 1500 μC/cm^2, (c) 2000 μC/cm^2, (d) 3000 μC/cm^2, (e) 5000 μC/cm^2, (f) 7000 μC/cm^2, (g) 8500 μC/cm^2, (h) 10000 μC/cm^2. Scale bars represent 1 μm.

S6. Schematic Energy distribution of an electron beam:

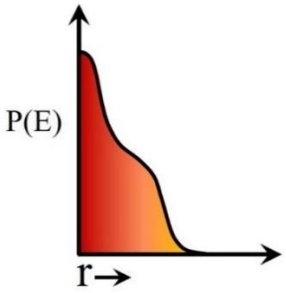

Figure S6. Schematic of the Energy distribution as a function of distance from the centre of the e-beam exposure (r).

S7. Effect of different exposure pitch:

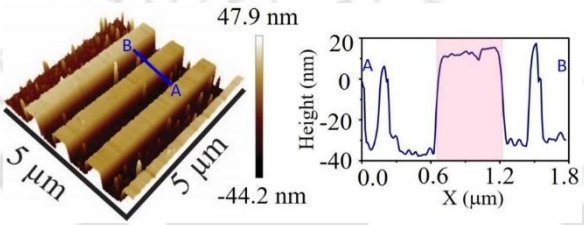

Figure S7. ~44 nm RCP film with ~500 nm exposure pitch with e-beam dose of 8000 µC/cm^2. Line scan AB reveals that the dewetted structure of polymer droplet having ~150 nm diameter is obtained.

S8. Effect of different film thickness:

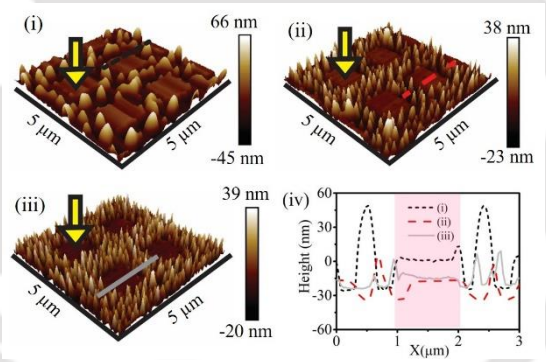

Figure S8. ~ 45 nm (i), ~ 22 nm (ii), and ~ 11 nm (iii) RCP film when exposued to 10000 µC/cm^2 e-dose havinf 2-D pattern of 1µm pitch. (iv) depicts the line scan revealing the miniaturization of dewetted droplet size with decreasing film thickness.

REFERENCE:

[1] A.C.F. Hoole, M.E. Welland, A.N. Broers, Negative PMMA as a high-resolution resist : the limits and possibilities, Semicond. Sci. Technol. 12 (1997) 1166–1170.

ANKUR PANDEY

Ph.D. Scholar

Department of Chemical Engineering

Indian Institute of Technology Guwahati,

CAREER OBJECTIVE

To become an independent researcher in the field of micro/nano-patterning of macromolecules, nanoparticle synthesis, and applications. Also, to secure a responsible career position to fully utilize my expertise and skills while making a significant contribution to society.

EDUCATIONAL QUALIFICATIONS

Ph.D. Department of Chemical Engineering, IIT Guwahati. *(Pursuing*).
M.Tech. with specialization in Chemical Process Design from Department of Chemical Engineering, National Institute of Technology Raipur, Chhattisgarh 4920210 as a GATE qualified candidate 7.34/10.

Completed B.E. in Chemical Engineering in 2013 from Manipal Institute of Technology, Madhav Nagar, Manipal, Taluk- Udupi, Karnataka-576104 with CGPA 6.67/10.

Passed CBSE All India Senior School Certificate Examination (AISSCE) in 2008 from Central School no. 2 Shivaji Nagar Bhopal (M.P.) with 72% marks.

Passed CBSE All India Secondary School Examination (AISSE) in 2006 from Holy Cross Convent School Ambikapur (C.G.) with 76% marks.

AREA OF EXPERTISE

Nanoparticles synthesis, Random copolymers, Photolithography, Electron Beam Lithography (EBL), Capillary Force Lithography, Atomic Force Microscopy (AFM), Field Emission Scanning Electron Microscopy (FE-SEM), X-Ray Diffraction (XRD), and Optical microscopy, Bio inspired complex hierarchical patterns.

PROJECTS UNDERTAKEN

Doctoral level: "Experimental investigation on the micro/ nano patterning of blended and random copolymer thin films" under the guidance of Dr. Partho S. G. Pattader, Department of Chemical Engineering, IIT Guwahati (*On going at Thesis submission stage*).
Graduate Level: "Study of synthesis of nickel nanoparticles" under the guidance of Dr. R. Manivannan, Department of Chemical Engineering, National Institute of Technology Raipur Chhattisgarh-492010 (*Completed*).
Undergraduate level: "Synthesis of Nickel Oxide and its applications in pollution abatement" under the guidance of Prof. S. Sivasankaran, Associate Professor, Department of Chemical Engineering, Manipal Institute of Technology, Madhav Nagar, Manipal, Taluk: Udupi 576104 (*Completed*).

LIST OF PUBLICATIONS

Research Articles

Ph.D.

1. **A. Pandey**, K. Murmu, P.S. Gooh Pattader, Non-equilibrium thermal annealing of a polymer blend in bilayer settings for complex micro/nano-patterning, RSC Adv. 11 (2021) 10183–10193.
2. **A. Pandey**, S. Maity, K. Murmu, S. Middya, D. Bandyopadhyay, P.S. Gooh Pattader, Self-organization of random copolymers to nanopatterns by localized e-beam dosing, Nanotechnology. 32 (2021) 285302.
3. P. Gogoi, S. K. Singh, **A. Pandey**, A. Chattopadhyay, P. S. Gooh Pattader, Nanometer Thick Superhydrophobic Coating Renders Cloth Mask Potentially Effective Against Aerosol-driven Infections, ACS Applied Bio Materials (Submitted).
4. D. Paul, **A. Pandey**, S. Neogi, Bacterial cell permeability study by metal oxide and mixed metal oxide nanoparticles: Analysis of the factors contributing to the antibacterial activity of nanoparticle, J. Photochem. Photobiol. B, Biol. (Submitted).

M.Tech.

1. **A. Pandey**, R. Manivannan, A Study on Synthesis of Nickel Nanoparticles Using Chemical Reduction Technique, Recent Patents Nanomed. 5 (2015) 33–37.

B.E.

1. **A. Pandey**,Piyush Ranjan, S. Sivasankaran, A Novel Ultrasound Assisted Advanced Oxidation Process for WaterPollution Abatement by Using Transition Metal Oxides, IJSER,4 (2013) 1587.

List of Conferences

1. **Ankur Pandey** and R. Manivannan “A study on synthesis of nickel nanoparticles using chemical reduction technique” presented at National Conference on Nanoscience and Nanotechnology-2014, Bhilai, Chhattisgarh (Second prize for best ORAL presentation).
2. Ankita Verma, **Ankur Pandey** and R. Manivannan, "Corrosion inhibition of mild steel in nitric acid using glycine (gly) as green corrosion inhibitor” CHEMCON-2014, Punjab Univeristy,Chandigarh.
3. **Ankur Pandey** and R. Manivannan“Synthesis of nickel nanoparticles using chemical reduction technique” International Conference on Nanotechnology-2015, HIT, Haldia, West Bengal
4. **Ankur Pandey**, Himanshu Raturi and Partho Sarathi Gooh Pattader, Multistage Patterning of Composite Polymeric Thin Film, International Conference on Functional Nanomaterials, IIT BHU, 2019.
5. **Ankur Pandey**, Surjendu Maity, Partho Sarathi Gooh Pattader and Dipankar Bandhyopadhyay, Biomimicking: Fabrication of insect eye type polymer structures using spin dewetting, Research Conclave, IITG, 2019. (2nd rank for poster presentation).
6. **Ankur Pandey** and Partho Sarathi Gooh Pattader, An experimental investigation of phase separation in polymer-polymer bilayer system, International Conference on Functional Materials-2020, IIT Kharagpur.
7. **Ankur Pandey**, Aniruddha Deb and Partho Sarathi Gooh Pattader, Phase separation in polymer-polymer bilayer systems, International Conference Advances in Chemical Engineering-2020, UPES, Dehradun.
8. **Ankur Pandey** and Partho Sarathi Gooh Pattader, A study on phase separation in polymer-polymer bilayer thin film, EMRS spring meeting 2020, Strasbourg-France. (Accepted for poster presentation).

Oral presentations

4. **Ankur Pandey**, Dipankar Bandhyopadhyay and Partho Sarathi Gooh Pattader, Investigation of blend and block copolymer self-assembly on thin polymer interlayer, REFLUX IIT G, 2018.

5. **Ankur Pandey**, Aniruddha Deb and Partho S G Pattader, Effect of a labile under layer on phase separation of PS-PMMA blend, ACS Spring 2021, 2021.
6. Aniruddha Deb, **Ankur Pandey** and Partho S G Pattader, Effect of vibration on spontaneous dewetting morphology, kinetics and self-assembly of thin films, ACS Spring 2021.

SOFTWARES KNOWN

MS-Office, Origin Pro 8, ADOBE PHOTOSHOP & ADOBE ILLUSTRATOR, Gwyddion

PERSONAL DETAILS

Parentage: Mrs. Jyoti Pandey & Mr. Aseem Kumar Pandey
Date of Birth: 11.08.1990.
Gender: Male.
Marital Status: Bachelor.
Nationality: INDIAN.
Religion: Hinduism.
Languages Known: English, Hindi.
Hobbies & Interests: Poetry, photography, reading, listening to music.
COVID Vaccination status: Vaccinated

PROFESSIONAL REFERENCES

Dr. Partho Sarathi Gooh Pattader

Department of Chemical Engineering
IIT Guwahati 781039
Email: psgp[at]iitg.ac.in

Prof. Dipankar Bandyopadhyay

Department of Chemical Engineering
IIT Guwahati 781039
Email: dipban[at]iitg.ac.in

DECLARATION

I hereby declare that the above information is correct to the best of my knowledge and belief.

(ANKUR PANDEY)

31 August 2021
Place: Guwahati